

INFORMATION TO USERS

This reproduction was made from a copy of a document sent to us for microfilming. While the most advanced technology has been used to photograph and reproduce this document, the quality of the reproduction is heavily dependent upon the quality of the material submitted.

The following explanation of techniques is provided to help clarify markings or notations which may appear on this reproduction.

1. The sign or "target" for pages apparently lacking from the document photographed is "Missing Page(s)". If it was possible to obtain the missing page(s) or section, they are spliced into the film along with adjacent pages. This may have necessitated cutting through an image and duplicating adjacent pages to assure complete continuity.
2. When an image on the film is obliterated with a round black mark, it is an indication of either blurred copy because of movement during exposure, duplicate copy, or copyrighted materials that should not have been filmed. For blurred pages, a good image of the page can be found in the adjacent frame. If copyrighted materials were deleted, a target note will appear listing the pages in the adjacent frame.
3. When a map, drawing or chart, etc., is part of the material being photographed, a definite method of "sectioning" the material has been followed. It is customary to begin filming at the upper left hand corner of a large sheet and to continue from left to right in equal sections with small overlaps. If necessary, sectioning is continued again—beginning below the first row and continuing on until complete.
4. For illustrations that cannot be satisfactorily reproduced by xerographic means, photographic prints can be purchased at additional cost and inserted into your xerographic copy. These prints are available upon request from the Dissertations Customer Services Department.
5. Some pages in any document may have indistinct print. In all cases the best available copy has been filmed.

**University
Microfilms
International**

300 N. Zeeb Road
Ann Arbor, MI 48106

8416535

Khondker, Abul Islam Mohammad Nazme Rahmani

THEORY OF CONDUCTION IN POLYCRYSTALLINE SILICON

Rice University

PH.D. 1984

University
Microfilms
International 300 N. Zeeb Road, Ann Arbor, MI 48106

RICE UNIVERSITY

THEORY OF CONDUCTION IN POLYCRYSTALLINE SILICON


BY


ABUL ISLAM MOHAMMAD NAZME RAHMANI KHONDKER

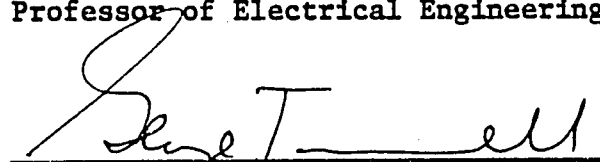
A THESIS SUBMITTED
IN PARTIAL FULFILLMENT OF THE
REQUIREMENTS FOR THE DEGREE

DOCTOR OF PHILOSOPHY

APPROVED, THESIS COMMITTEE


Dae Mann Kim
Professor of Electrical Engineering


Thomas A. Rabson
Professor of Electrical Engineering


George Trammell
Professor of Physics

HOUSTON, TEXAS

JULY, 1983

بِسْمِ اللَّهِ الرَّحْمَنِ الرَّحِيمِ

In the name of Allah, the Beneficent, the Merciful

ACKNOWLEDGEMENTS

I Would like to express my sincere gratitude to my thesis director, Dr. Dae Mann Kim, for his constant guidance, enthusiasm, and many helpful suggestions. I would also like to thank Professors T. A. Rabson and G. Trammel for serving in my thesis committee.

I would also like to thank Dr. Rajiv Shah, Dr.W.L. Wilson, T. Estle for their constructive comments on the subject matter of the thesis. The help of S.S. Ahmed and T.I. Liou is also greatly appreciated.

D. Dhamdhere and R. Covington generously shared their wide knowledge of computers with me through this research. I acknowledge their help gratefully.

V. Hoff also deserves thanks for helping me process and type this thesis.

Finally, I would like to express my gratitude to my parents Mr. and Mrs. Golam Rabbani Khondker, my brothers and sister for their support, patience and encouragement. I would also like to acknowledge the encouragement, help and constant companionship of my wife Jane Giesberg Khondker during the writing of my thesis.

TABLE OF CONTENTS

	PAGE
ACKNOWLEDGEMENTS.....	i
TABLE OF CONTENTS.....	ii
CHAPTER ONE: INTRODUCTION.....	1
1.1 PRELIMINARIES.....	1
1.2 POLYCRYSTALLINE SEMICONDUCTORS	2
1.3 REVIEW OF PREVIOUS THEORIES.....	8
1.4 GRAIN BOUNDARY ALTERATION.....	22
1.5 MOTIVATION.....	25
1.6 ORGANIZATION.....	28
CHAPTER TWO: THEORY OF AMORPHOUS SEMICONDUCTORS.....	30
2.1 PRELIMINARIES.....	30
2.2 TRANSPORT THEORY OF AMORPHOUS SEMICONDUCTORS.....	31
2.3 TEMPERATURE DEPENDENCE OF AMORPHOUS CONDUCTIVITY.....	34
2.4 I-V CHARACTERISTICS OF AMORPHOUS SEMICONDUCTORS.....	36
2.5 PASSIVATION OF AMORPHOUS SILICON.....	37
CHAPTER THREE: CONDUCTION THEORY IN POLYSILICON.....	39

3.1 PRELIMINARIES.....	39
3.2 SMALL SIGNAL THEORY.....	39
CHAPTER FOUR: GENERALIZED CONDUCTION THEORY	
OF POLYCRYSTALLINE SILICON.....	55
4.1 PRELIMINARIES.....	55
4.2 GENERAL I-V CHARACTERISTICS.....	56
CHAPTER FIVE: RESULTS AND DISCUSSION.....	
5.1 COMPARISON WITH EXPERIMENT: SMALL SIGNAL LIMIT.....	68
5.2 GENERAL I-V CHARACTERISTICS FOR UNDOPED POLYSILICON.....	80
5.3 DISCUSSION: SMALL SIGNAL THEORY.....	88
5.4 EFFECT OF LASER RESTRUCTURING AND	
GRAIN BOUNDARY ALTERATION.....	90
5.5 COMPARISON WITH EXPERIMENT: GENERAL J-V CHARACTERISTICS.....	100
CHAPTER SIX: CONCLUSION.....	
6.1 PRELIMINARIES.....	115
6.2 VOLTAGE PARTITION.....	116
6.3 $\ln \rho$ VS. T^{-1}	119
6.4 ARTIFICIAL FACTOR, f	120
REFERENCES.....	124
APPENDIX I: ANALYSIS OF CONDUCTANCE DATA OF REF. [64].....	134

ABSTRACT

A comprehensive theory of conduction in polycrystalline silicon is presented. The present approach fundamentally differs from previous theories in its treatment of the grain boundary. This theory regards the grain boundary as an amorphous conducting medium and invokes drift-diffusion as the mechanism of conduction. This model explains the electrical properties of polysilicon in terms of the inherent electronic and structural parameters of the material and is in excellent agreement with the experimental data. The theory is valid for arbitrary grain size, temperature, doping concentration, and applied voltage. Therefore, this model is suitable for describing electrical characteristics of laser restructured and/or plasma passivated polysilicon and of devices fabricated therein. Also, the present approach critically examines, theoretically and experimentally, the grain boundary scattering potential, $q\chi$, introduced in previous theories. Specifically, the emission mode of conduction based on $q\chi$ is shown to suffer from the inconsistencies in its voltage partition scheme and theoretical I-V predictions. The present model consistently incorporates the effect of mobile carrier redistribution under bias and accounts for the high field switching in amorphous grain boundary. Microscopic mobilities used for describing the carrier transport provides a physical basis for introducing the grain voltage (V_g) across the unit cell of polysilicon system and V_g , in turn, distributes itself to preserve a constant current density therein. This new criterion yields a new voltage partitioning scheme, and a general expression for corresponding response function of current is derived in terms of pertinent system parameters.

CHAPTER ONE

INTRODUCTION

1.1 PRELIMINARIES

Devices fabricated with polycrystalline semiconductor thin films have existed for a long period of time [1]. In the LSI circuit fabrication processes, chemically vapor deposited polycrystalline silicon was used in the past decade in numerous ways [2], e.g. interconnections, gate electrodes, passivation and isolation layers in poly I^2L , high value load resistors in RAM's [3], and monolithic distributed RC filters [4]. Thin film transistors, field effect and Schottky barrier diodes, photoconductors, luminescent thin film devices also have promising potential commercial applications [1]. Thin film device technology, in response to the ever expanding demand for higher density and faster speed integrated circuits have progressed to a point where polysilicon devices are commanding increasing attention [5-9]. A major breakthrough in the semiconductor industry appears possible if vertical integration (3-D) could be implemented vis-a-vis the reduction in device dimensions. The current prevailing consensus is that the 3-D integration of semiconductor devices will possibly be realized via the use of laser and electron beam processed polysilicon and grain boundary passivation techniques [10-36]. Extensive research has already been carried out to fabricate resistors [10,28], p-n junctions and Schottky barrier diode [11-14], MOSFETS and bipolar structures in laser processed polysilicon [15-27]. However, the low carrier mobility, high series resistance, short carrier lifetimes,

high leakage currents and turn-on voltage, low breakdown voltages, lack of controllability and reproducibility in its electrical properties are the main bottlenecks for more pervasive use of polysilicon in the integrated circuit industries [7-9,27]. Factors which further inhibit the use of polysilicon are a large temperature dependency of resistivity at low doping concentration, incomplete impurity activation, and diffusion and segregation of impurities to the grain boundaries [37]. The recent development in laser processing technology has changed the situation and has considerably enhanced the possibility for the application of polysilicon in VLSI and VHSI circuits [33-36]. It has been demonstrated in recent years that the beam processing techniques can produce defect free, device quality single crystal islands in polycrystalline silicon films deposited on suitable insulating substrates [19,20,22,25]. This increase in grain size is generally accompanied by a reduction in resistivity and increase in mobility. These radiation processed polysilicon thin films have also been used as low cost, high performance substitutes for silicon on sapphire, for fabrication of solar cells and MOS transistors for large area display [7,38].

1.2 POLYCRYSTALLINE SEMICONDUCTORS

Because of the growing importance of polysilicon in semiconductor industries a comprehensive understanding of its physical and electrical properties has become rather imperative. This section highlights the various factors which describe the overall behavior, properties and performance of polysilicon [37].

1.2.1 DEPOSITION

Thermal decomposition of silicon containing gas (e.g. silane) on silicon substrates in atmospheric-pressure cold wall reactors (APCVD) has been the standard method for chemical-vapor deposition of polycrystalline silicon. However, in recent years, low-pressure chemical-vapor deposition technique (LPCVD) has drastically reduced the cost of deposition. Because of its high yield this method of deposition has been rapidly accepted in the integrated circuit industry. The deposition temperature is rather low (620°C) at a pressure of 0.2 to 1 torr compared to APCVD (650°C to 1200°C) [37].

1.2.2 CRYSTAL STRUCTURE

The crystal structure of polysilicon determines its optical properties, rate of oxidation, etching, diffusion of dopant atoms into films and other electrical properties. [37,39]. Polycrystalline materials are composed of small grains of single crystal joined together at the boundary [2,40-41]. The structure of the polysilicon and grain size are sensitive to the deposition temperature and the thermal processing steps. It has been observed that the grain size increases with the increasing deposition temperature and film thickness [39]. However, acceptable surface roughness, lithography resolution and smaller device geometry limit the maximum size of the grain [39]. If the deposition temperature is above 600°C , polycrystalline films are formed. Amorphous films are formed at lower temperature [37]. The crystallite grains are generally believed to be formed by a random and independent nucleation and growth process. The islands of crystallites grown are randomly oriented and are separated from each other by the boundary region [2]. The films deposited at 620°C has insignificant change after annealing at 800°C or 1000°C . But grain

size increases significantly at 1100°C and 1200°C [37]. The grains have a columnar structure which increases the diffusivity of dopants compared to single crystals [2,39]. The diffusion of dopants is difficult to control because the process itself depends on grain structure and deposition temperature. Ion implantation and subsequent annealing is used to achieve better control.

1.2.3 ELECTRICAL PROPERTIES

Extensive experimental investigation has been carried out [39-47] to characterize the differences in electrical properties between polysilicon and the single crystal silicon. Specifically Hall and resistivity measurement have been performed on polycrystalline silicon over a wide range of temperature and dopant concentration ($10^{15} - 10^{20}\text{ cm}^{-3}$). These results are summarized in Fig. 1.1.

1.2.3.1 RESISTIVITY

At room temperature, the resistivity of polysilicon is higher than that of single crystal by more than a factor of 10^6 (Fig. 1.1) for small doping concentration (10^{15} cm^{-3} or less) [39,41]. The resistivity, however, decreases slowly as the doping density is increased until a critical concentration, N^* , is reached when it drops very sharply by several orders in magnitude for a slight increase in doping concentration. At higher doping levels, the resistivity decreases almost linearly and approaches that of single crystal to within a factor of 2 to 5.

The resistivity is significantly dependent on temperature for low and medium doping concentration. The plot of logarithm of resistivity

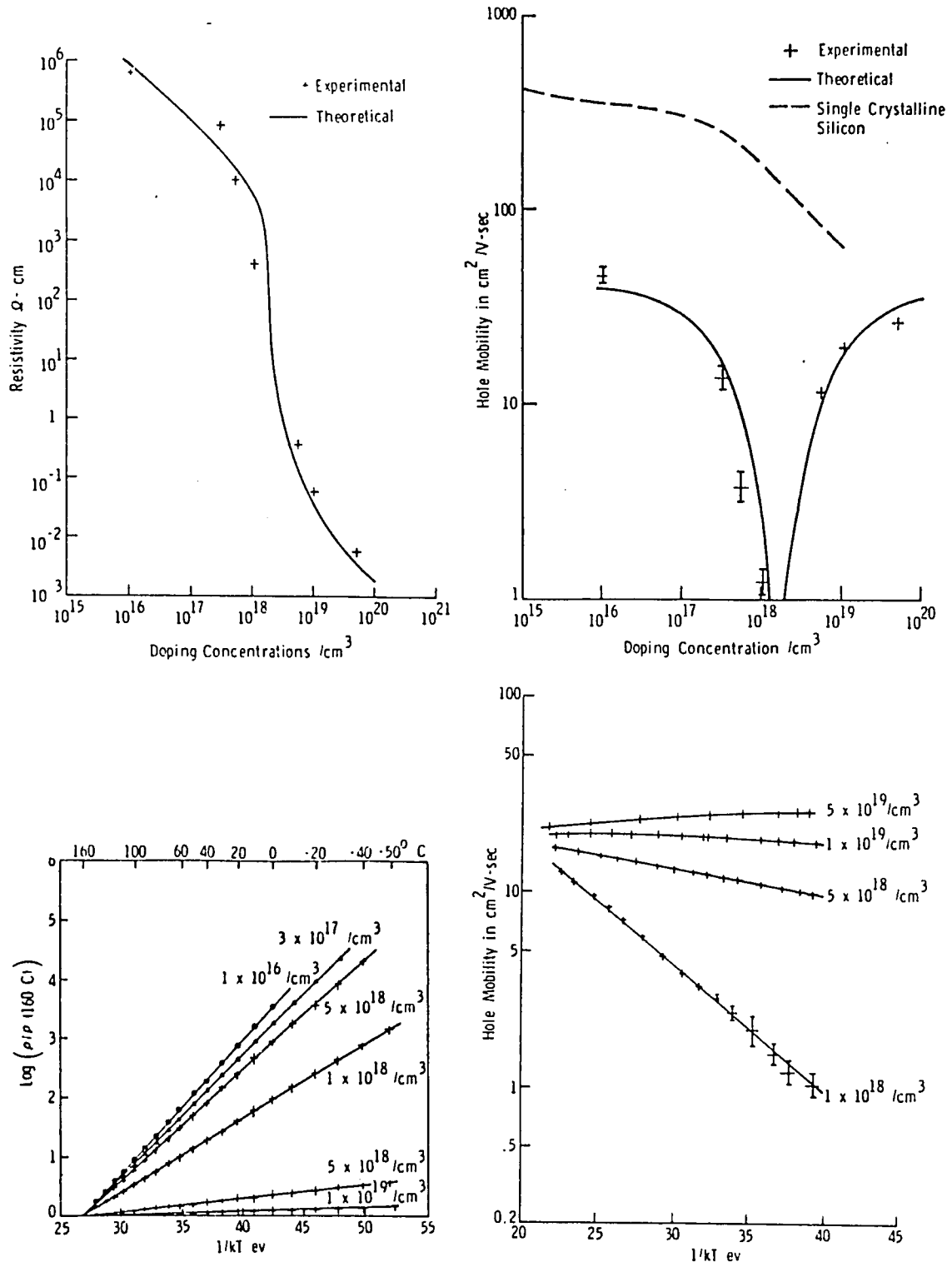


Fig. 1.1 Polysilicon data [41].

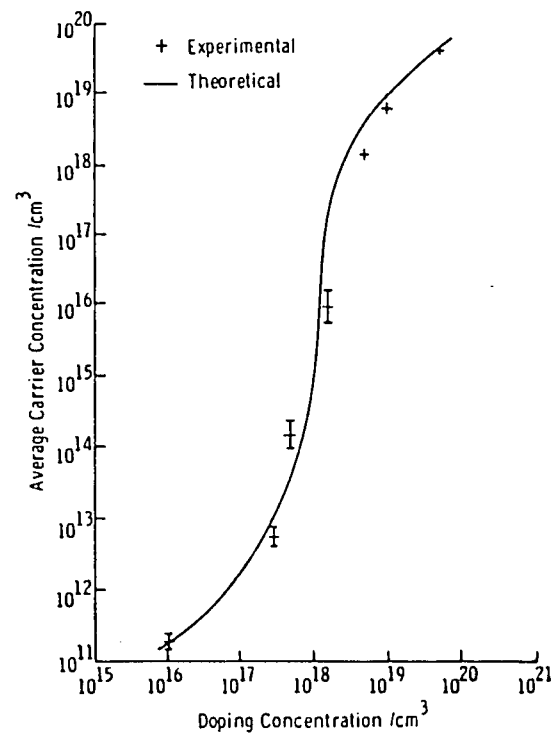


Fig. 1.2 Carrier concentration vs. doping concentration [41].

versus inverse temperature ($1/kT$) is linear if temperature is not very low ($T > -40^{\circ}\text{C}$) [39,41,43]. This Arrhenius behavior of resistivity can thus be characterized in terms of an activation energy, E_a , defined as the slope of this curve. The activation energy is about 0.56 eV at low impurity concentration. As the doping level is increased the activation energy slowly decreases at first till N^* is reached when it sharply decreases and vanishes at higher concentration. At very low temperature [43] the slope of $\ln\rho$ versus $1/kT$ curve, however, decreases gradually and becomes constant below a certain temperature.

1.2.3.2 MOBILITY

The Hall mobility of polysilicon is, in general, considerably lower than the corresponding single crystalline mobility at low doping levels [39-41]. As doping concentration is increased the mobility remains fairly insensitive. Near the critical concentration, N^* , however, the mobility sharply decreases to a value which is several orders in magnitude smaller than the corresponding single crystalline value at the same doping concentration. With further increase in doping level, mobility rapidly rises and approaches single crystal mobility within a factor of 2 to 5. The logarithm of Hall mobility, μ , has been plotted as a function of $1/kT$ (Fig. 1.1). At medium concentration $\ln(\mu)$ decreases linearly with increasing $1/kT$. The slope of this curve decreases with increasing impurity level.

1.2.3.3 CARRIER CONCENTRATION

The carrier concentration in polysilicon is, in general, lower than the corresponding value in single crystalline silicon (Fig. 1.2) [39-41].

For low doping concentration it remains very close to the intrinsic value. As dopant concentration is raised, it increases slowly until N^* is reached. Above N^* level the carrier concentration rapidly increases and essentially merges with the corresponding single crystalline value.

1.3 REVIEW OF PREVIOUS CONDUCTION THEORIES

1.3.1 SEGREGATION THEORY

Several models have been proposed to explain the electrical properties of polycrystalline silicon. In these models the polycrystalline material is regarded as small crystallites which are joined together at the grain boundary. Inside the crystallite the atoms are periodically arranged as in single crystal with its orientation random with respect to that of the other crystallite. Thus at a grain boundary the angle between the adjacent orientation can be very large. This gives rise to a high concentration of defects and incomplete bonding at the grain boundary. These defects and the dangling bonds are capable of trapping and immobilizing dopant atoms and/or free charge carriers. There are two schools of thought regarding the effect of grain boundary on the electrical properties of polycrystalline semiconductors. One school believes that the effective resistivity of polysilicon is large because the dopant atoms are mainly segregated and trapped passively at the grain boundary [58,59]. Thus there are less carriers in the crystallite region. However, this theory fails to explain the observed mobility minimum (dip) and the temperature dependences of resistivity. Besides it has been reported [41] that in the case of boron no appreciable segregation has been observed for dopant atoms. Failure to explain these observations has led

to a second model for conduction.

1.3.2 CHARGE TRAPPING THEORY

T.I. Kamins reported Hall measurement on polycrystalline silicon films deposited on SiO_2 surface by thermal decomposition of silane [40]. The average grain size was about 5000\AA and the doping density of both acceptor and donor type was varied from 10^{16} cm^{-3} to about 10^{19} or 10^{20} cm^{-3} . It was observed that the mobility in both n and p type increases from a low value and reaches a maximum of about $40\text{ cm}^2/\text{V-sec}$ at a free carrier concentration of 10^{18} cm^{-3} . Kamins explained this observation by considering that i) a polycrystalline material is composed of small crystallites joined together at a grain boundary, ii) because of the disordered nature of grain boundary there is a large number of defects arising from incomplete atomic bonding and iii) the dangling bonds form trapping states and are capable of trapping mobile carriers from the grain, thereby giving rise to a space charge regions of very high resistivity near the grain boundary. This process in turn reduces the mobility and could increase the resistivity by several orders of magnitudes. Kamins also observed that as the number of carriers trapped in grain boundary is increased, the trap levels could approach saturation. Beyond this point it no longer traps any mobile carriers from the grain. This will eventually lead to a very small width of barrier, compared to the grain size, which will no longer have limitation on the conductivity and the material behaves as though it is single crystal. This effect is more pronounced in the case of samples having larger grain size and thickness for the same doping density.

1.3.3 THERMIONIC EMISSION

In 1975, John Y.W.Seto [41] reported the first quantitative theory describing conduction in polycrystalline silicon films. Based on the measurement of electrical properties of polysilicon films (implanted with boron) and Kamin's trapping theory, Seto proposed a one dimensional model for current density where the polysilicon is considered to be composed of identical crystallites of grain size L cm. The conduction data were then specified in terms of three physical parameters, viz. the trap level, E_t , the trap density, Q_t , and L . These trap levels are capable of capturing mobile charge carriers donated by the dopant atoms and become charged. Depending on whether the total number of carriers available in the grain is less ($LN < Q_t$) or greater ($LN > Q_t$) than the available number of traps, the grain is either completely depleted or partially depleted of carriers respectively. In this abrupt depletion approximation the Poisson's equation reads (Fig.1.3):

$$\frac{d^2V}{dx^2} = \frac{qN}{\epsilon} \quad (1.1)$$

where ϵ is the dielectric constant of polysilicon. Using the boundary condition that $V(x) = V_{vo}$ and $dv/dx = 0$ at the edge of the depletion depth ($x = l$) gives

$$V(x) = (qN/2\epsilon)(x - l)^2 + V_{vo} \quad l < |x| < \frac{L}{2} \quad (1.2)$$

where V_{vo} is the potential of the valence band edge. When the grain is completely depleted of carriers ($l = 0$) the potential energy maximum is given by

$$V_B = qL^2N/8\epsilon \quad (1.3)$$

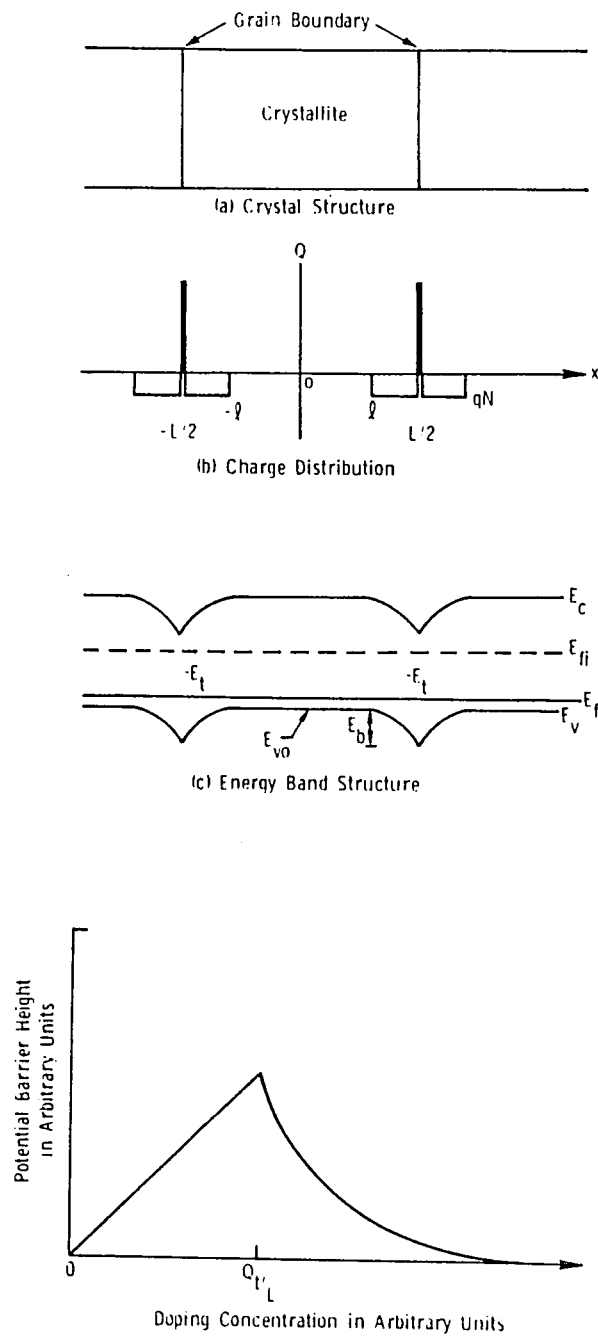


Fig. 1.3 Seto's model [41].

For partially depleted case $l > 0$ and V_B is given by

$$V_B = qQ_t^2 / 8\epsilon N \quad (1.4)$$

Using Boltzmann statistics, the mobile carrier concentration, $p(x)$, is given by

$$p(x) = N_V \exp(-[qV(x) - E_F]/kT) \quad (1.5)$$

The Fermi level is determined from the charge conservation by equating the number of carriers captured to the total number of trapping states occupied. Finally Seto invoked thermionic emission theory of current across the grain boundary. The current density is then given by

$$J_{th} = qp_a \left(\frac{kT}{2m^*\pi}\right)^{1/2} \exp\left(-\frac{qV_B}{kT}\right) \left[\exp\left(\frac{qV_a}{kT}\right) - 1\right] \quad (1.6)$$

where p_a is the average carrier concentrations obtained by integrating $p(x)$ from $-L/2$ to $L/2$ and dividing by L . If $qV_a \ll kT$, the conductivity is given by

$$\sigma = L q^2 p_a \left(\frac{1}{2\pi m^* kT}\right)^{1/2} \exp\left(-\frac{qV_B}{kT}\right) \quad (1.7)$$

Using the relationship $\sigma = qp\mu$, the mobility is given by

$$\mu_{eff} = Lq \left(\frac{1}{2\pi m^* kT}\right)^{1/2} \exp\left(-\frac{qV_B}{kT}\right) \quad (1.8)$$

The dip in mobility is described in the following way. When $LN < Q_t$ the potential barrier increases linearly (eqn.1.3) with N until a critical value, N^* is reached such that $LN^* = Q_t$ (Fig. 1.3). Beyond this concentration the potential barrier decreases as $1/N$ and rapidly vanishes.

Although Seto's model was successful in explaining the general trends of the experimental data it required two artificial factors to fit the data quantitatively. These two fitting parameters entered the in expression

of conductivity in the form

$$\sigma = fLq^2 \left(\frac{1}{2\pi m^* kT} \right)^{1/2} \exp\left(-\frac{qV_B}{nkT}\right) \quad (1.9)$$

with $f=0.12$ and $n=6.49$.

N.C.C. Lu et al [42] included the resistivity of the undepleted crystalline grain, ρ_C , within the framework of Seto's model. This modification was necessary because if ρ_C is neglected, the resistivity of large grain polysilicon becomes smaller than that of single crystal for doping level more than $3 \times 10^{18} \text{ cm}^{-3}$. In this modification the total resistivity of polysilicon was expressed as a weighted sum of resistivities of depleted and undepleted regions in the grain. The resistivity expression thus read

$$\rho = \rho_C \left(1 - \frac{2l}{L}\right) + \rho_B \quad (1.10)$$

where ρ_B is the barrier resistivity in the depletion region given by eqn.(1.9). However, this theory could not attribute any physical significance to the artificial factors f and n . The absence of these parameters in the eqn.(1.6) continued to predict a current density larger than the actual value by more than an order in magnitude. The values of artificial factors, f and n , required to fit the data was taken as 0.06 and 1.22 respectively.

In an effort to eliminate one of the artificial factors, namely n , from the ρ expression N.C.C. Lu extended their previous model [42]. This theory is basically similar, in concept, to the previous theory. However, they proposed that if instead of the average value of the concentration p_a one uses the carrier concentration at the center of the grain, $p(0)$, the artificial factor n is no longer required in the expression for

resistivity (eqn.(1.9)). The artificial factor f retained in this model was then attributed to a smaller value of effective Richardson constant because of smaller effective mass of the carriers compared to single crystal value. It was suggested that the artificial factor may also represent a transmission probability arising when carriers are passing through the disordered grain boundary by either scattering or recombination. Lu et al, however, improved Seto's charge neutrality equation which is required to calculate the Fermi level, E_F , for $N < N^*$ and depletion length for $N > N^*$:

$$2N^+1 = \frac{Q_t}{1 + 2\exp[(E_F - e_t + qV_B)/kT]} \quad (1.11)$$

In this equation N^+ was used instead of N to account for the incomplete ionization of dopants. The term qV_B recognizes the fact that the trap levels are lowered by qV_B when the grain boundary potential is lowered by the same amount. The theoretical activation energy, defined as the slope of $\ln(\rho)$ versus $1/kT$ curve ($E_a = \partial(\ln(\rho))/\partial(1/kT)$), predicted by this theory, however, is constant (about 0.425 eV) for $N < N^*$, whereas the measured value actually starts from 0.56 eV for low concentration and gradually decreases with increasing doping concentration. The I-V measurements taken in the polysilicon were observed to be nonlinear. Lu et al made an attempt to explain this nonlinear relationship within the framework of the thermionic model. Specifically, Lu et al proposed that the theoretical I-V characteristics should be described via the use of hyperbolic sine functional format.

1.3.4 THERMIONIC AND/OR FIELD EMISSION (Fig. 1.4)

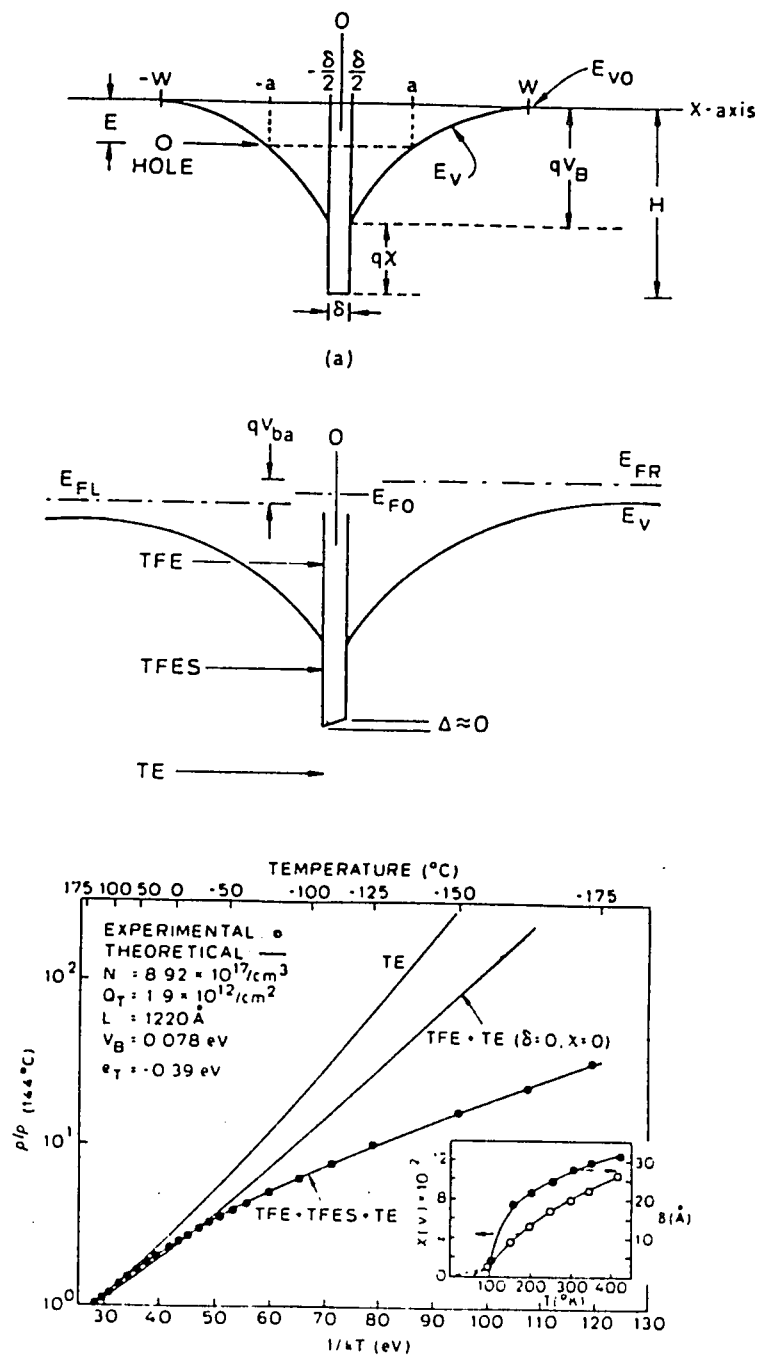


Fig. 1.4 Energy diagram [43] and graph of resistivity vs. $1/kT$.

The previous models, based on thermionic emission mode of conduction, were able to fit the experimental data at room temperature with the help of the above mentioned artificial factors. As discussed earlier, these factors were introduced, primarily, to reduce the current density at room temperature. However, there was essentially no physical reasoning upon which the use of these factors could be justified. Besides, at low temperature ($T < -40^{\circ}\text{C}$), the data for current density revealed that these factors were diminishing the calculated value of the current, more than it should, in these range of temperatures. In other words, the theory predicts a higher resistance at low temperature whereas the experimental curves had a gradual downward bending trend for $T < -40^{\circ}\text{C}$. The only remedy for this unsatisfactory situation was to decrease the artificial factors at lower temperature which was, of course, even harder to justify. In order to remove these inherent inadequacies of their previous models and also to explain the use of f and n , Lu et al [43] proposed a new conduction model for polysilicon. In this model, Lu et al, brought in a concept of grain boundary scattering effect on charge carriers that replaced the factors from f and n from the current expressions. In order to simulate the above mentioned scattering of carriers from grain boundary, the authors employed an additional scattering potential on the top of the usual barriers used in the trapping models. This barrier was rectangular in shape and has a height χ and a width δ . and was attributed to the mobility gap of the grain boundary. As can be expected, the scattering potential lowered the calculated current density at room temperature because the number of charge carriers which are now able to cross the grain boundary is decreased. Charge carriers, in this model, are required to overcome the combined potential barrier by thermionic

and/or field emission. However, the fit to the resistivity versus $1/kT$ curves was achieved by reducing the χ and the δ as temperature is decreased. The authors suggested that as the temperature drops, χ and δ , whose product represents the scattering strength of the grain boundary, are expected to decrease because there is less phonon scattering at these temperatures. It should be noted, however, that no effort was made to justify the aforementioned functional behavior of χ and δ with temperature. It should also be mentioned that these temperature dependences of χ and δ , calculated to fit the resistivity data for doping concentration of $8.92 \times 10^{17} \text{ cm}^{-3}$ was not capable of satisfactorily fitting the $\ln(\rho)$ vs $1/kT$ curve, for polysilicon doped with different concentration.

1.3.5 COMBINED TRAPPING AND SEGREGATION MODEL

M.M. Mandurah et al combined the aforementioned two approaches, viz. the trapping and segregation models [44] to explain resistivity variation with dopant concentration in polysilicon. Recall that the trapping model concerns with resistivity variation due to the change in barrier height resulting from trapping of free carriers at the grain boundary, while the second model considers the dopant segregation to the grain boundary. In this work the authors noted a difference in resistivity value for same dopant concentration when dopant types are different. In addition, it was observed that there is a reversible change in resistivity, for arsenic and phosphorus doping, with higher and lower temperature annealing cycle. Mandurah et al suggested that this change in resistivity can only be explained if one takes into account the dopant segregation effect in the grain boundary. Using Gibbs absorption equation and Ising-like model it was shown that segregation effect is dominant in phosphorus and arsenic.

In the case of boron, the dopant atoms are more likely to be depleted from the boundary or surface rather than segregating. The average dopant concentration in the grain (N_G) was calculated using the equation :

$$\ln\left(\frac{N-N_G}{N_G}\right) = \ln \frac{AQ_s}{N_{si}} + \frac{Q_o}{kT_A} \quad (1.12)$$

where N is the total number dopant density (cm^{-3}), N_{si} , the total number of bulk and grain boundary sites (cm^{-3}), Q_s , the density of grain boundary sites in the system. A is the pre-exponential factor, Q_o , the dopant heat of segregation and T_A is the final annealing temperature.

1.3.6 TRAP DISTRIBUTION AND DENSITIES

G. Baccarani, B. Ricco and G. Spadini proposed a modified version of charge trapping model [45] to clarify the electrical properties of polysilicon in the intermediate concentrations (near N^*). This model considered δ -shaped trapping states as in previous theories and continuous energy distribution of interface states within the band gap in grain boundaries. Using the thermionic emission theory they found that the former is in better agreement with the experimental results. Baccarani et al also pointed out that although trapping and segregation theory have been regarded as alternative explanations for high resistivity values, Hall measurement provides evidence that in phosphorus doped sample the active dopant concentration is considerably smaller than total doping concentration. This led them to justify the use of both theories in the explanation of observed data. The trap density was determined to be $3.8 \times 10^{12} \text{ cm}^{-2}$ in accordance with carrier life time measurement performed on CVD films.

C.H. Seager and T.G. Castner [46] characterized the electrical transport properties of neutron-transmutation-doped polycrystalline silicon. Their polysilicon had quasiparallel rod like grain having typical dimensions of $25 \times 25 \times 100$ – $200 \mu\text{m}$. With four-probe techniques they made ~~zero-bias~~ measurement of resistance as a function of temperature on both bulk and individual grain boundaries in this material. It was observed that below a doping level of $2 \times 10^{15} \text{ cm}^{-3}$ of phosphorus, the logarithm of resistivity is linear with temperature with an activation energy of 0.55 eV. With increasing donor concentration the activation energy started to decrease with decreasing temperature. Traveling potential probe measurements were carried out on heavily doped polycrystalline silicon and it was found that the impedance of individual boundaries could vary to a large extent. In other words, there is a large range of potential barriers present across the grain boundaries. The authors summarized these observations by concluding that at lower doping densities ($N < 2 \times 10^{15} \text{ cm}^{-3}$), the largest barriers control the activation energy, although not all the barriers are of this size. Seager et al examined the mechanism of current flow when grain boundary potentials are present in the material. The authors used thermionic emission theory and derived an expression for activation energy of ρ :

$$E_a \equiv k \frac{\partial \ln(\rho)}{\partial (1/T)} = q[V_B - T \frac{\partial V_B}{\partial T}] \quad (1.13)$$

Using three types of trap densities , namely, 1) energy independent 2) monoenergetic 3) exponentially dependent trap distribution , the activation energy was calculated for polysilicon. It was found that the exponential density of states better explained the experimental data than the other two types of states. The comparisons also led to the conclusion

that the largest grain boundary state density was $6 \times 10^{11} \text{ cm}^{-2}$ located within ~ 0.2 eV from the center of the forbidden gap. The tendency for the slope of $\ln(\rho)$ versus $1/kT$ to drop below 220° K is attributed to the inhomogeneous nature of the material which may give rise to a decreased activation energy at lower temperature. Authors suggested that some form of impurity conduction along the grain boundary may also be responsible for this behavior.

1.3.7 APCVD VERSUS LPCVD FILMS

T.I. Kamins reported [47] that there is a marked difference between the resistivities of polysilicon, doped with phosphorus, at low pressure and high temperature, atmospheric pressure. For moderately doped polysilicon, the sheet resistance of low pressure films are higher than the atmospheric pressure films. However, the LPCVD film resistivities approaches that of high pressure ones as the dopant concentration is increased to high values. This behavior has been explained by arguing that the LPCVD films are deposited at a lower temperature and this may lead to a higher trap density.

1.3.8 EFFECTS OF ILLUMINATION

H.P. Maruska et al measured Hall mobility [48] in the dark and under illuminated conditions in order to evaluate the transport of carriers in polysilicon solar cells. The grain size of their sample was 1 μm . The resistivity of the samples were also measured in the above two conditions. In the dark, the resistivities of the samples slowly decreases in the range of 400° K - 350° K , then rapidly increases to 200° K , and finally saturates below 200° K . When the samples were exposed to light, the

resistivity decreased from its dark value at low intensities, and at about solar intensities the curve inverts in the range below 350°K and becomes thermally inactive. The authors suggested that with illumination of light, the barrier potential is removed. This argument appears reasonable because the hole generated by photon induced band to band excitation of electron-hole pairs in the n type samples are attracted to the grain boundary, where they could eliminate the trapped electrons by recombination process. The measured carrier concentration was found to be independent of supply voltage, temperature and level of illumination. The authors further argued that this is the free carrier concentration of the grain which shows bulk properties. They defined an effective mobility of polysilicon which is measured by the Hall effect. Under illuminated condition, this effective mobility approaches bulk mobility at high temperature. However, at low temperature the intrinsic properties of the depleted regions (e.g. mobile carriers) influence the conduction mechanism.

1.3.9 DYNAMICS OF POTENTIAL BARRIER FORMATION

K.R. Kumar and M. Satyam presented a modified version of Seto's model [49] by including the dynamics involved in capturing and releasing mechanisms of free carriers by the grain boundary in order to estimate the barrier potential height. The authors, however, included the bulk resistance into their calculation. By considering the thermionic emission theory as the mechanism of carrier transport across the grain boundary barrier, the authors defined an effective mobility using an f-factor of 0.25.

1.4 GRAIN BOUNDARY ALTERATION

1.4.1 HYDROGEN PASSIVATION

As has been discussed thus far one of the major roles of the grain boundary is to capture a mobile carriers from the grain and thereby giving rise to a potential barrier. This potential barrier then deters the carrier transport across the grain boundary. Recently considerable work has been carried out to reduce the effect of grain boundary by decreasing the number of traps contained therein [2,29-32].

A method for modifying the electronic properties of the grain boundary in polysilicon via the introduction of monoatomic hydrogen has been reported by Seager et al [29]. It has been suggested that monoatomic hydrogen and few other species may be introduced within the grain boundary to tie up the dangling bonds which arise from atoms which are not tetrahedrally coordinated. Thus, the introduction of hydrogen plasma may remove grain boundary trap states. The resistivity of these hydrogenated polysilicon has been found to be lower than the original polysilicon. Also this passivation of grain boundary changes the temperature characteristics of the grain boundary. The conductance of the virgin polysilicon decreases as temperature is decreased. In a $\ln(\sigma)$ vs $1/kT$ plots, $\ln(\sigma)$ decreases at a constant rate near room temperature and above. However, at lower temperature the curve becomes non-linear and its slope decreases. The hydrogen passivated polysilicon shows a weaker temperature variation compared to the virgin samples. At a high doping concentration it may lose its activation nature and take the temperature characteristics of single crystals where mobility is determined by simple scattering for majority carriers. The authors also found that (i) plasmas of O_2 ,

SF_6 , N_2 increase the trap density of states and as a result resistivity of the polysilicon increases, (ii) molecular hydrogen has no effect on the grain boundary state density. Seager et al believe that these passivation techniques can significantly enhance the thin film solar cell performance where the grain boundary recombination of photogenerated current has the most detrimental effect.

Campbell [30] showed that an enhancement of the polysilicon conductivity by a factor as large as 10^3 can occur when the grain boundaries are passivated by hydrogen plasma. The activation energy in the sample was also reduced as a result of this passivation technique. The author, however, discovered that this passivation technique is reversible. A hydrogenated sample was heat treated at 500°C for 30 minutes in an oil-free vacuum of 1.3×10^{-4} pa. It was found that this film was restored to its original state. It was assumed that this is due to the vacuum desorption of hydrogen from the grain boundary. Campbell et al [31] further investigated the effects of exposing the polycrystalline film to atomic hydrogen from hydrogen plasma. The conduction properties of hydrogenated polycrystalline silicon were improved in comparison to the unhydrogenated one. In Seto's theory the mobility can be expressed as the following:

$$\mu = \mu_0 \exp[-qV_B/KT] \quad (1.14)$$

where μ_0 is a parameter having units of mobility. Campbell et al [31] explained that because of plasma hydrogenation, the number of traps, Q_t , is decreased. As a result, the barrier height for partially depleted grains and filled traps will be lower at a given concentration. This can be understood in relation to eqn.(1.1-1.4). The critical concentration

at which the V_B reached its maximum value (or the point the mobility attains its minimum value) is shifted to the lower concentration region. This follows because $N^* = Q_t/L$. However, for the fully depleted grains, the value of qV_B and hence the value of mobility is expected to remain unchanged. In their experiment, Campbell et al found that Q_t has been reduced from $3.8 \times 10^{12} \text{ cm}^{-2}$ by a factor of about 1/3. The authors also compared the electron spin resonance signal (ESR) on both virgin and hydrogen passivated polysilicon and found that the spin density of the dangling bonds had systematically decreased. The authors concluded that different types of traps may exist within the grain boundary. Therefore, to reduce all the traps different methods of passivation may be required. For example, as Redfield shows [60], an oxygen trap segregated in the grain boundary may cause the grain boundary to become more electrically active. Since Si-O bonds are relatively stable, this may not be removed by a hydrogen passivation only, and this may contribute to the two-thirds trap density that remains in the grain boundary.

1.4.2 LITHIUM PASSIVATION

R.T. Young et al investigated the effects of passivation of the grain boundary by diffusion of lithium into the n-type polysilicon [32]. The carrier mobility was found to increase for the lithium diffused polysilicon samples. The authors generated photoresponse map on p-n junction solar cells using scanning light spot (SLS) technique. The grain boundaries have a detrimental effect on the photogenerated currents through minority-carrier recombination at the grain boundaries [61]. It was shown that these adverse effects were significantly reduced after the introduction of Li into the solar cell. It was postulated that the Li^+

ions can diffuse into the negatively charged recombination sites in an n-type polysilicon and neutralize them. This process, therefore, reduces the recombination cross sections of trap centers. The authors claimed that the Li passivation technique may be better than the hydrogen passivation because it is difficult to introduce atomic hydrogen uniformly into the grain boundary.

1.5 MOTIVATION

1.5.1 MAJOR DRAWBACKS OF THE PREVIOUS THEORIES

So far we have discussed the previous models which have been proposed to explain the conduction characteristics of polycrystalline silicon. These models have brought out some important physical mechanisms responsible for electrical conduction. However, these models have several drawbacks which make these theories very unattractive. Seto's model [41], for example, neglects the grain resistivity. But it was found that for very high doping concentration and for large grain size, the grain resistivity becomes important. As a result, the model is good only up to a grain size of 600 \AA . Lu et al [42], included the grain resistivity for the case of high dopant concentrations. In their theory the crystalline grain region has been partitioned into two regions, viz the undepleted neutral region and the depleted space charge region. In the undepleted region, carriers are taken to be transported via drift mode of conduction. The drift current is described by the mobility of the charge carriers. In this picture the carriers are constantly scattered by lattice imperfection and vibration, dopant atoms, and so forth, which reduces the mobility. When the carriers enter the depleted region of the grain,

however, it was tacitly assumed to behave as free particles and cross the grain boundary via thermionic emission. Obviously this description is unsatisfactory and should run into a major difficulty when the depletion depth is larger than the mean free path. It should also be noted that the thermionic emission theory can be satisfactorily applied for high mobility materials [62]. Note that for the case of high doping concentration where the impurity scattering is predominant the mobility is reduced by about one order of magnitude from its intrinsic value [62,41]. In Seto's model, the grain boundary width has been neglected. We believe, this approximation is a gross simplification and has led to the use of an artificial factor to reduce the current density. Lu et al on the other hand considered a finite thickness of the boundary. However, to account for the artificial factor, f , a new scattering potential χ having a finite width δ has been postulated. As discussed in sec. 1.3 the product $\chi \delta$ was suggested to represent the scattering strength of the grain boundary. In this regard the width, δ , of this scattering potential did not correspond to the width of the grain boundary. This scattering potential, $q\chi$, which has been ascribed to mobility shoulder was successful in reducing the current density and hence the artificial factor, f , could be dropped from the resistivity expression. Mandhurach et al also introduced this additional potential and attributed it to the optical band gap of the disordered grain boundary [54]. Lu et al made a further attempt to quantitatively explain the bending tendency of $\ln(\rho)$ versus $1/kT$ curve over a wide range of temperature observed in polysilicon. In their modeling, $q\chi$ and δ have been continuously adjusted as a function of temperature. The physical justification for this procedure remains unresolved. Seager et al [46], attributed the bending trend to the random network

nature of the polycrystalline semiconductors. Young, et al [63] and Werner et al [64], however, singled out a grain boundary in a bicrystal and observed a similar bending trend in the $\ln(\rho)$ versus $1/kT$ curve. It is, therefore, apparent that this bending tendency is intrinsically associated with the conduction processes within the grain boundary. Wu et al [57], considered Rutherford scattering of carriers from fixed charge centers believed to be present in the boundary. However, the resulting attenuation factor of current was insufficient to explain the data and also it is unknown whether the temperature characteristics of the resulting attenuation factor is consistent with the downward bending trend.

An ultimate goal of modeling conduction is to have a quantitative understanding of general I-V characteristics. The previous theories have considered thermionic and/or field emission as a mechanism for transporting carriers across the boundary. The expressions for I-V relationship in this model can be summarized in the form [55]:

$$I = I_s \sinh(qV/2kTN_g) \quad (1.15)$$

Here, V is the external voltage applied across the poly-resistor and N_g is the average number of grains contained therein. I_s is Schottky emission current is given by $I_s = 2kTN_g/qR_s$ with R_s denoting the small signal ($V \ll N_g KT$) resistance value. A major difficulty in using the above I-V expression lies in that the actual fit to the data requires the introduction of an unphysical fitting parameter N_{eff} in place of N_g [56]. This parameter for effective number of grains in the resistor, N_{eff} , has to be varied continuously and nonmonotonically over a range of 300 to 800 in a doping range of 10^{15} - 10^{18} cm^{-3} , whereas the actual value of N_g was about 150. Additionally, N_{eff} has also to be adjusted to fit the I-V data at

different temperatures. Furthermore, eqn.(1.15) appears to suffer from a basic built-in inconsistency. The resistance of a polysilicon resistor at a very high doping concentration ($N > 10^{18} \text{ cm}^{-3}$) is larger than the corresponding single crystal resistor by a factor, 2-5. The resistance at any voltage, V , from the above expression is given by

$$R(V) = \frac{R_s}{\sinh(z)/z} \quad (1.16)$$

where $z = qV/2kTN_g$. As the value of z is increased above 5, the resistance, $R(V)$, drops by more than an order in magnitude. Consequently, the current drawn in a polysilicon resistor becomes higher than that of a single crystal resistor at a same applied voltage. Obviously, this is an unphysical consequence.

We have seen that, in the previous models, the grain boundary played the role of trapping the carriers and creating a potential barrier. From the conduction standpoint, the boundary was regarded strictly as an insulator, and the applied voltage was thus partitioned to the boundary via electrostatic consideration [54]. The resulting voltage partitioning consideration leads to a negligible voltage drop across the grain boundary for the case of low doping concentration. Conductance measurements performed on a grain boundary [64] of a lightly doped ($N \approx 10^{15} \text{ cm}^{-3}$) bicrystal shows, however, that the voltage dropped across the boundary is about 2 - 3 times larger than that across the grain at room temperature [64]. This clearly indicates that the grain boundary has a very high resistivity. In addition, its temperature characteristics have been observed to resemble closely the polycrystalline data.

1.6 ORGANIZATION

The thesis has been arranged in six chapters. In the first chapter we have discussed a few pertinent properties of polycrystalline silicon, previous theories of electrical conduction and their drawbacks, and the necessity of developing a new conduction theory. In the second chapter, we summarize the electronic and structural properties of amorphous polysilicon. Different conduction mechanisms in amorphous semiconductors are discussed and Passivation and electrical switching theory of amorphous semiconductor are also briefly reviewed. In this chapter we present a physical basis for modeling charge transport in grain boundary. Based on the theory of conduction in amorphous semiconductors, we present a new theory of conduction in polysilicon in chapter three. A brief outline of this theory has been reported elsewhere [65-67]. Here, we analyze the current response in the limit of small ($\ll kT/q$) applied voltage. In chapter four we generalize the small signal theory to the case of arbitrary applied voltage. Chapter five summarizes the results obtained from our model and compare with the experimental data obtained from various sources. In chapter six we give the conclusion and some limitations of this theory and suggest possible remedies.

CHAPTER TWO

THEORY OF AMORPHOUS SEMICONDUCTORS

2.1 PRELIMINARIES

In the past 15 years considerable progress has been made in understanding the properties of amorphous semiconductors. Amorphous semiconductors are essentially noncrystalline material which lack long range periodic ordering of their constituent atoms but they are not completely disordered in the atomic scale [68,69]. The diffraction pattern of the amorphous semiconductors is characterized by diffuse rings rather than sharply defined Bragg rings or spots as is observed in single crystalline semiconductors. As opposed to amorphous semiconductors, polycrystalline semiconductors are composed of grains. These grains contain a periodic array of atoms which are surrounded by a boundary layer of atoms. These boundary atoms serves the purpose of interconnecting different grains. As the size of these grains decreases, the boundary region of the grains has a large number of atoms. In the limit of very small grain sizes, the distinction between the crystallite grain and the boundary disappears completely. At this point the concept of a periodic microcrystallite regions loses its meaning. Amorphous semiconductors are normally subdivided into two basic categories: (i) the tetrahedrally coordinated materials, and (ii) chalcogenide glasses. Silicon and germanium fall within the first category [68].

Amorphous semiconductors have complex structural configuration. Many idealized models have been proposed to correlate the structural disorder

to the electrical properties of the amorphous semiconductors. In this chapter the theoretical concepts of electronic states of an amorphous semiconductor are briefly outlined. We describe the electronic transport mechanism and summarize the formulae appropriate to describe the conduction process. A brief review of electrical switching phenomenon and passivation of amorphous semiconductors has also been included.

2.2 TRANSPORT THEORY OF AMORPHOUS SEMICONDUCTORS

Considerable progress has been made in understanding the properties of amorphous semiconductors in recent years. Specifically extensive effort [68] has been made to correlate the structural disorder to the electrical properties of amorphous semiconductors. This section contains the theory of the transport mechanism for the carriers contained therein. In contrast to the crystalline semiconductor, there is no long-range structural order in amorphous solid. Short range orders such as (i) the interatomic distances and (ii) valence angles are, however, believed to be preserved [68]. This is understood in the light of tight binding approximation theory where atomic wave functions of individual atoms are primarily perturbed by those of the nearest neighbors. Mott[69] suggested that the spatial fluctuations in potentials arising from long-range configurational disorder may result in the formation of localized states in the band tail in contrast to the sharply defined edges of density of states in valence and conduction band. Mott also suggested a sharp boundary to demarcate two different types of conduction channels, namely the extended states and the localized tail states. As the name extended states specifically suggests that the electron wave function in this energy states are extended over the entire crystal length whereas in the

localized states an electron does not diffuse at zero degree Kelvin. At higher temperature the electrons in the localized states can move by exchanging energy with a phonon. The above mentioned sharp energy level is known as the mobility shoulder and in Mott-Davis model a pseudo-energy gap is defined in terms of the mobility shoulder instead of a sharply defined band edges. Experimental evidence for localized gap states has been observed from luminescence, photoconductivity and drift mobility measurements [68]. The above model also proposes a band of compensated levels near the mid-gap of the pseudo-energy gap which also originates from defects in the random network, e.g. vacancies and dangling bonds etc. The center band may again be split into two bands, namely the acceptor and donor bands which will pin the Fermi level at the mid gap. Thus the Mott-Davis model for band structure leads to three distinct channel for conduction [69,70].

2.2.1 THE EXTENDED STATE MOBILITY

If a charge carrier in the extended states is not strongly influenced by the lattice disorder, its motion is described by a mobility associated with a free particle having an effective mass, m^* and a relatively long mean free path. However, it was pointed out that mean free path of the carriers are of the order of interatomic spacing and the charge transport may be described by a Brownian or diffusive type motion [68]. The diffusion coefficient is given by

$$D = (1/6) v a^2 \quad (2.1)$$

where $a = 2\text{\AA}$ is the interatomic separation and $v \approx 10^{15} \text{ sec}^{-1}$ is the jump frequency associated with the interatomic transfer integral, $J = \hbar v$.

Using Einstein's relation $\mu = qD/kT$, the extended state mobility is given by

$$\mu_{\text{ext}} = \frac{1}{6} q v a^2 / kT \quad (2.2)$$

The typical value of μ_{ext} has been estimated to be equal to 2 to 12 $\text{cm}^2 \text{V}^{-1} \text{sec}^{-1}$.

2.2.2 THE HOPPING MOBILITY

The charge carriers in the localized band tail can be transported via thermally activated hopping process. Since hopping is a phonon assisted mechanism, the mobility associated with it will also have a thermally activated nature

$$\mu_{\text{hop}} = \mu_0 \exp[- H(E)/kT] \quad (2.3)$$

where the pre-exponential factor μ_0 is given by

$$\mu_0 = (1/6) v_{\text{ph}} q R^2 / kT \quad (2.4)$$

Here $v_{\text{ph}} \approx 10^{13}$ is the phonon frequency and R the distance covered in one hop. With $H \approx kT$, μ_{hop} was estimated to be of the order of $10^{-1} \text{cm}^2 \text{V}^{-1} \text{sec}^{-1}$ at room temperature which is smaller than the extended state mobility by at least a factor of 100. This drop in mobility has been called the mobility shoulder [68,69].

2.2.3 THE TUNNEL STATE MOBILITY

Carriers in the localized defect states near the midgap can also move between states via phonon-assisted tunneling which is analogous to the impurity conduction in heavily doped semiconductors at low tempera-

ture. The mobility has the following form

$$\mu_{\text{tun}} = \mu_0' \exp - (A/T^{1/4}) \quad (2.5)$$

Here, quantities,

$A = 2.1[\alpha^3/kN(E_F)]^{1/4}$, $\mu_0 = [q/4(2\pi)^{1/2}] \cdot v_{\text{ph}} [1/\alpha N(E_F)kT]^{1/2} (1/kT)$ are represented by a scale factor (α) for the spatial extent of wave functions (inverse length), attempt frequency v_{ph} and density of states factor, $N(E_F)$. This mobility is smaller than the above mentioned values by several orders of magnitude.

2.3 TEMPERATURE DEPENDENCE OF AMORPHOUS CONDUCTIVITY

The total conductivity of amorphous semiconductor is, therefore, given by [69]

$$\sigma = q \int dE g(E) \mu(E) f(E) \quad (2.6)$$

where $g(E)$ is the density of states factor which includes the defect states near the midgap, localized states in the band tail and the extended states beyond the mobility shoulder; $\mu(E)$ is the mobility associated with the three conduction channels and $f(E)$ is the Fermi probability factor. The temperature dependence of conductivity is thus determined by the combined effect of the above conduction channels. For a given E_F and at room temperature and above, the dominant contribution to the above integral arises from the carriers in the extended states. This is because there is an appreciable amount of mobile carriers beyond the mobility shoulder and μ_{ext} is much larger than the mobilities associated with the localized states. As the temperature is lowered, however, the Fermi probability factor for extended states is rapidly reduced, in which

case the prevalent channel of conduction should be the hopping of carriers in the bandtail. With further decrease in temperature, charge transport is, by the same reasoning, due to the tunneling of carriers between defect states near the midgap. As a consequence, the plot of $\ln \sigma$ vs. $1/T$ is not characterized by a straight line over a wide range of temperatures. Rather, there exist three different slopes, each having its own dominant range of temperature [71]. This theoretical temperature dependence of σ is experimentally supported by the drift mobility measurements in amorphous solids [68]. This bending trend of the slope, when transcribed into the resistivity curve is strikingly similar to that observed in polycrystalline silicon [43,46]. Herein lies the basic experimental link between the grain boundary and amorphous solids and also the attractive possibility of explaining the temperature dependency of polysilicon resistivity on a general physical ground. As mentioned earlier, the resistivity data reported by Young et al and Werner et al [63,64], using a bicrystal explicitly suggests that the bending trend of $\ln \rho$ vs $1/T$ curve is determined by the grain boundary property itself. This, coupled with the strikingly similar and consistent behavior of $\ln \sigma$ vs. $1/T$ curve in an amorphous semiconductor lends strong credence to the point of view, namely that the grain boundary not only gives rise to a potential barrier, but also provides an actual conducting medium through which carriers are microscopically transported. The effective mean free path of carriers associated with the various conduction channels are approximately equal to or less than the lattice spacing. Since the grain boundary is generally believed to consist of at least a few lattice sites, there is no physical ambiguity for assigning these conduction channels to the grain boundary.

2.4 I-V CHARACTERISTICS OF AMORPHOUS SEMICONDUCTORS

The current-voltage characteristics of amorphous materials is strictly ohmic for low applied voltages. However, as the applied voltage is increased to a certain critical voltage, V_{th} , the material converts from a highly resistive to a highly conductive state. When the voltage is reduced, the material may revert back to its original state. This phenomenon is known as the threshold switching. In the case where the material continues to remain in the high conducting state even if the voltage is decreased, the transition is known as memory switching. This electrical switching phenomena has been observed in amorphous thin films of silicon, germanium and various semiconducting glasses [72]. Much research has been done in the field of threshold switching to identify the mechanisms responsible in this transition [73]. Materials which exhibit switching are typically disordered and contain a large concentration of carrier traps [72]. Another feature common to these substances is their low mobility and the corresponding high resistivity. This makes it possible to apply high electric field across the films [72]. Investigations in this field has thus far revealed that this switching may be either electronic or thermal in nature or a combination of both [73]. The widely accepted viewpoint for this transition is the electrothermal theory. This theory suggests that at high voltage some filamentary current channels are formed in the material which increases the overall conductivity of the thin film. This at the end leads to an avalanche-like condition and causes the film to switch. There has been proposed an empirical relationship existing between the switching voltage, V_{th} , and the thickness of the amorphous films [73]. For silicon

$$V_{th} \propto d^{1/2} \quad (2.7)$$

where d is the film thickness. The constant of proportionality, M , has been determined experimentally to be $\approx 9.4 \times 10^2 \text{ V/cm}^{1/2}$ [73]

2.5 PASSIVATION OF AMORPHOUS SILICON

Amorphous silicon is normally characterized by a presence of a large number of dangling bonds [68]. This has been demonstrated by a large electronic spin resonance (ESR) by Brodsky and Tittle [74]. in Ge and Si. For pure evaporated and sputtered material, the ESR signal is very large and it shows a presence of high density of paramagnetic centers ($10^{19} - 10^{20} \text{ cm}^{-3}$). The electron energy levels of the dangling states lie between the valence and the conduction states of the fully paired and bonding electrons [68]. If these silicon dangling bonds can not be paired to each other, it is possible to pair them with other atomic orbitals, e.g. hydrogen, nitrogen, oxygen, fluorine etc [68]. It has been observed that the glow discharge plasma decomposition of silane or sputtering in the presence of hydrogen tends to reduce the ESR signal, showing large decrease in the paramagnetic spin centers in the bulk amorphous silicon [75]. In the glow discharge deposition method, the hydrogen concentration depends on the deposition conditions such as substrates temperature, SiH_4 pressure, SiH_4 flow rate etc. It has been observed that the hydrogen content decreases as the substrate temperatures is increased [76]. Based on absorption measurement, it has been estimated that the amount of bonded hydrogen (a-Si:H) is typically 35-52 atomic percent for substrates maintained at 300°K whereas for 520°K specimen the corresponding number was lower (14-25 atomic percent) [77]. These a-Si:H has been used to make relatively efficient solar cells [76]. Thus, the passivation of the

defect states may enhance the possibility of using amorphous semiconductor thin films in fabricating useful devices. However, it has been revealed that hydrogen and other additives may enlarge the band gap (alloying with Si), changing the lattice-electron coupling etc. For that reason, the amount of hydrogen incorporation in the a-Si has to be carefully chosen to optimize the use of a-Si:H in the semiconductor industries [78].

CHAPTER THREE

CONDUCTION THEORY IN POLYSILICON

3.1 PRELIMINARIES

In this chapter we present a new approach in modeling conduction in polycrystalline silicon. This model introduces a conceptually novel treatment for conduction in the disordered (amorphous) grain boundary — based on the extended state, hopping and tunneling mobilities, and uses drift and diffusion theory to describe current in both the single crystalline grain and amorphous boundary regions. This model is capable of explaining previous data on conduction in polysilicon, using a fixed set of physically meaningful parameters, determined only by the structural properties of the material. This comprehensive theory aptly demonstrates the internal consistency, in stark contrast with other models, by extensive comparison with previously reported experimental results. Furthermore, the model can successfully predict the electrical properties of polysilicon for a given set of structural parameters or vice versa.

3.2 SMALL SIGNAL THEORY

The present theory of conduction in polycrystalline silicon is derived with the following assumptions and simplifications. The validity of these assumptions will be demonstrated in the rest of the theory.

(a) Polysilicon is composed of uniform size cubic grain which are joined together at the grain boundary. The current is mainly due to one-dimensional charge transport. We define an unit cell of length L , which

consists of a disordered grain boundary and a crystalline grain.

(b) The grain boundary is amorphous in nature and has a fixed width δ . The density of states in the boundary is described by Davis-Mott energy band and is specified by a band tail (Δ) and a mobility shoulder (Δ'). Kamin's trapping model is adopted but traps are interpreted as the non vanishing defect states near the mid gap with a trap density of $Q_t/\delta \text{ cm}^{-3}$ and at a level E_T . These trap distribution is either monoenergetic or gaussian in nature.

(c) Space charge potential is treated by Poisson equation in the abrupt depletion approximation. The barrier potential is considered flat within the boundary. As a result the hole concentration remains constant in the grain boundary.

(d) Dopant atoms are assumed to enter the grain substitutionally. The effect of dopant segregation can be treated in a manner same as Mandhurah et al [44]. Atoms segregated in the grain boundary are passively accommodated by the defect sites.

(e) Current density, J , is due to drift and diffusion of carriers in the two regions in an unit cell. Hence J is proportional to the product of carrier concentration, $p(x)$, and the local slope of quasi-Fermi energy.

(f) To calculate the carrier density, the Fermi-Dirac function, $f(E)$, has been approximated by Maxwell-Boltzmann statistics.

3.2.1 POISSON EQUATION

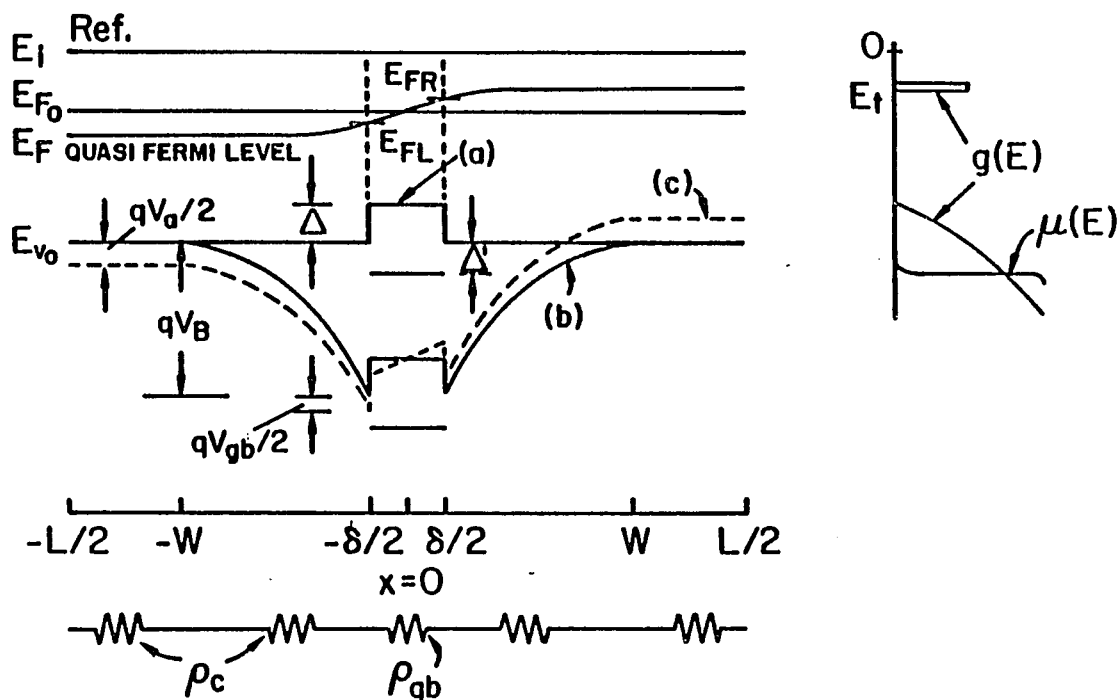


Fig.3.1 Energy level diagram of a unit cell in polysilicon (a) undoped, (b) doped, and (c) doped and biased conditions. Also shown are the density of states factor, $g(E)$, and mobility, $\mu(E)$, for undoped polysilicon: V_a , V_{gb} represent the applied voltages across the unit cell and the grain boundary, respectively. Δ represents the band tailing, and Δ' the mobility shoulder.

Consider a boron doped p-type polycrystalline silicon doped at a concentration level of $N_A \text{ cm}^{-3}$. Using the abrupt depletion approximation, the Poisson equation is written as shown below.

$$\frac{\delta^2 V}{\delta x^2} = \frac{qN_A}{\epsilon} \quad W \leq |x| \leq \delta/2 \quad (3.1)$$

With the boundary condition, $V=0$ and $\frac{\delta V}{\delta x} = 0$, one calculates the bending of the band edges. The resulting expressions for the valence band edge is given by

$$E_v(x) = E_{v0} - \left(\frac{qN_A}{2\epsilon}\right)(|x| - W)^2 \quad (3.2)$$

in the depletion depth, W . Here, E_{v0} represents the valence band edge at the grain center ($x = |L/2|$). As a result, the energy band of all the states within boundary is lowered by the barrier potential, qV_B where

$$V_B = \frac{qN_A}{2\epsilon}(W - \delta/2)^2 \quad (3.3)$$

Figure 2.1 shows schematically the energy band diagram for undoped, doped and doped with an external bias voltage. In the case of doped case the valence band bends down because of the depletion of charge carrier in accordance with eqn.(3.2).

3.2.2 DRIFT-DIFFUSION EQUATION FOR CURRENT DENSITY

Under bias, the current density in the grain is given by $J = \mu_c p(x) \delta E_F / \delta x$, where μ_c is the single crystalline silicon mobility which is a function of both N_A and temperature T . The hole concentration, $p(x)$, is given in terms of the quasi Fermi energy, E_F , and at any x is given by

$$p(x) = N_v \exp[- (E_F(x) - E_v(x))/kT]. \quad (3.4)$$

Therefore, one may write

$$\frac{J}{\mu_c} \int dx e^{-\frac{E_v}{kT}} = N_v \int dE_F e^{-\frac{E_F}{kT}} \quad (3.5)$$

When the applied voltage, V_a , is much smaller than kT/q , the depletion width change is almost negligible. Therefore, the band edges and the quasi-Fermi levels remains very close to the thermal equilibrium value. Hence upon inserting eqn.(3.2) in eqn.(3.5) and integrating the left hand side with respect to x over the undepleted crystalline grain, viz. $[-L/2, -\delta/2]$ and $[L/2, \delta/2]$ and the corresponding right hand side with respect to E_F , one obtains

$$JL F_c^{(0)} / \mu_c p(-L/2) = 2kT [\sinh(\frac{qV_a}{2kT}) - \sinh(\frac{qV_{gb}}{2kT})] \quad (3.6)$$

Here V_{gb} is a portion of applied voltage, V_a , dropped across the grain boundary. In this integration we have assigned

$$E_F(-L/2) = E_{F0} - qV_a/2 \quad (3.7a)$$

$$E_F(-\delta/2) = E_{F0} - qV_{gb}/2 \quad (3.7b)$$

$$E_F(+\delta/2) = E_{F0} + qV_{gb}/2 \quad (3.7c)$$

$$E_F(L/2) = E_{F0} + qV_a/2 \quad (3.7d)$$

In the eqn.(3.6), terms arising from the integration on the right hand side are, however, linearized because $V_a \ll kT/q$. Thus we have

$$JL F_c^{(0)} / \mu_c p(-L/2) = q(V_a - V_{gb}) \quad (3.8)$$

The hole concentration at the center of the grain, $p(-L/2)$, is given by

$$p(-L/2) = N_v \exp[- (E_{F0} - E_{v0})/kT] = n_i e^{-\frac{E_{F0}}{kT}} \quad (3.9)$$

$F_c^{(0)}$ is a dimensionless factor which results from the integration on the left side of eqn.(3.5).

$$F_c^{(0)} = 1 - \frac{2W}{L} + \left[\frac{2W-\delta}{L} \right] \frac{D \left[(qV_B/kT)^{1/2} \right]}{\left[qV_B/kT \right]^{1/2}} e^{\frac{qV_B}{kT}} \quad (3.10)$$

where D is the dawson integral defined as [79]

$$D(a) = e^{-a^2} \int_0^a e^{t^2} dt \quad (3.11)$$

3.2.3 THE CURRENT DENSITY IN THE GRAIN BOUNDARY

In the above expression for current density (eqn.(3.8)) one needs to specify V_{gb} in order to obtain current density as a function of V_a . To do that one needs to partition the voltage V_a in the undepleted region, depleted region and the boundary in a way such that the current density remains constant. Within the grain boundary there is no depletion region and the carrier density is uniform. As a result the grain boundary acts as a passive resistor. In other words, the edge of the band tail and the quasi-Fermi level undergo a parallel shift from the thermal equilibrium with a slope, V_{gb}/δ . This implies also that the number of holes trapped in the boundary remains unchanged as a result of external bias. The current density, J , in the boundary is given by

$$J = q\mu_{gb}p_{gb} \frac{V_{gb}}{\delta} \quad (3.12)$$

here $q\mu_{gb}p_{gb}$ represents the effective conductivity σ_{gb} of the boundary channels and is given by the eqn.(2.6). The numerical value of σ_{gb} is calculated in the following manner. In the small signal theory the effective conductivity is strictly given by the mobility and the carrier concentration in the barrier. However, if the voltage across the barrier is large, the barrier may behave as though it is a thin amorphous film. The conductivity in this case has to be determined by the switching properties of the amorphous thin films as discussed in chapter two.

3.2.4 ENERGY STATES IN THE GRAIN BOUNDARY

We approximate the Mott-Davis energy states, $g(E)$, in the boundary, by the crystalline density of state factor in the valence band and raising it above E_{vo} by an amount Δ . The energy states between $E_{vo} - qV_B + \Delta$ and $E_{vo} - qV_B - \Delta$ represents the localized tail states (Fig 2.1). Below energy level $E_{vo} - qV_B - \Delta$ all the states are in the extended states.

Thus

$$g(E + qV_B) = \frac{\sqrt{2}m_p^*}{\pi^2 h^3} [E_{vo} - qV_B + \Delta - E]^{1/2} \quad (3.13a)$$

where m_p^* is the hole effective mass and h , the Planck's constant. The term qV_B appears in these expressions because of the fact that all the energy states in the boundary has been lowered by the barrier potential, qV_B . The tail states, however, has been approximated in many different ways in the literature [2]. One other possibility is

$$g_{\text{hop}}(E) = \frac{g_{\text{ext}}(E)}{(\Delta E)^s} (E_A - E)^s \quad (3.13b)$$

where $g_{\text{hop}}(E)$ is the density of states in the localized hopping states, $g_{\text{ext}}(E)$ is the density of states in the extended states, E_A is the edge of the band tail and s is some exponent. In our approximation the total concentration p_{gb} is given by

$$p_{\text{gb}} = \int_{-\infty}^u dE g(E + qV_B) f(E) \quad (3.14)$$

Here, $u = E_{\text{vo}} - qV_B + \Delta$. Upon integration one obtains

$$p_{\text{gb}} = p(-L/2) \exp[- (qV_B - \Delta)/kT] \quad (3.15)$$

where $p(-L/2)$ is the hole concentration at the center of grain and is given by

$$p(-L/2) = n_i e^{-\frac{E_F}{kT}} \quad (3.16)$$

The hole concentration below mobility shoulder p_{ext} is obtained by replacing u by $E_{\text{vo}} - qV_B - \Delta'$ in eqn. (3.14). Thus p_{ext} is given by

$$p_{\text{ext}} = p_{\text{gb}} \gamma \quad (3.17)$$

Here the γ factor is given in terms of complementary error function as

$$\gamma = \text{erfc}\left[\frac{\Delta + \Delta'}{kT}\right]^{1/2} + \frac{2}{\sqrt{\pi}} \left[\frac{\Delta + \Delta'}{kT}\right]^{1/2} \exp\left[-\frac{\Delta + \Delta'}{kT}\right] \quad (3.18)$$

For simplicity we have chosen constant values of μ_{ext} and μ_{hop} in extended and hopping states. Thus the conductivity within the grain boundary is given by

$$\sigma = p_{gb} \left[(\gamma \mu_{ext}) + (1-\gamma) \mu_{hop} \right] \quad (3.19)$$

The above equation is an analytic expression for the boundary conductivity in the context of mean value theorem as applied to the general integral representation of σ in eqn.(2.6) and are summarized in Table I. In the above equation we have neglected any contribution to σ_{gb} from the defect states near the mid gap. However, situations may arise when this contribution may become dominant, especially when E_F is near the mid gap and very low temperature, when it can no longer be neglected.

3.2.5 CURRENT DENSITY EXPRESSION

Upon inserting eqn.(3.12) in the right hand side of eqn.(3.8) and carrying out the algebra, there results

$$J = q p(-L/2) \mu_{eff}^{(0)} \frac{V_a}{L} \quad (3.20)$$

with

$$\mu_{eff}^{(0)} = \mu_c / [F_c^{(0)} + F_{gb}^{(0)}] \quad (3.21)$$

and

$$F_{gb} = \frac{\delta}{L} \frac{\mu_c}{\mu_{gb}} \frac{p(-L/2)}{p_{gb}} \quad (3.22)$$

$$\rho = [F_c^{(0)} + F_{gb}^{(0)}] / q \mu_c p(-L/2) \quad (3.23a)$$

or equivalently

$$\rho = \frac{1}{q \mu_{eff} p(-L/2)} \quad (3.23b)$$

The effective mobility (eqn.(3.21)) reflects the composite nature of the

Table I

Summary of Mathematical Formulas

$$p(-L/2) = n_i \exp - E_{F0}/kT$$

$$p_{gb} = p(-L/2) \exp (\Delta - qV_B)/kT$$

$$p_{ext} = p_{gb}\gamma ; \quad p_{hop} = p_{gb}(1-\gamma)$$

$$\gamma = \operatorname{erfc}\kappa + \frac{2}{\sqrt{\pi}}\kappa \exp -\kappa^2$$

$$\mu_{gb}p_{gb} = \mu_{ext}p_{ext} + \mu_{hop}p_{hop}$$

$$D(x) = e^{-x} \int_0^{2x} e^{t^2} dt$$

$$N_A L = \Delta Q_t + \delta p_{gb} ; \quad N_A < N^*$$

$$2WN_A = \Delta Q_t + \delta p_{gb} ; \quad N_A < N^*$$

$$\text{See eqn. (3.27) for } \Delta Q_t ; \quad \kappa = \left(\frac{\Delta + \Delta'}{kT} \right)^{1/2}$$

polycrystalline systems. In the grain, the mobility is dictated mainly by the phonon and impurity scattering. But in the boundary the mechanism of charge transport is via hopping and brownian or diffusive type scattering. The expression for ρ can be interpreted as a weighted sum of individual resistivities of the undepleted, depleted and the grain boundary.

3.2.6 DISTRIBUTED CIRCUIT MODEL

This small theory is amenable to a straightforward interpretation. The unit cell is a distributed circuit system, because the hole concentration in W is nonuniform and also because hole mobilities are different in two subregions. These different local resistivities, when summed up accordingly determine the net resistivity, ρ . The local resistivity at any region i is given, in terms of the carrier concentration, $p(x)$, and mobility, μ_i , by $\rho(x) = 1/(qp(x)\mu_i)$. Integrating $\rho(x)$ over the entire region and dividing the resulting expression by the length of the region, one obtains the resistivity of the region, i.e.

$$\rho_i = \frac{1}{L_i} \int \rho(x) dx \quad (3.24)$$

In this model $p(x)$ is given by

$$p(x) = p(-L/2) \quad W < |x| < L/2 \quad (3.25a)$$

$$= p(-L/2) \exp(-qV(x)/kT) \quad \delta/2 < |x| < W \quad (3.25b)$$

$$= p_{gb} \quad 0 < |x| < \delta/2 \quad (3.25c)$$

The values of μ_i are μ_c and μ_{gb} in the grain and the boundary. Inserting eqn.(3.25) in eqn.(3.24) and performing the corresponding integration one obtains the resistivity of the undepleted, depleted and the grain

boundary regions. The polysilicon resistivity is now expressed in terms of these individual resistivities as a distributed circuit model, i.e.

$\rho = \sum_i \rho_i l_i / L$. The resulting expression is identical as eqn.(3.23).

3.2.7 DETERMINATION OF THE FERMI LEVEL

3.2.7.1 CHARGE NEUTRALITY CONDITION

The conductivity of polysilicon is now fully described under small bias when the Fermi level E_{F0} is specified from charge neutrality condition. For the case where grain boundary is fully depleted, using abrupt depletion approximation, we have

$$N_A L = \delta \int_{-\infty}^{-qV_B} dE g(E+qV_B) f(E, E_F) - \delta \int_{-\infty}^0 dE g(E) f(E, 0) \quad (3.26)$$

Here $g(E)$ is the total density of states within the grain boundary. It includes the trap or defect states, band tail and the extended states beyond the mobility shoulder and $f(E, E_F)$ is the Fermi factor for hole occupancy. The trap states are modeled as either a δ -function distribution at a trap level E_t and having a density of $Q_t \text{ cm}^{-3}$ or a Gaussian distribution having a full width at half maximum point, Δ_t . It has been found that for the interpretation of most of the available data the former is as good as the latter distribution. But the Gaussian distribution probably represents the actual defect states better than the first one. This charge neutrality equation suggests that the total number of exposed ions (negatively charged) must be equal to the carriers trapped from the grain. This charge neutrality is valid only for p type semiconductor. The term in the left hand side represents the total number (cm^{-2}) of negatively charged dopant atoms. The first term in the charge

neutrality represents the amount of holes present for a certain E_{F0} and T . The second term represents the density of intrinsic holes present in the boundary before dopant incorporation. Since minority carriers are neglected this second term actually ensures that the Fermi level is pinned at mid gap as N_A approaches zero. Absence of this term in the simplified charge neutrality equations normally raises the Fermi level above the intrinsic Fermi level, E_i for very low dopant concentration. This can lead to an erroneous result for activation energy. In eqn.(3.26) we have considered that all the dopant atoms are ionized which is true for most dopant concentrations when E_{F0} is few kT above the acceptor level, E_a . In the case when E_{F0} is close to E_a at the grain center, because of band bending $E_{F0} - E_a$ increases as one moves towards the grain boundary. For the case of heavily doped case, the impurity band broadens and merges with the valence band. All the holes would, therefore, be virtually free to enter the valence band. Experimental data for hole concentration tends to support this simplifying assumption. This simplification is, however, non essential and one can easily incorporate the fact that not all of the atoms are ionized by considering a spatial dependence of ionization energy, E_A . The transition from completely depleted case to the partially depleted case occurs when $p(-L/2)$ is equal to the dopant concentration. Above this transition concentration, N_A^* , E_{F0} is determined by the fact that $p(-L/2) = n_i \exp(-E_{F0}/kT) = N_A$. The depletion width, W , can be determined if one replaces the L by $2W$ in the above charge neutrality condition. The integrations in the charge neutrality equation can be solved analytically and is derived in the next section.

3.2.7.2 ANALYTIC DESCRIPTION OF CHARGE NEUTRALITY CONDITION

Consider eqn.(3.26) representing the conservation of charges. The discussion divides into two parts: (i) holes trapped in the defect states near the midgap, and (ii) holes residing in hopping and diffusive bands, i.e. δp_{gb} . The second term has been analysed in section(3.2.4).

The number of holes trapped in the boundary can be defined explicitly from eqn.(3.26) by

$$\Delta Q_t = \int_{-\infty}^{\infty} Q_t(E + qV_B) f(E, E_F) dE - \int_{-\infty}^{\infty} Q_t(E) f(E, 0) dE; \quad (3.27)$$

where the defect density of states has been transcribed into the total number of trap states in the boundary via $\delta g(E) = Q_t(E)$. The trap states are taken in our analysis to be of a Gaussian distribution centered at E_t below the midgap:

$$Q_t(E) = Q_t \frac{1}{\sqrt{\pi}\Delta\epsilon} \exp - [(E + E_t)^2 / \Delta\epsilon^2] \quad (3.28)$$

The full width at half maximum points is thus given by

$$\Delta_t = 2(\ln 2)^{1/2} \Delta\epsilon \quad (3.29)$$

The hole occupancy factor, $f(E, E_F) = [1 + \exp(E_F - E)/kT]^{-1}$, appearing in the integrand can be accurately approximated by

$$(1 + e^x)^{-1} = \begin{cases} \frac{1}{2} \exp - (0.1x^2 + 0.52x); & x > 0 \\ 1 - \frac{1}{2} \exp - (0.1x^2 - 0.52x); & x < 0 \end{cases} \quad (3.30)$$

Upon inserting eqn.(3.28) and eqn.(3.30) into eqn.(3.27), the first term in eqn.(3.27), for example, takes the form,

$$Q_t \frac{kT}{\sqrt{\pi}\Delta\epsilon} \int_0^{\infty} dx \frac{1}{2} e^{-[kT(x-a)/\Delta\epsilon]^2 - (0.1x^2 + 0.52x)}$$

$$+ \int_{-\infty}^0 dx e^{-[kT(x-a)/\Delta\epsilon]^2} [1 - \frac{1}{2}e^{-(0.1x^2-0.52x)}] \quad (3.31)$$

with $a = (E_F + E_t + qV_B)/kT$. These integrals can be readily performed and the results are obtained in terms of complimentary error functions:

$$\Delta Q_t = \frac{1}{2} Q_t [G(E_F, E_t, qV_B) - G(0, E_t, 0)] \quad (3.32)$$

with

$$G(E_F, E_t, qV_B) = \text{erfc}\Lambda_0 + \frac{1}{2}e^{\Lambda_0^2} (e^{\Lambda_-^2} \text{erfc}\Lambda_- - e^{\Lambda_+^2} \text{erfc}\Lambda_+) \quad (3.33)$$

$$\Lambda_0^2 = (E_F + E_t + qV_B)/\Delta\epsilon \quad (3.34)$$

$$\Lambda_-^2 = (0.26\Delta\epsilon/kT - \Lambda_0)/[1 + 0.1(\Delta\epsilon/kT)^2]^{1/2} \quad (3.35)$$

$$\Lambda_+^2 = (0.26\Delta\epsilon/kT + \Lambda_0)/[1 + 0.1(\Delta\epsilon/kT)^2]^{1/2} \quad (3.36)$$

Therefore, below N^* eqn. (3.26) takes the form

$$N_A L = \Delta Q_t + \delta p_{gb} \quad (3.37)$$

and E_F is determined with $qV_B = q^2 N_A L^2 / 8\epsilon$. Above N^* where E_F is known and given by $n_i \exp - E_F/kT = N_A$ and $qV_B = q^2 N_A W^2 / 2\epsilon$, W is determined from

$$2WN_A = \Delta Q_t + \delta p_{gb} \quad (3.38)$$

3.2.8 ACTIVATION ENERGY

As mentioned earlier, the slope of the plot of $\ln(\rho)$ versus $1/kT$ is defined as the activation energy. The temperature dependency of resistivity is mainly via $p(-L/2)$ and qV_B . At very low concentration, N_A , E_{F0} is nearly pinned down at the mid gap and qV_B is negligible. As a result

$E_a \approx 0.56$ eV. If E_{F0} is not a sensitive function of temperature, i.e. $\partial E_{F0}/\partial(1/kT) \approx 0$, which is almost true if the Gaussian trap distribution is assumed, E_a should vary as $E_{F0} - E_{v0}$ as a function of N_A . However, near N_A^* , qV_B term becomes significant. Beyond N_A^* $p(-L/2) \approx N_A$. As a result, most of the temperature dependence is because of qV_B . To a first order approximation the activation energy can be found in the following manner. Taking the logarithm on the both side of eqn.(3.23b)

$$\ln(\rho) = -\ln(q) - \ln(\mu_{eff}) - \ln(p(-L/2)) \quad (3.39)$$

and differentiating both sides with respect to $1/kT$, we have

$$E_a = \frac{qV_B(F_c^{(0)} - 1 + \frac{2W}{L}) + (qV_B + \Delta') \left(\frac{\delta\mu_c p(-L/2)}{L\mu_{gb} p_{gb}} \right)}{F_c^{(0)} + \frac{\delta\mu_c p(-L/2)}{L\mu_{gb} p_{gb}}} + (E_{F0} - E_{v0})U(N_A^* - N_A) \quad (3.40)$$

Here, $U(a)$ is the unit function defined as

$$U(a) = 1 \quad \text{if } a > 0 \quad (3.41a)$$

$$= 0 \quad \text{if } a < 0 \quad (3.41b)$$

In the above derivation the temperature sensitivity of E_{F0} has been ignored and only the temperature dependence of exponential terms are considered to contribute to the activation energy.

CHAPTER FOUR

GENERALIZED CONDUCTION THEORY OF POLYCRYSTALLINE SILICON

4.1 PRELIMINARIES

In the chapter three we presented a new approach to modeling conduction in polycrystalline semiconductor system. The theory was based on regarding grain boundary as amorphous conducting medium. This viewpoint was shown to be strongly supported by its ability to explain the experimental data for resistivity versus temperature in the small signal limit.

In this chapter, we generalize the small signal theory to the general case of arbitrary applied voltage. In any I-V theory, proper voltage partitioning constitutes a key element. As discussed in chapter three, the present approach models the unit cell of polycrystalline semiconductor to consist of two conducting media in equilibrium contact and describes current via the intrinsic carrier mobilities therein. Hence, this treatment has the inherent advantage of bringing in naturally the concept of grain voltage, V_a . It also results in a voltage partition scheme within the unit cell, which is drastically different from the previous analyses. One may recall that in previous emission theories the grain boundary was treated as an insulator. Therefore, the external voltage dropped across it via electrostatic considerations is practically negligible, especially for low doping concentrations. In the present model, however, the grain boundary voltage, V_{gb} , can constitute a dominant fraction of V_a over a wide range of doping concentration. This implicitly suggests that the general I-V characteristics can be predom-

inantly influenced by the electrical properties of amorphous grain boundary.

Amorphous semiconductor thin films generally exhibit (i) high resistivity for small voltage, and (ii) threshold and/or memory switching for high applied voltage [72,73]. In this regard, it is important to note that these switching phenomena, characteristic of amorphous material, have in fact been observed in undoped polysilicon [80]. We believe that this experimental observation lends rather direct and additional credence to the viewpoint that the grain boundary is a high resistivity conducting medium, which can also be driven to exhibit nonlinear current response by a high applied voltage.

In this chapter we comprehensively analyse the general I-V characteristics in polysilicon, incorporating, (i) the field-dependent conductivity in the disordered grain boundary, and (ii) the modification in band bending specifically brought about by the external field induced redistribution of mobile charge carriers.

4.2 GENERAL I-V CHARACTERISTICS

In deriving J for any applied voltage and dopant concentration we use the same approximations as were made in Sec.(3.2). Due to the enormous complexity of high field I-V phenomena a few additional assumptions or simplifications are made as follows:

(i) Under a bias the depletion depths on both sides of a grain boundary are taken to change such that the total equilibrium length, $2W$, is preserved [54]. Equivalently, the number of carriers residing within the boundary is assumed to remain unchanged under bias. Since the concentra-

tion profile of carriers within the thin grain boundary is approximately uniform, both the imref and the edge of band tail should undergo a parallel linear shift therein. Hence, it is reasonable to make this assumption.

(ii) The grain boundary is regarded as a high resistivity conducting medium for small applied voltage with its resistivity specified via hopping and extended state mobilities as in sec. 3.2. With increasing external voltage, the disordered boundary is taken to be driven to threshold and/or memory switching or breakdown. This sudden transition in I-V characteristics is modeled phenomenologically in analogy with the diode breakdown.

(iii) A new additional critical voltage is introduced with regard to changing depletion depths under bias. With increasing applied voltage across the unit cell, V_a , the depletion depth on one side of the boundary eventually shrinks to zero. Beyond this critical voltage, V_a^m , the external field induced change in band bending ceases to be operative, and carrier concentration profile in the grain remains fixed at the configuration determined at V_a^m . Hence, for $V_a > V_a^m$ the grain is taken to be transformed into ohmic resistor with its resistivity specified at V_a^m .

(iv) Drift-diffusion theory is used to describe J. However, the diffusion theory of current (or for that matter emission theory) is derived from the assumption that the barrier potential, qV_B , is much greater than kT [62]. The theory could thus lead to erroneous results for the case of high applied voltage and low doping concentration, where $qV_B \leq kT$. This difficulty is circumvented as follows. For $N < N^*$ and $qV_B/kT \leq 2$, the effect of qV_B is neglected and the carrier concentration in the grain is

taken to be uniform at a value determined from the charge neutrality condition at the grain center. Equivalently, the grain is regarded as a passive resistor, while the amorphous boundary is treated in a manner as discussed in (ii).

4.2.1 VOLTAGE PARTITION

Consider again p-type polysilicon doped at a level $N_A \text{ cm}^{-3}$. Under a bias, the depletion depth to the left of boundary, W_L shrinks from the equilibrium value W , while W_R increases such that,

$$W_L + W_R = 2W \quad (4.1)$$

Eqn. (4.1) implies a significant modification in the band edge specifically brought about by the bias voltage (Fig. 4.1). For convenience, we use a new unit cell of length, L ranging from $-W_L$ to $L - W_L$ (Fig. 4.1). The voltage, V_a , assigned to the unit cell partitions into the boundary region (V_{gb}), undepleted region, (V_{ud}) and depleted region on both sides of the boundary (V_{dL}, V_{dR}). Expressing depletion depths in eqn.(4.1) in terms of the corresponding barrier potentials, one may write

$$2V_B^{1/2} = (V_B - V_{dL})^{1/2} + (V_B + V_{dR})^{1/2}, \quad (4.2)$$

where V_B is the equilibrium barrier potential. Now, V_d is defined as the total voltage drop in W_L, W_R :

$$V_d = V_{dL} + V_{dR} \quad (4.3)$$

Upon inserting eqn.(4.3) into eqn.(4.2) one obtains a quadratic equation for, say V_{dL} in terms of V_B, V_d . Hence there results

$$V_{dL} = \frac{1}{2} V_d - V_d^2 / 16V_B \quad (4.4a)$$

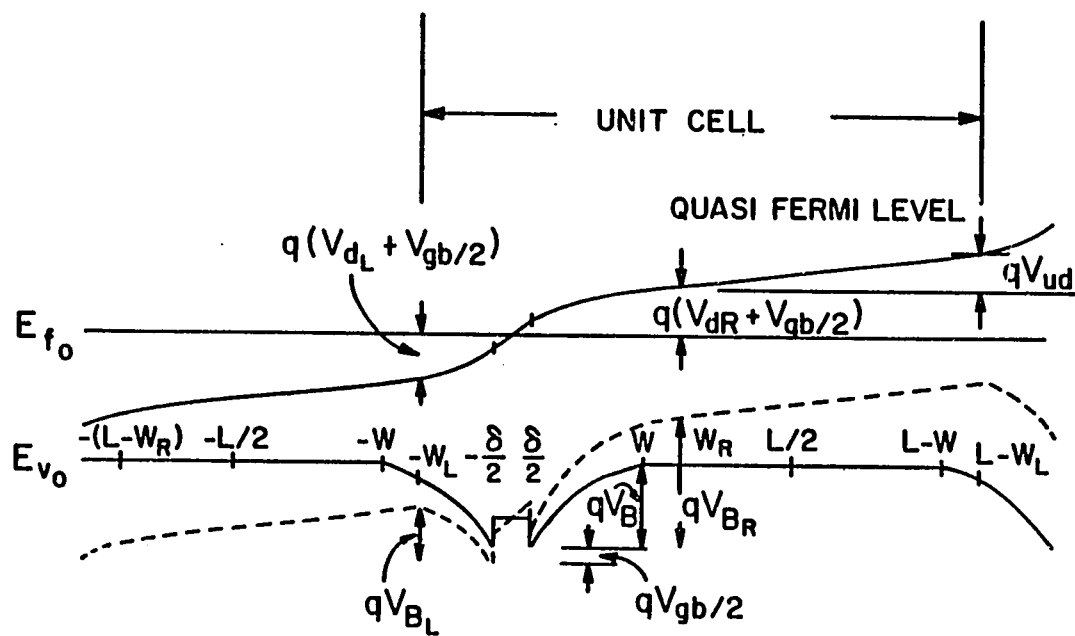


Fig.4.1 Schematic energy level diagram of a unit cell for polysilicon under (i) doped and (ii) doped and biased conditions.

$$V_{dR} = \frac{1}{2} V_d + V_d^2/16V_B \quad (4.4b)$$

The total voltage dropped to the left and right of grain boundary center reads, respectively, as

$$V_L = V_{dL} + V_{gb}/2 \quad (4.5a)$$

$$V_R = V_{dR} + V_{gb}/2 + V_{ud} \quad (4.5b)$$

4.2.2 DRIFT-DIFFUSION FORMULATION FOR J

Next, J can be derived in a manner similar to the small signal theory. As shown in Fig. 4.1, the valence band edge in the interval $-W_L$ to $-\delta/2$ is given under bias by

$$E_v(x) = E_{v0} - qV_L - q^2 N_A (x + W_L)^2 / 2\epsilon \quad (4.6a)$$

In the grain boundary the edge of band tail is modified as,

$$E_v(x) = E_{v0} + \Delta - qV_B + (qV_{gb}/\delta)x \quad (4.6b)$$

In the interval, $\delta/2$ to W_R one can similarly write,

$$E_v(x) = E_{v0} + q(V_R - V_{ud}) - q^2 N_A (W_R - x)^2 / 2\epsilon, \quad (4.6c)$$

while in the undepleted region, W_R to $L - W_L$

$$E_v(x) = E_{v0} + q(V_R - V_{ud}) + [qV_{ud}(x - W_R)/(L - 2W)] \quad (4.6d)$$

Now, since J and μ are constant for a given N_A and T in a homogeneous medium, one may write

$$(J/\mu) \int \exp[-E_v(x)/kT] dx = N_v \int \exp[-E_F(x)/kT] dE_F \quad (4.7)$$

We insert eqn.(4.6) into eqn.(4.7) and perform the x -integration in the crystal grain region, i.e. in $[-W_L, -\delta/2]$ and $[\delta/2, L - W_L]$ and the

corresponding E_F integration, obtaining

$$JLe^{-E_{vo}/kT} F_c/\mu_c = N_V kT \{ \exp - [E_F(-W_L)/kT] - \exp - [E_F(-\delta/2)/kT] \\ - \exp - [E_F(\delta/2)/kT] + \exp - [E_F(L - W_L)/kT] \} \quad (4.8)$$

where the dimensionless integration factor

$$F_c = e^{v_L} \frac{1}{2} \frac{2W_L - \delta}{L} e^{\frac{\Lambda_L^2}{\Lambda_L} \frac{D(\Lambda_L)}{\Lambda_L}} + e^{-(v_R - v_{ud})} \left[\frac{1}{2} \frac{2W_R - \delta}{L} e^{\frac{\Lambda_R^2}{\Lambda_R} \frac{D(\Lambda_R)}{\Lambda_R}} \right. \\ \left. + (1 - \frac{2W}{L})(1 - e^{-v_{ud}})/v_{ud} \right] \quad (4.9)$$

is given in terms of the Dawson integral, D [79] defined in Sec. 3.2 and the dimensionless shorthand notations

$$v_j = qV_j/kT \quad (4.10)$$

$$\Lambda_j^2 = q^2 N_A (W_j - \delta/2)^2 / 2\epsilon kT \quad (4.11)$$

Here, the subscript j denotes the different regions in the unit cell.

The quasi-Fermi level, E_F , appearing in eqn.(4.8) can be expressed via equilibrium Fermi level, E_{F0} and external voltages dropped across the three regions as

$$E_F(-W_L) = E_{F0} - qV_L \quad (4.12a)$$

$$E_F(L - W_L) = E_{F0} + qV_R \quad (4.12b)$$

$$E_F(-\delta/2) = E_{F0} - \frac{1}{2} qV_{gb} \quad (4.12c)$$

$$E_F(\delta/2) = E_{F0} + \frac{1}{2} qV_{gb} \quad (4.12d)$$

With the use of eqn.(4.12) in eqn.(4.8) and the identification,

$$p(-L/2) = N_v \exp - (E_{F0} - E_{v0})/kT, \quad (4.13)$$

$p(-L/2)$ denoting the hole concentration at the grain center, eqn.(4.8) becomes

$$\frac{JLF_c}{\mu_c} = p(-L/2)kT \left(e^{\frac{qV_L}{kT}} - e^{-\frac{qV_R}{kT}} - 2 \sinh \frac{qV_{gb}}{2kT} \right) \quad (4.14)$$

4.2.3 NONLINEAR GRAIN BOUNDARY CONDUCTIVITY

In the grain boundary where the hole concentration, p_{gb} , in the hopping band and extended state is uniform, the applied voltage, V_{gb} gives rise to an electric field, V_{gb}/δ . We now formally express the terminal J-V characteristics therein in a form

$$J = \sigma_{gb}(V_{gb})(V_{gb}/\delta) \quad (4.15)$$

Here, $\sigma_{gb}(V_{gb})$ has the unit of conductivity and represents the effective field-dependent conductivity of the grain boundary. In the limit of small applied voltage $\sigma_{gb}(V_{gb})$ reduces to

$$\sigma_{gb}(0) = q\mu_{gb}p_{gb} \quad (4.16)$$

This small signal expression represents the actual conductivity of the amorphous boundary and has been extensively discussed in chapter three. As V_{gb} approaches the threshold voltage, V_{th} , for switching $\sigma_{gb}(V_{gb})$ loses its usual meaning and can be phenomenologically represented by

$$\sigma_{gb}(V_{gb}) = J/(V_{gb}/\delta) \quad (4.17)$$

Here, the value of J is now limited by the resistivity of the crystalline grain.

As mentioned earlier, the I-V relationship observed in amorphous thin films exhibits threshold or memory switching when the applied voltage approaches the threshold voltage [72,73]. This switching phenomenon usually occurs in disordered material with high resistance, low mobility, and a large concentration of carrier traps. Since the same switching phenomena have also been observed in undoped polysilicon film [80], and since the grain boundary provides the only disordered region of polysilicon film, it is apparent that this observed electrical switching effect should be attributed to the intrinsic grain boundary property itself. Furthermore, an apparent electrical breakdown of Ge grain boundary has been observed by Taylor, et al [82]. In the present theory we, therefore, describe the voltage dependence of σ_{gb} via this switching and/or breakdown.

4.2.4 J-V RELATIONSHIP

The expression for current density in eqn.(4.14) can be cast into a more transparent form with the use of eqn.(4.15). Upon using the identity,

$$2kT \sinh(qV_{gb}/2kT) = J[q\delta/\sigma_{gb}(V_{gb})][\sinh(qV_{gb}/2kT)/(qV_{gb}/2kT)] \quad (4.18)$$

in eqn.(4.14) and rearranging the terms, there results

$$J(V_a) = [\mu_c p(-L/2)kT/LF] \left(e^{\frac{qV_L}{kT}} - e^{-\frac{qV_R}{kT}} \right) \quad (4.19)$$

where the factor

$$F = F_c + \frac{\delta}{L} \frac{q\mu_c p(-L/2)}{\sigma_{gb}(V_{gb})} \frac{\sinh(qV_{gb}/2kT)}{(qV_{gb}/2kT)} \quad (4.20)$$

depends now explicitly on V_a . Although the J-expression is somewhat

complex in its format, the underlying physics is simple and straightforward. When V_a is applied, mobile holes in the grain are rearranged and, consequently the depletion depths change. This significantly modifies the energy band from the symmetrical equilibrium configuration and gives rise to the V_a -dependent form factor, F_c . This, together with the non-linear conductivity of the grain boundary is responsible for the non-linear I-V characteristics in polysilicon.

4.2.5 SELF-CONSISTENCY CONDITION

The current density is fully described by eqn.(4.19) with an explicit partition of a given V_a into V_{gb} , V_d , and V_{ud} . This can be achieved as follows. In the undepleted region, for $N > N^*$, where the hole concentration is uniform at a value $p(-L/2)$, J is given by the slope of imref , i.e.

$$J = q\mu_c p(-L/2) [V_{ud}/(L - 2W)] \quad (4.21)$$

Here, μ_c is the crystalline mobility. Since J is constant, it follows from eqn.(4.15) and eqn.(4.21) that

$$V_{ud} = V_{gb} \left(\frac{L-2W}{\delta} \right) \left[\frac{q\mu_c p(-L/2)}{\sigma_{gb}(V_{gb})} \right] \quad (4.22)$$

Hence, the total voltage, V_a , consisting of V_d , V_{gb} , and V_{ud} , is given by

$$V_a = V_d + V_{gb} \left[1 + \frac{L-2W}{\delta} \cdot \frac{q\mu_c p(-L/2)}{\sigma_{gb}(V_{gb})} \right] \quad (4.23)$$

Now, we impose a self-consistency condition, namely that J given in eqn.(4.19) be identical to the value, say within the grain boundary:

$$J(V_a) = \sigma_{gb}(V_{gb})(V_{gb}/\delta) \quad (4.24)$$

With the use of eqns.(4.4), (4.5), (4.19) and (4.23), eqn.(4.24) can be written in terms of a given input voltage V_a and an unknown V_{gb} component. The V_{gb} -value can be easily determined numerically from this transcendental relation (24) and once V_{gb} is determined, V_d , V_{ud} can be found from eqn.(4.22), eqn.(4.23)

4.2.6 CRITICAL VOLTAGE, V_a^m

Thus far, V_a has been distributed in the unit cell via two physical mechanisms; (a) the changes in depletion depths, W_L , W_R , induced by V_a and (b) given this realignment, the local slope of imref appropriately adjusted to keep J constant throughout the unit cell. The first process ceases to be operative any further when $W_L - \delta \propto (V_B - V_{dL})^{1/2}$ shrinks to zero, i.e., $V_{dL} = V_B$. In this limiting case it follows from eqn.(4.4) that, $V_{dR} = 3V_B$ and $V_d = 4V_B$. The value of external voltage corresponding to this final configuration is given from eqn.(4.23) by

$$V_a^m = 4V_B + V_{gb}^m \left[1 + \frac{L-2W}{\delta} \cdot \frac{q\mu_c p(-L/2)}{\sigma_{gb}(V_{gb}^m)} \right] \quad (4.25)$$

where V_{gb}^m is the boundary component computed numerically from eqn.(4.24).

The physical significance of this limiting case is that any further increase in V_a does not change the mobile hole concentration profile within the grain. Equivalently, the grain becomes strictly ohmic. Thus any increase in current density, ΔJ , arising from the excess voltage beyond V_a^m , i.e. $\Delta V_a = V_a - V_a^m$ in the grain must be attributed to the change in imref, ΔE_F :

$$\Delta J = \mu_c p^m(x) \frac{\partial}{\partial x} \Delta E_F. \quad (4.26)$$

Since ΔJ is constant, with the identification

$\Delta E_F(\delta/2) - \Delta E_F(L - \delta/2) = q\Delta V_c$, one finds

$$\Delta J = \Delta V_c / L \rho_c^m \quad (4.27)$$

where ΔV_c denotes the fractional excess voltage applied to the grain and ρ_c^m is the grain resistivity given by

$$\rho_c^m = (1/L) \int_{-\delta/2}^{L-\delta/2} [q\mu_c p^m(x)]^{-1} dx \quad (4.28)$$

Note that the superscript, m is introduced to represent various quantities at V_a^m .

Now, the voltage dependence of the effective polysilicon resistivity, ρ beyond V_a^m can be generally discussed as follows. We define the resistivity at V_a^m as

$$\rho^m = \frac{V_a^m}{LJ^m} = \frac{\delta}{L} \rho_{gb}^m + \frac{L-\delta}{L} \rho_c^m \quad (4.29)$$

where

$$\rho_c^m = V_c^m / (L - \delta) J^m \quad ; \quad V_c^m = V_d^m + V_{ud}^m \quad (4.30)$$

$$\rho_{gb}^m = V_{gb}^m / \delta J^m \quad (4.31)$$

are the grain and the boundary component of ρ , respectively, which are specified in terms of $V_a^m (\equiv V_c^m + V_{gb}^m)$ and V_{gb}^m from eqn.(4.24). For $\Delta V_a > 0$, the grain resistivity, ρ_c , should remain constant at ρ_c^m , as mentioned earlier. Hence, ρ reads as

$$\rho = (\delta/L) \rho_{gb}(V_{gb}) + [(L - \delta)/L] \rho_c^m \quad (4.32)$$

The voltage dependence of ρ is now clearly seen to arise from $\rho_{gb}(V_{gb})$. With increasing ΔV_a , $\rho_{gb}(V_{gb})$ gradually decreases monotonically, followed

by a sharp decrease near the switching and/or breakdown voltages. Near these critical voltages $\rho_{gb}(V_{gb})$ becomes practically negligible and the polysilicon transforms into a passive resistor with the effective resistivity given by ρ_c^m . Therefore, the I-V relationship eventually becomes strictly ohmic. The incorporation of V_a^m is essential to insure that J in a polyresistor never surpasses that in a corresponding crystalline resistor at any applied voltage and doping concentration.

CHAPTER FIVE

RESULTS AND DISCUSSION

5.1 COMPARISON WITH EXPERIMENT: SMALL SIGNAL LIMIT

5.1.1 ρ , μ , E_a vs N_A :

We now explain the conduction data obtained in the small signal limit. The procedure is as follows. Polysilicon is characterized by the average grain size ($L-\delta$), boundary width (δ) and a Davis-Mott energy band with trap density ($Q_t \text{ cm}^{-2}$) and distribution (E_t, Δ_t). For a given N_A and T , the crystalline mobility (μ_c) in the grain and the composite mobility (μ_{gb}) in the boundary are specified. The charge neutrality condition determines E_{F0} and hence qV_B , $p(-L/2)$, p_{gb} , and W . These quantities are used in the appropriate expressions in our theory (eqn.(3.21), eqn.(3.23)).

Figures 5.1 and 5.2 present the room temperature hole mobility and resistivity vs. N_A , measured in polysilicon whose average grain size is about 250 Å in diameter [41]. The optimal theoretical curves have been generated, using the physical and material parameters, whose values are listed in Table II. Note that the present theory does not rely on the ideality or scaling factors. Previous theories attributed the mobility dip near N^* to qV_B which attains its maximum value near N^* and thereby reduces drastically the number of holes thermionically crossing the barrier. In contrast, the role of qV_B in our theory is to lower the mobility shoulder and to reduce the number of holes in the extended state conduction mode. This, coupled with the fact that μ_{ext} constitutes the dominant channel at room temperature is responsible for the dip (see

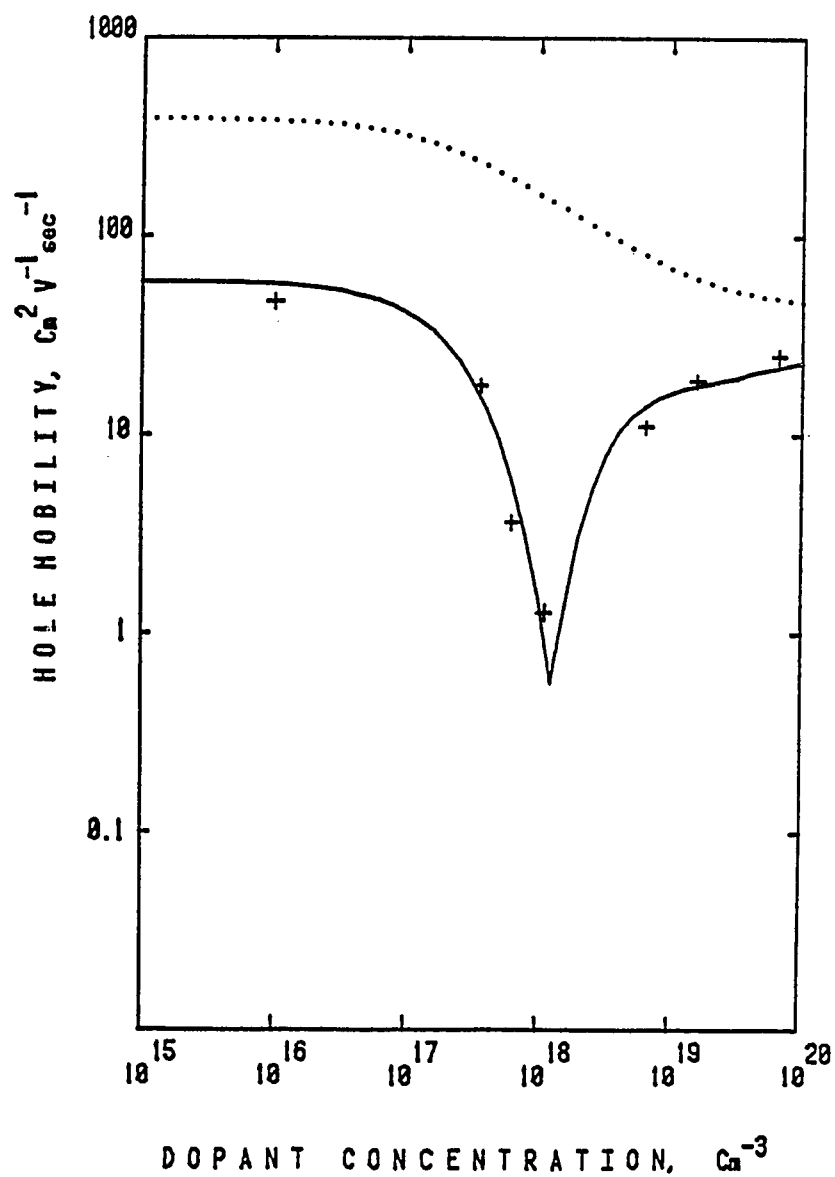


Fig. 5.1 Mobility vs. doping concentration (B-implanted poly-Si):
 + represents the data of Ref. [41], and the dotted line
 is the hole mobility in single crystal silicon.

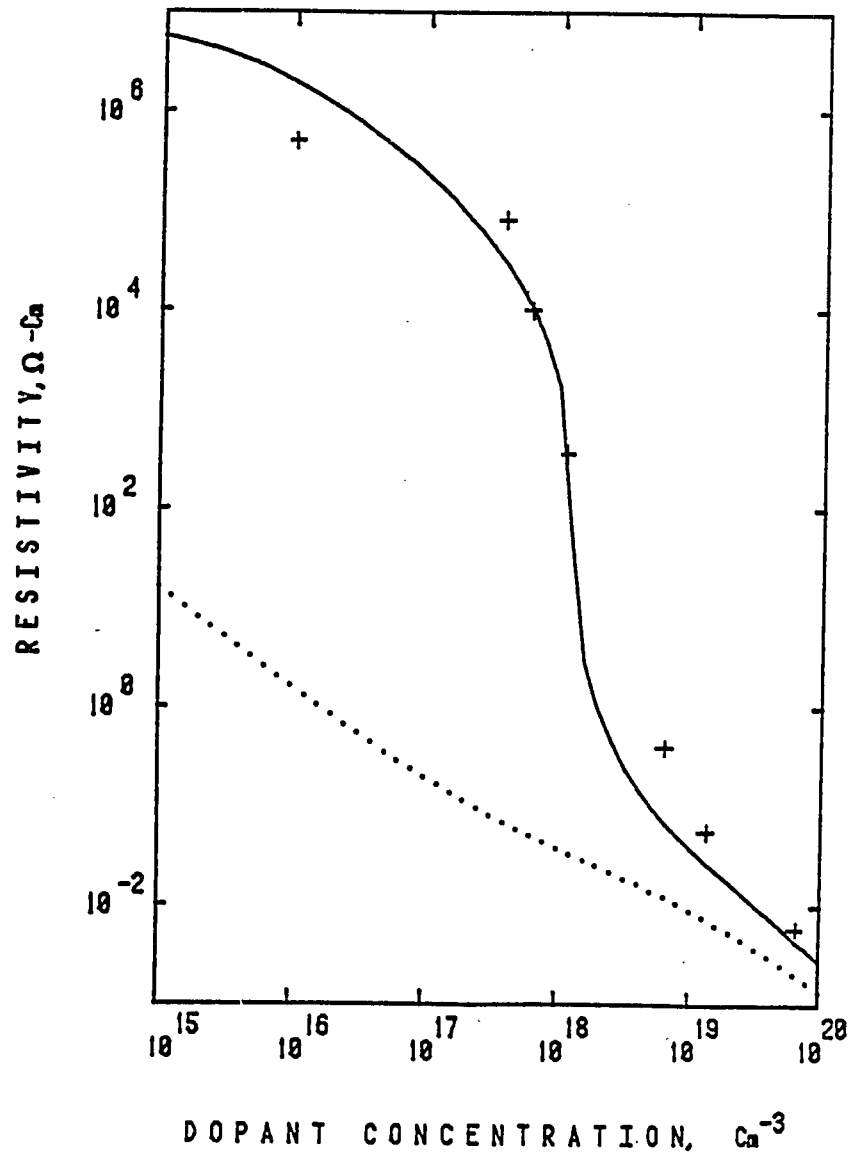


Fig. 5.2 Resistivity vs. doping concentration (B-implanted poly-Si): + represents the data of Ref. [41], and the dotted line is the crystalline resistivity.

eqn.(3.21)). The resistivity is again predominantly contributed by the boundary, the contribution from the depletion depth being overshadowed by the boundary component. With increasing N_A ($> N^*$), E_{F0} is lowered and the level of hole concentration profile is significantly enhanced. Consequently, ρ decreases monotonically with N_A . In the limit of large N_A , $qV_B \rightarrow 0$ and $p(-L/2) = N_A \approx p_{gb}$. Hence, ρ approaches the crystalline value to within a factor of 2-3. Fig. 5.3 shows the activation energy, E_a for ρ measured as a function of N_A in Ref. [44]. The theoretical curve has been obtained from the slope of ρ vs. T^{-1} curve (see eqn.(3.23)), which is linear in the temperature range, -40°C to 150°C . E_a is primarily determined by E_{F0} via $p(-L/2)$, as expected and the effect of qV_B is significant near N^* on both sides. Because E_{F0} is pinned near midgap for small N_A , $E_a \approx 0.56$ eV. With increasing N_A , E_{F0} is lowered monotonically, and E_a should decrease accordingly to become essentially zero for large N_A ($> 10^{18} \text{ cm}^{-3}$).

Figures 5.4, 5.5 and 5.6 show the data for μ , ρ , and E_a vs. N_A , reported in Ref. [39] from a slightly larger grain polysilicon ($L \sim 0.2 \mu\text{m}$). Theoretical curves have been generated in a similar way (see Table II) and physical discussions of the data are generally the same as in the preceding case. A slight discontinuity in E_a curve near N^* is due to the abrupt depletion approximation used in the theory. The effect of larger grain size is, (a) to shift N^* value to a lower doping level and (b) to increase the barrier potential for a given trap density, which enhances the mobility dip (Fig. 5.4). The agreement between theory and experiment is excellent, as shown in Figs. 5.1-5.6. Our main thrust is, however, directed towards understanding the general behavior of the data, rather than to fit the data precisely. A basic assumption of the present

Table II

Parameter Values Used to Explain Data of Polysilicon					
Data Source	E_t	Q_t	L	δ	f
from	(eV)	(cm^{-2})	(\AA)	(\AA)	
Ref. [19]	-.18	3.34×10^{12}	270	0	0.12
This Work	-.17	3×10^{12}	235	10	—
Ref. [24]	-.17	1.9×10^{12}	1220	25[25]	0.06
This Work	-.17	1.5×10^{12}	1550	25	—

$$\Delta = 0.05 \text{ eV}; \Delta' = 0.07 \text{ eV}; \Delta_t = 0.083 \text{ eV}$$

$$\mu_{\text{ext}} (300^\circ\text{K}) = 12 \text{ cm}^2/\text{V}\cdot\text{sec.}; \mu_{\text{hop}} (300^\circ\text{K}) = 10^{-1} \text{ cm}^2/\text{V}\cdot\text{sec.}$$

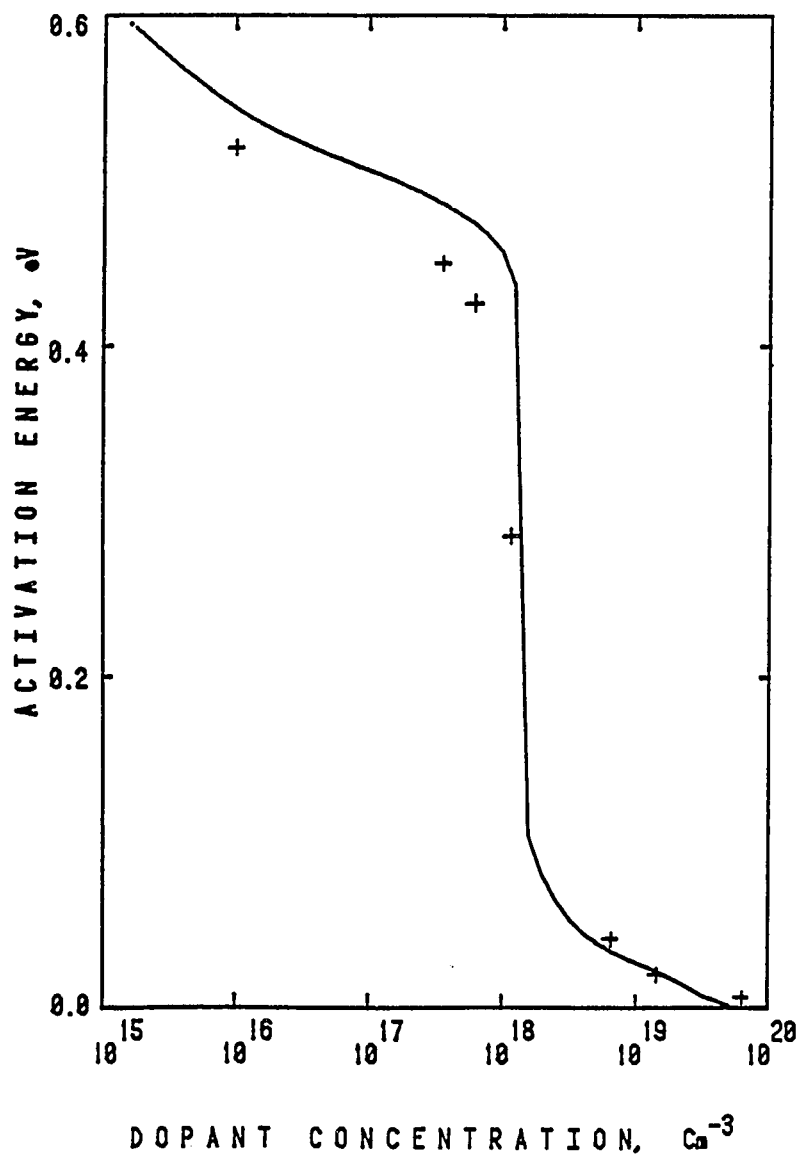


Fig. 5.3 Activation energy vs. doping concentration (B-implanted poly-Si): + represents the data of Ref. [41].

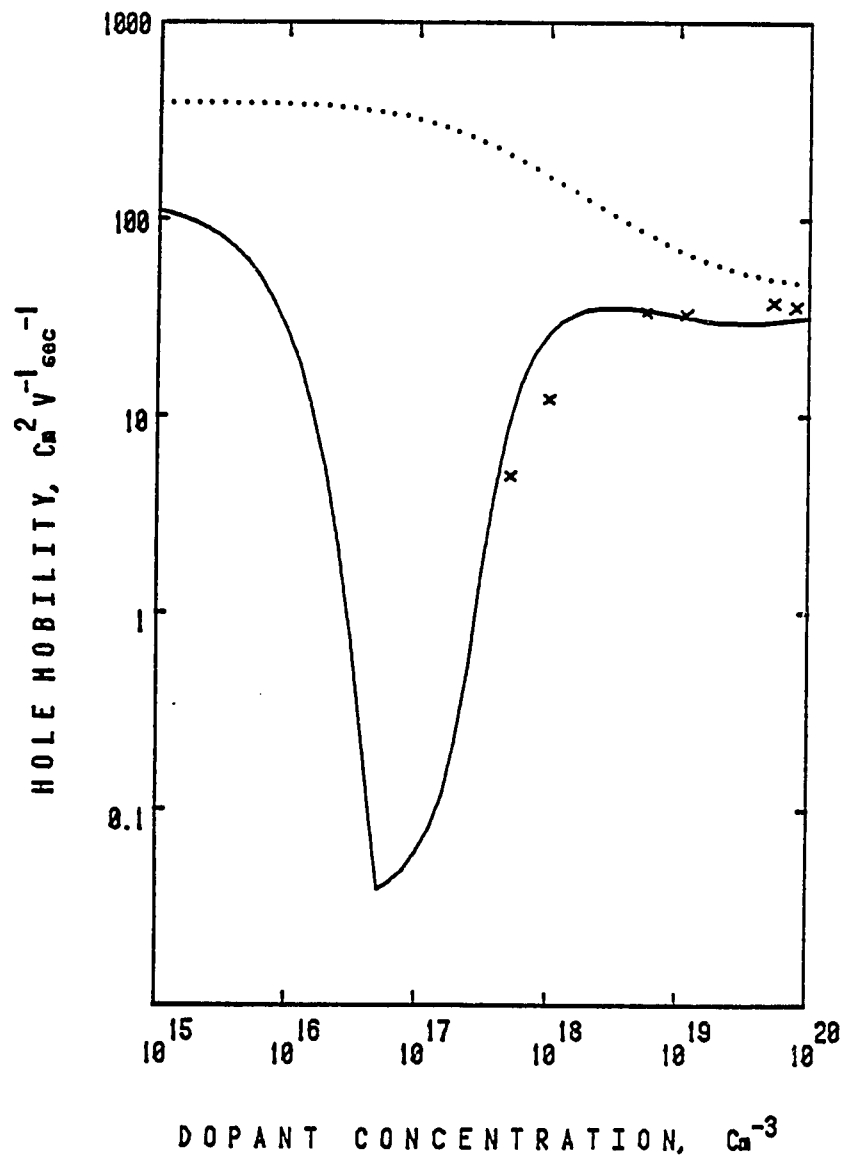


Fig. 5.4 Mobility vs. doping concentration (B-implanted poly-Si):
 x represents the data of Ref. [39] and the dotted line
 is the single crystal hole mobility.

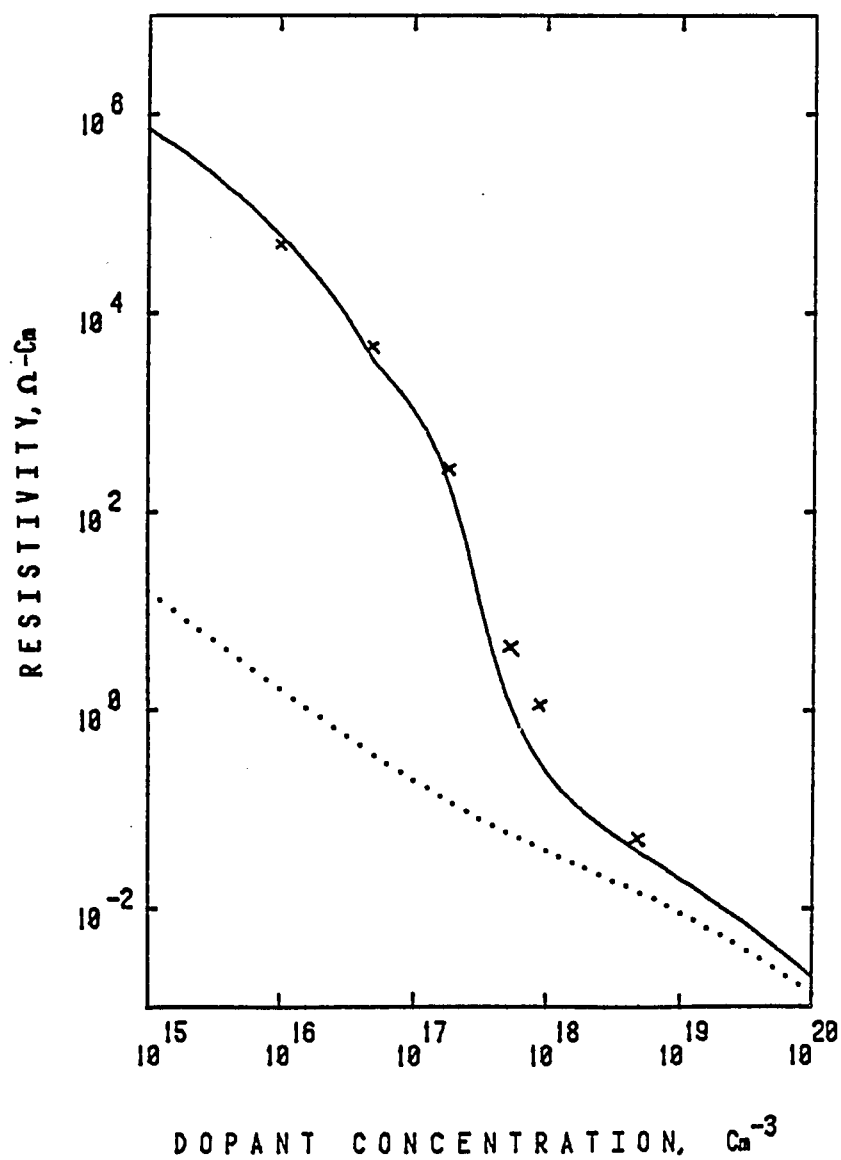


Fig. 5.5 Resistivity vs. doping concentration (B-implanted poly-Si):
 x represents the data of Ref. [39] and the dotted line
 is the crystalline resistivity.

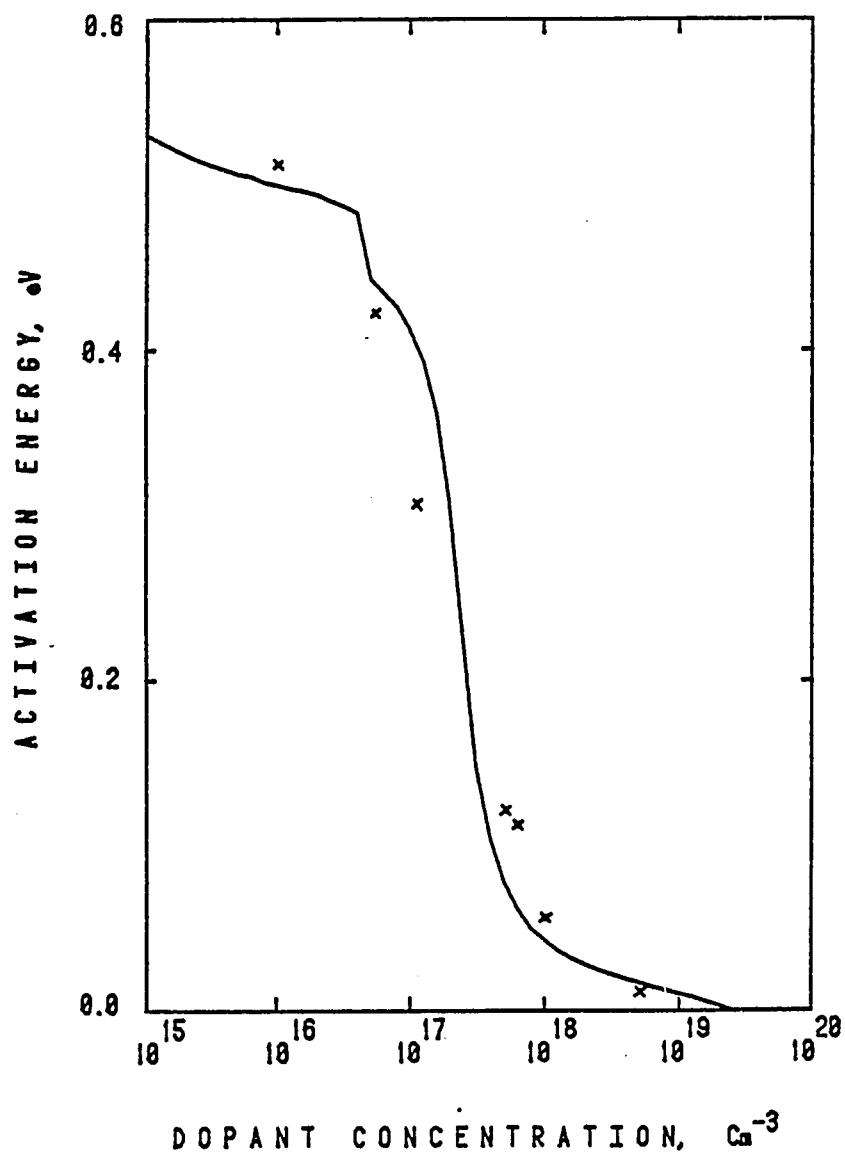


Fig. 5.6 Activation energy vs. doping concentration (B-implanted poly-Si): x represents the data of Ref. [39].

approach is that many of the inherent boundary properties should be the same regardless of the average size of the grains. This is illustrated by the fact that the theoretical curves for two sets of data in Ref. [44] and [39] have been generated, using common values for E_t , Δ_t , μ_{gb} and so forth. The only differing parameters are the measured value of L , the boundary width δ , and Q_t (Table II). This is in contrast with previous theories where a quantitative fit to the data requires significant readjustment of the artificial factor itself from $f = 0.12$ for $L \sim 250 \text{ \AA}$ in Ref. [44] to $f = 0.06$ for $L \sim 0.2 \text{ \mu m}$ in Ref. [39].

5.1.2 ρ vs. T :

A major advantage of the present theory consists of its capability in explaining comprehensively the general temperature characteristics of polysilicon resistivity. The plot of $\ln \rho$ vs. $1/kT$ is linear in the temperature range, 150°C to about -40°C . As T is lowered further, say down to -200°C , the slope appreciably changes and decreases from the high temperature value. To explain this bending trend and to simultaneously provide a physical basis for the f -factors, Lu, et al. [43] proposed that a scattering potential, $q\chi$, is associated with the grain boundary. The physical inadequacy in postulating $q\chi$ will be further dealt with separately in sec. 5.2. As mentioned earlier, if $q\chi$ is attributed to the mobility shoulder, its position should be kept independent of T as the demarcation energy level for μ_{ext} and μ_{hop} . Furthermore, since μ_{hop} is phonon-assisted it should decrease with decreasing T , while μ_{ext} should increase. These temperature characteristics make the demarcation line more prominent. The lowering of $q\chi$ with decreasing T , as adopted by Lu, et al. [43] could have been mathematically justified if μ_{ext} and μ_{hop}

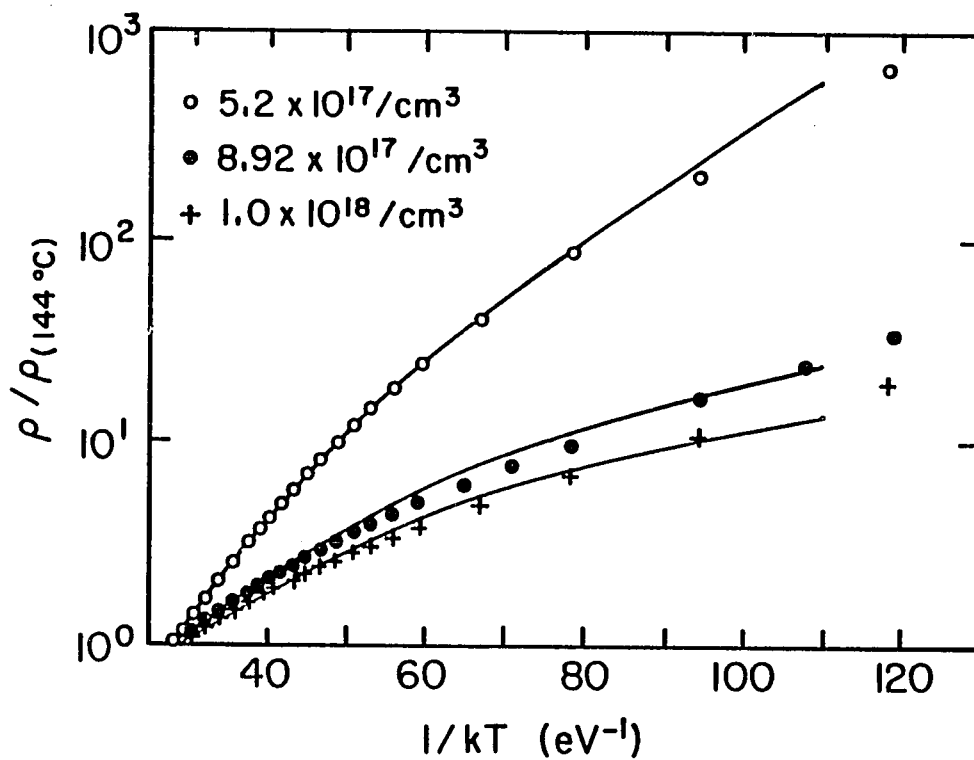


Fig. 5.7 $\ln \rho$ vs. $1/kT$ (B-implanted poly-Si): Data points are taken from Ref. [43].

approached each other with decreasing T , such that the mobility shoulder disappeared. From a practical standpoint, the necessity of continuous adjustment of χ and δ as a function of T itself is a mathematical artifice, which is not only unjustifiable but also undesirable. Furthermore, because the f -factor depends on the grain size, $q\chi$ should also depend sensitively on L , which is again hard to justify. In our model the bending of $\ln \rho$ vs. T^{-1} curve is simply explained as follows. For $Q_t \sim 10^{12} \text{ cm}^{-2}$ and $L \leq 0.3 \text{ } \mu\text{m}$, ρ is dominantly contributed by the boundary component. Also, near room temperature or above, conduction through the boundary is primarily due to μ_{ext} , as pointed out earlier. The difference in energy between E_{F0} and this conduction channel below the mobility shoulder, i.e. E_g is large, and hence the slope of $\ln \rho$ vs. T^{-1} is large. As T is lowered, Fermi statistics dictate that the prevalent channel for conduction be the hopping mode above the valence band edge and the mobility shoulder. Additionally, E_{F0} tends to be lowered with decreasing T . This results in decreasing E_g , and hence the value of the slope. Fig 5.7. shows the experimental data for $\ln \rho$ vs. T^{-1} reported in Ref. [43]. The theoretical curves have been produced, using eqn.(3.23) for ρ and eqn.(3.26) for E_{F0} , eqn.(3.2) for qV_B , and choosing an optimal set of values for μ_{ext} and μ_{hop} from the range of values available in the literature [68,69] (see Table II). The agreement between theory and experiment is excellent and we assert that our theory is equally applicable for any L , large or small. For a given set of N_A , Q_t , L , etc., the weighting factors for crystalline grain and boundary contributions to ρ are specifically given by the material and physical properties of polysilicon (see eqn.(3.23)). These general predictions of our theory can be readily tested by experiments.

We have shown that the present theory can describe unambiguously all the small signal conduction data. An additional attractive feature of this approach is the consistency of the formulation. The composite mobility and resistivity of polysilicon reduce to the corresponding values for either crystalline silicon or amorphous silicon in appropriate limits. We next discuss the physical differences between the present model and the previous theories on a more basic level.

5.2 GENERAL I-V CHARACTERISTICS FOR UNDOPED POLYSILICON

5.2.1 THEORETICAL CONSIDERATION

A fundamental difference between the present and previous theories centers around the scattering potential, qx . Note that p was initially attributed in emission models primarily to the depleted region in the grain. This led to the overestimation of current by a factor 10-20 and the necessary attenuation factor was sought by postulating qx in the boundary. The emission or tunneling process would then be further deterred by qx . The validity of emission models, therefore, hinges upon the existence of qx . In our model the major portion of p is also contributed by the boundary component for $L < 0.3 \mu\text{m}$. However, there is no qx and carriers instead diffuse or drift through the boundary medium via Brownian random scattering (μ_{ext}) or hopping (μ_{hop}). An undoped polysilicon provides a convenient testing ground for these differing viewpoints.

In undoped polysilicon, there is essentially no space charge barrier potential although the sample tends to be slightly p-type [3]. Hence, E_{F0} is pinned near midgap and the hole concentration profile in the grain and the boundary is uniform at a level p_i and p_{gbi} , respectively. Under

a bias, the band edge and the imref should undergo parallel linear shifts in a manner similar to the crystalline case, except that there are two slopes to keep J constant, in the grain ($\mu_c p_i$) and in the boundary ($\mu_{gb} p_{gbi}$) (Fig. 5.8). Because of these parallel shifts, the equilibrium carrier profile remains unchanged for any V_a . In this case, eqn.(3.5) representing the hole current, $J_p = \mu p \partial E_f / \partial x$ simplifies to,

$$J_p \int_{-\frac{1}{2}L}^{\frac{1}{2}L} \frac{1}{\mu p} dx = E_F(\frac{1}{2}L) - E_F(-\frac{1}{2}L) . \quad (5.1)$$

Dividing the x -interval into grain and boundary regions, in each of which μp is constant, and identifying $qV_a = E_F(L/2) - E_F(-L/2)$ one finds

$$J = q p_i \left[\mu_c / \left(1 - \frac{\delta}{L} + \frac{\delta}{L} \mu_c p_i \mu_{gb} p_{gbi} \right) \right] \frac{V_a}{L} . \quad (5.2)$$

Here, the third term in the denominator can be explicitly read off from Table I as a special case where $qV_B = 0$. The electron current density can also be obtained from eqn.(5.2) with an obvious replacement of the proper quantities. The total current is due to these two components:

$$J_{total} = J_p + J_n \quad (5.3)$$

An important conclusion is that J-V relationship in the present theory is strictly linear in undoped polysilicon for arbitrary applied voltage, provided the electrical field at any point does not exceed the critical field strength for breakdown. This is in direct contrast with the distinctly nonlinear I-V behavior predicted by emission theories (see eqn.(1.15)). Because there is no space charge potential in this case, the nonlinearity, if any, should strictly be due to qx [43]. A careful measurement of current as a function of voltage will, therefore, provide

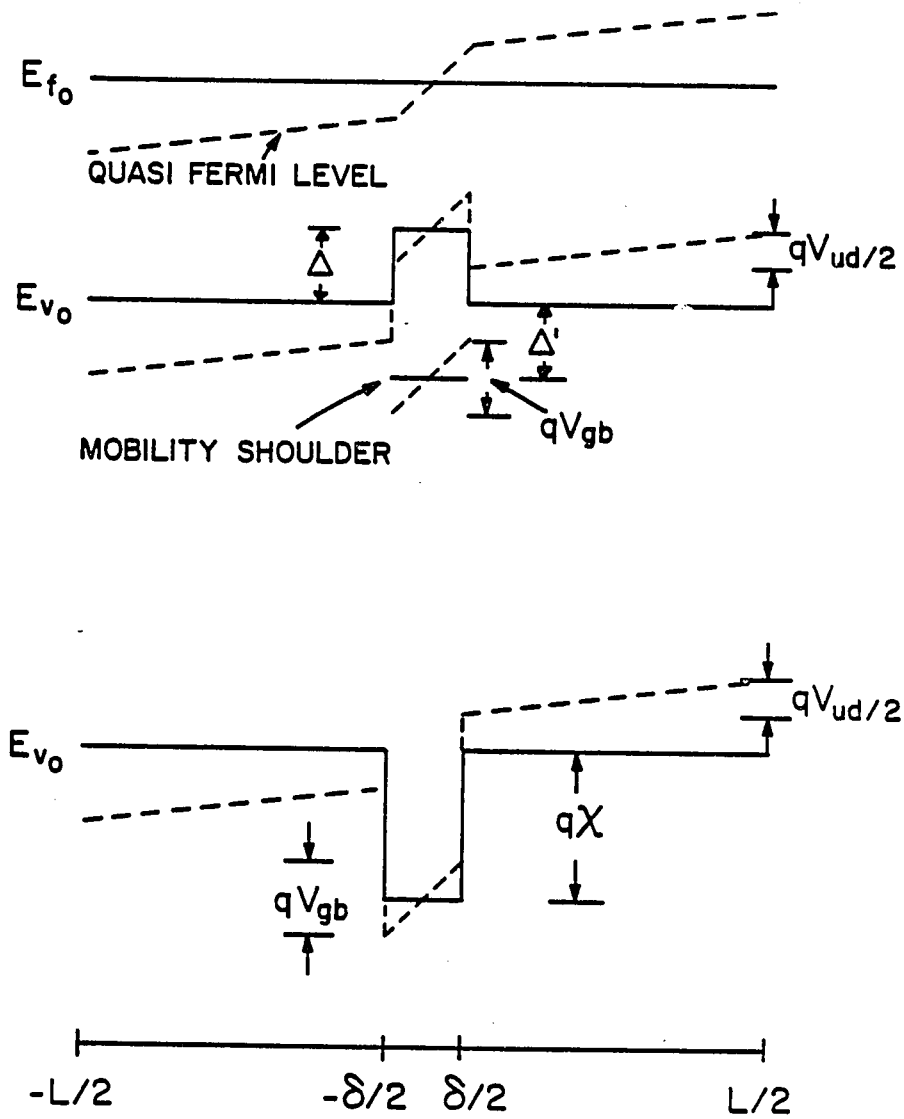


Fig. 5.8 Energy level diagram of a unit cell in undoped poly-Si under equilibrium and biased conditions. The corresponding energy diagram of Ref. [43] is also shown.

an unambiguous experimental test for these two different predictions.

5.2.2 EXPERIMENTAL DATA

Test resistor structures for I-V measurements are usually fabricated with heavily doped contact pads. For the case of undoped polysilicon the current measured is then due to two n^+-i or p^+-i junctions operating in forward and reverse bias modes in series with the resistor. The effect of these two junctions have been normally neglected in I-V analysis. However, these two junctions could significantly mask the intrinsic I-V characteristics of polysilicon, as has been detailed by Mahan, et al. [3]. In our I-V measurement these complications have been bypassed by resorting to the two point spreading resistance probe technique [81]. Undoped $0.4\text{ }\mu\text{m}$ polysilicon films were deposited via LPCVD technique unto $1\text{ }\mu\text{m}$ SiO_2 layer thermally grown on a p-type silicon wafer. Two probe points ($25\text{ }\mu\text{m}$ in diameter) were pressure contacted onto the film at a distance $50\text{ }\mu\text{m}$ apart (defined between two nearest rims). For a given applied voltage, current flowing into and out of probe pads was measured. For each set of V,I, 100 independent measurements were performed on the same slice and the resulting mean values and standard deviations were recorded. Because the thickness, t of the film deposited on an insulating layer is much less than the probe radius, a , the current is essentially two dimensional. The measured resistance, $\Delta V/I$ can therefore be converted to the resistivity via the correction factor [81],

$$\rho = (\Delta V/I)\pi t / \ln(2s/a) \quad (5.4)$$

s being the distance between two center points of probe pads. The quantity, a , represents in practice the effective contact radius: because it

enters eqn.(5.4) via \ln -format, an uncertainty in a , by a factor as much as 2 still does not affect ρ appreciably.

In Fig. 5.9 we present the resistance, $\Delta V/I$ and the corresponding I-V data obtained in the voltage range, 0-90 V. The current is clearly seen to exhibit a strictly linear response to applied voltage. Also there is no voltage dependence of R over the entire range of V . The slight dip of R for small V may perhaps be due to the contact potential between the probe pad and the film. The voltage range used was sufficiently large, so that the grain voltage ($L \sim 300 \text{ \AA}$) covered a range of 2 times the value of kT/q at room temperature. Also, we have chosen a geometry, in which the potential drop across the film between two probe points ($\ln r/a$) did not depart appreciably from linearity. Hence, the averaging effect arising from locally varying electric field was minimal. Additionally, because of the extremely high sheet resistivity involved in our measurement the problem of contact resistance, R_c does not appear to significantly affect the data. The effect of R_c , if any, could have resulted in nonlinear I-V behavior. The resistivity value obtained via eqn.(5.4) is about $0.9 \text{ M}\Omega \text{ cm}$. This value is consistent with the result reported by Seto [41] in the limit of a low dopant concentration. This lends further credence to our resistance measurement and the corresponding I-V data.

The resistivity of undoped polysilicon can be theoretically estimated from eqn.(5.3). By using the intrinsic crystalline mobilities for electrons and holes, and $\mu_{gb} \sim \mu_{ext} = 10 \text{ cm}^2 \text{ V}^{-1}$ for both electrons and holes and with the choice of $\delta \sim 10 \text{ \AA}$, $L \sim 300 \text{ \AA}$, ρ is found to be about $0.76 \text{ M}\Omega \text{ cm}$. This remarkable agreement between theoretical and experimental ρ -values appears to provide additional evidence for the extended

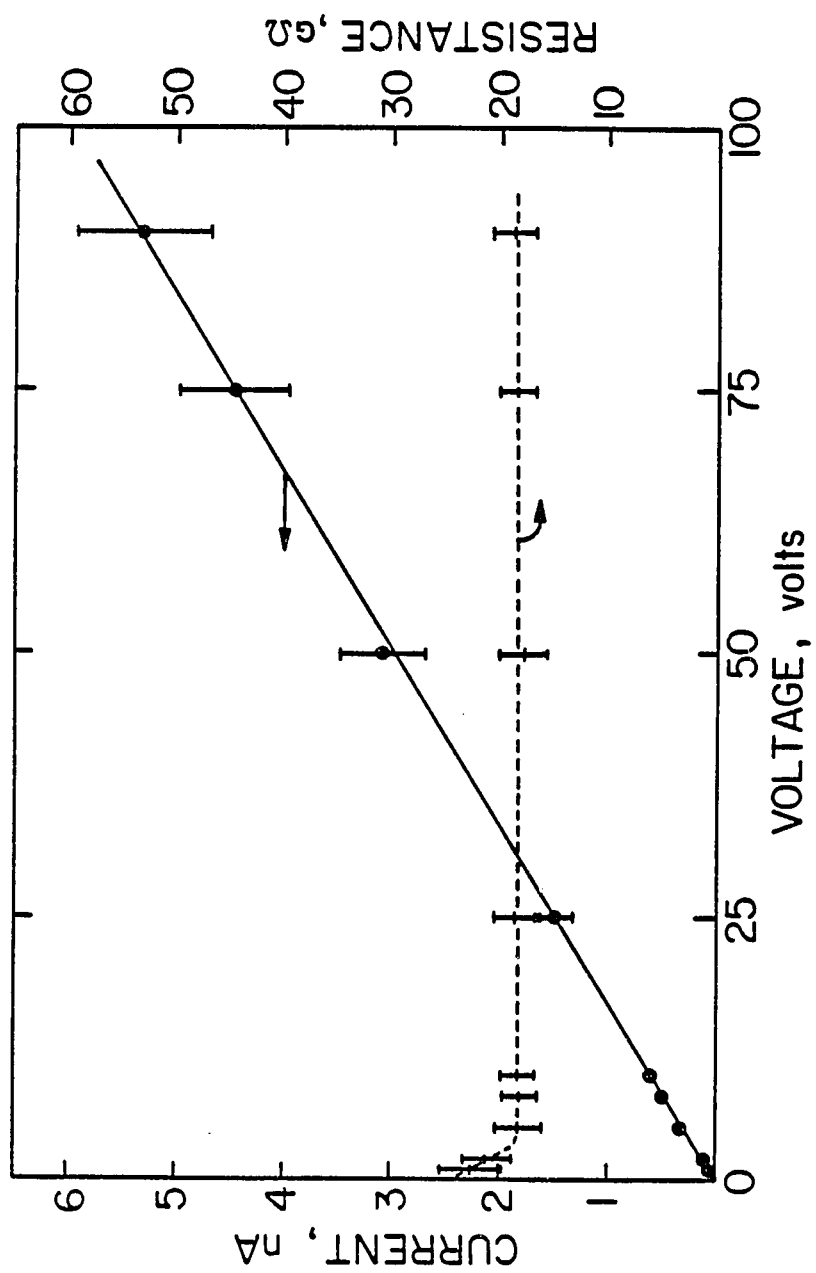


Fig. 5.9 Current and resistance vs. applied voltage in undoped poly-Si.

state mobility operative within the grain boundary. More importantly, the strictly linear I-V data constitutes a direct experimental evidence against the existence of q . Rather, the data explicitly supports the viewpoint that the boundary is a high resistivity conducting medium.

5.2.3 COMPARISON WITH EXPERIMENTAL DATA OF Ref. [3]

We now correlate our data with the I-V curves taken by Mahan, et al. [3], using resistors of varying lengths fabricated in undoped polysilicon. Their work explicitly showed the significant role played by back-to-back $n^+ - i$ junctions operating in series with resistors. Because of this we have reproduced in Fig. 5.10 their I-V data. Mahan et al modeled the resulting I-V behavior, based on the avalanche breakdown of the reverse-biased $n^+ - i$ junction together with the hyperbolic sine functional I-V relationship within the resistor. The theoretical fit to the data achieved within a narrow voltage range (0-10 V) remains unsatisfactory, and furthermore the disagreement becomes extremely severe when both curves are extrapolated to the high voltage range, where the nonlinear voltage drop across the resistor, if operative, could have been a dominant factor.

A quantitative analysis of I-V data requires a theory applicable to junction diodes fabricated in polysilicon. Such a theory is not available at present. Furthermore, the performances of junction diodes in polysilicon are generally characterized by widely varying I-V behavior, depending on annealing conditions used. Nevertheless, the intrinsic I-V data for undoped polysilicon can be extracted with the assumption, that $n^+ - i$ diodes are more or less similar in behavior for all resistors fabricated. In the I-V data by Mahan et al we consider only the current range

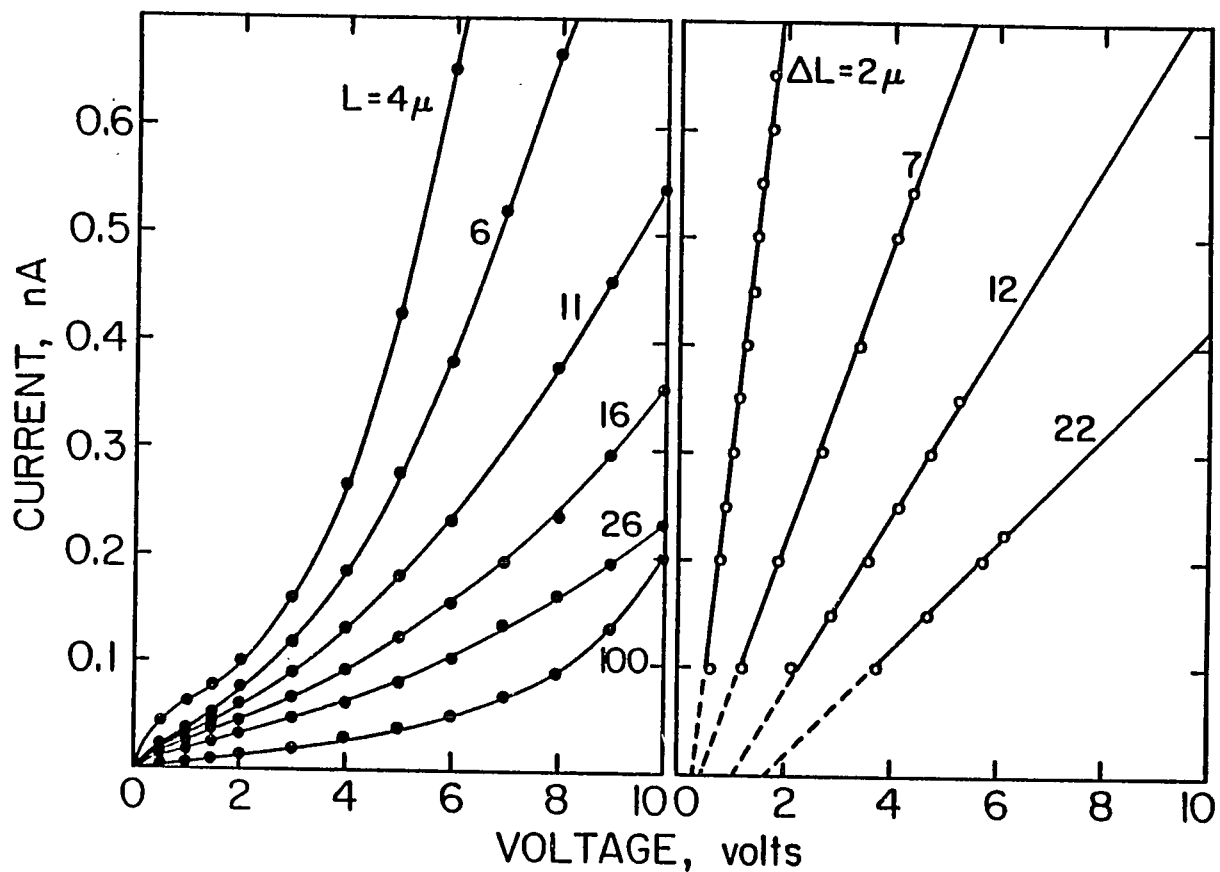


Fig. 5.10 Current vs. applied voltage in undoped poly-Si: The I-V curves on the left are for $(n^+ - i)$ -resistor- $(i - n^+)$ system reported in [3]. Curves on the right are extracted I-V data for resistor only. The cross-sectional area of the resistor is $4 \times 10^{-8} \text{ cm}^2$.

beyond 0.1 na, which is believed to be beyond the breakdown voltage for the reverse-biased n^+-i junction. We next choose two I-V curves corresponding to two different resistors and read off the voltage difference, ΔV between the curves at a fixed current. Now, we have two nominally identical forward biased junctions operating at the same current but connected to two different resistors, whose difference in length is, say Δl . Clearly, ΔV is then the amount of extra voltage required to compensate the additional voltage drop across a resistor of length Δl . By finding ΔV 's for different currents and plotting I vs. ΔV one can extract the inherent I-V characteristics for polysilicon resistors.

In view of the absence of n^+-i junction diode theory in polysilicon, this graphical procedure is essential. In Fig. 5.10 we have plotted several sets of I-V data for undoped polysilicon which have been extracted in the manner described above. We have chosen the I-V curve for resistor with 4 μm nominal length as the reference line and found ΔV for all other curves above 0.2 nA current. These data points are clearly seen to be accurately described by straight lines, which is in contrast to the predictions of the thermionic emission theory. The resistivity is easily determined from the slopes of these lines and was found to be $0.4 \pm 0.043 \text{ M}\Omega \text{ cm}$, a value smaller than our result by a factor of about 2. These curves do not go through the origin perhaps because of the slightly different breakdown voltages of n^+-i junctions.

5.3 DISCUSSION: SMALL SIGNAL THEORY

We have shown by comparison with different and independent experimental data that the concept of $q\chi$ in the context of tunneling or emission is not valid. This entails a few fundamental theoretical

implications. If there does not exist q_x on top of the conduction and/or valence band edge for undoped polysilicon where $qV_B = 0$, obviously emission approaches can not be adopted to describe current. Rather, the drift and diffusion theory is the only alternative approach available in this case. Furthermore, the barrier potential, qV_B does not increase rapidly with increasing doping level especially for small grains. This suggests that over a substantial range ($10^{15} - 10^{17} \text{ cm}^{-3}$ for $L \approx 250 \text{ \AA}$) of dopant concentration conduction mechanisms for polysilicon are more or less similar to those in the undoped case. This unavoidably raises the question; at what doping density does emission model become operative? As mentioned earlier, the boundary resistivity for the case of small grain size is the dominant component of ρ . Modeling this component by postulating q_x in conjunction with the emission mode of conduction is based implicitly on two additional assumptions: (i) carrier mobility (μ_{ext}) in the energy range beyond q_x or, equivalently mobility shoulder is the same as the crystalline grain region (same m^*) and (ii) there is no density of states for carriers within q_x so that the tunneling probability can be calculated, using WKB approximation. We have pointed out in detail that these assumptions are not compatible with the concept of mobility shoulder.

Our alternative approach bypasses these theoretical difficulties in a simple manner. In our model the unit cell consists of two conducting media and current is explicitly described via various mobilities involved. Specifically, μ_{ext} , μ_{hop} or μ_{tun} are much less than μ_c , and hence there is no need for attenuation factors in various formats. It is further pointed out that these mobilities are based on scattering potential but on a microscopic level, viz molecular scattering potentials.

This approach has been extended to describe the high field conduction processes, as will be discussed in detail in sec.5.5. Also, the expressions for ρ and μ derived in eqn.(3.21) and eqn.(3.23), respectively, provide a convenient basis, with which to consider the electrical properties of large grain polysilicon system.

5.4 EFFECT OF LASER RESTRUCTURING AND GRAIN BOUNDARY ALTERATION

We examine in this section the effect of laser restructuring on polysilicon. The primary result of laser processing of polysilicon is to increase the grain size. Without resorting to techniques such as lateral or vertical seeding, spatial or temporal temperature profile shaping or encapsulation, i.e., with random nucleation during laser recrystallization, one can change the grain size from a few hundred Å's to typically 2 to 10 μ m. This has been extensively reported [33-36], using either cw or pulsed laser processing. Concurrently with this increase in grain size, one may also expect that the melting and recrystallization processes substantially modify and, most likely, decrease the trap density at the grain boundaries, although no experimental observations have been reported to that effect. This trap density is a key parameter affecting the overall electrical performance of polysilicon and can be modified with the use of other alteration techniques such as plasma passivation. It is, therefore, important to examine the ensuing changes in electrical properties, specifically ρ and μ over a wide range of L and Q_t .

5.4.1 EFFECTS OF INCREASING L

In Fig. 5.11 we have plotted ρ vs. N_A for different grain sizes at a fixed Q_t ($3 \cdot 10^{12} \text{ cm}^{-2}$). ρ decreases monotonically with increasing N_A for the reasons discussed in sec. 3.2. The rate with which ρ decreases is rather drastic near N^* . This is partly due to the abrupt depletion approximation used in the analysis. In this approximation, the hole concentration at the grain center, $p(-L/2)$ changes abruptly across N^* , and gives rise to the sharp reduction in ρ . Incorporation of the mobile holes present in the grain in the charge neutrality condition naturally could have rendered the change in ρ near N^* considerably less pronounced. The effect of increasing grain size, L at a fixed Q_t is to shift N^* to the left on the N_A -axis. This is understandable because N^* can be accurately estimated by a simplified charge neutrality condition, i.e., $Q_t^+ \simeq N^* L$. Additionally, with increasing L , ρ is substantially reduced. For instance, at $N_A = 10^{15} \text{ cm}^{-3}$ ρ decreases from about $2 \text{ M}\Omega \text{ cm}$ at $L = 500 \text{ \AA}$ to about $5 \text{ K}\Omega \text{ cm}$ at $L = 10 \text{ }\mu\text{m}$, a reduction factor of 400. Also, above N^* the ρ -value becomes essentially identical to single crystal value with increasing L as the mobility shoulder goes up allowing extended state conduction through the grain boundaries. These general trends can be understood by recalling that ρ is a composite quantity contributed by both the crystalline grain and boundary components. Increasing L , therefore, physically corresponds to increasing the weighting factor of the crystalline component and ρ tends to resemble the crystalline case.

In Fig. 5.12 we present the room temperature μ vs. N_A curves for the same set of grain sizes and same Q_t as in Fig. 12. Note the appreciable and systematic shift of the mobility dip toward lower dopant concentration with increasing L . This is because the mobility dip occurs near N^* and N_{sup}^* shifts to the left on the N_A -axis with increasing L . For a

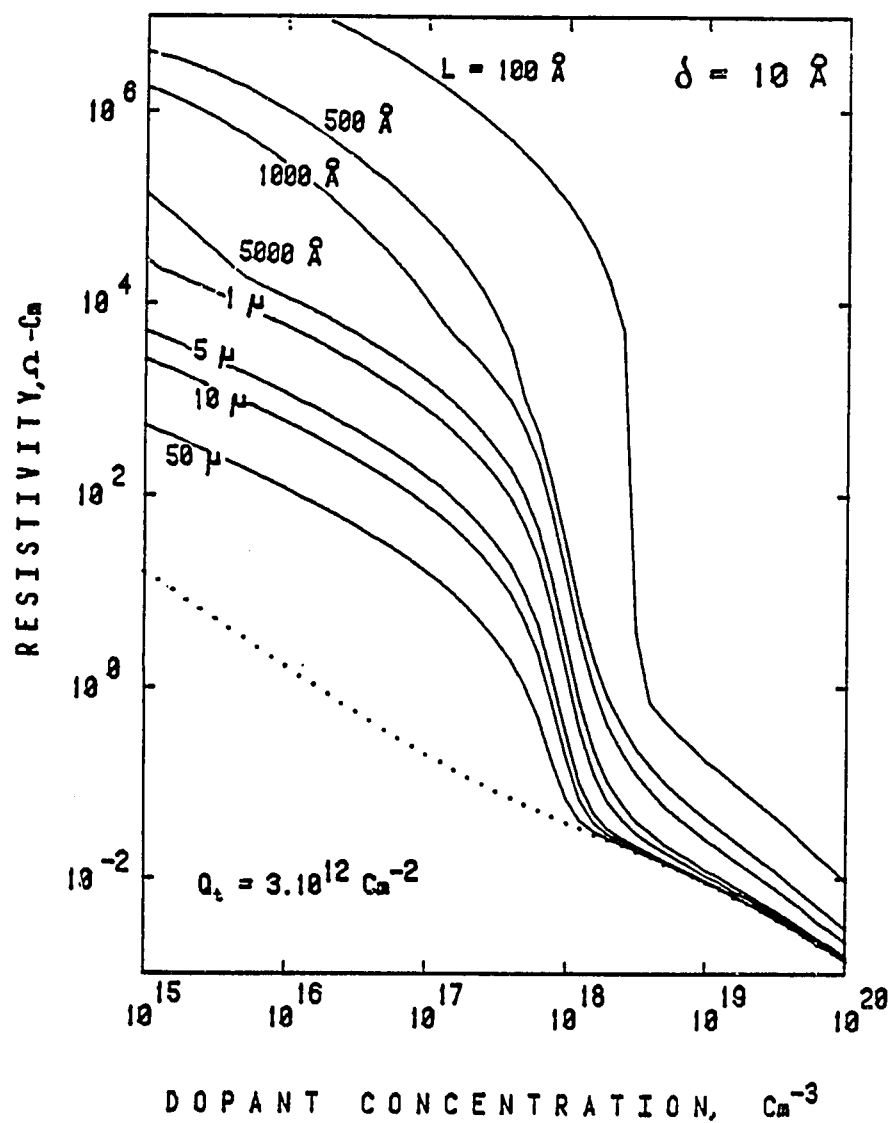


Fig. 5.11 Theoretical ρ vs. N_A for different L .

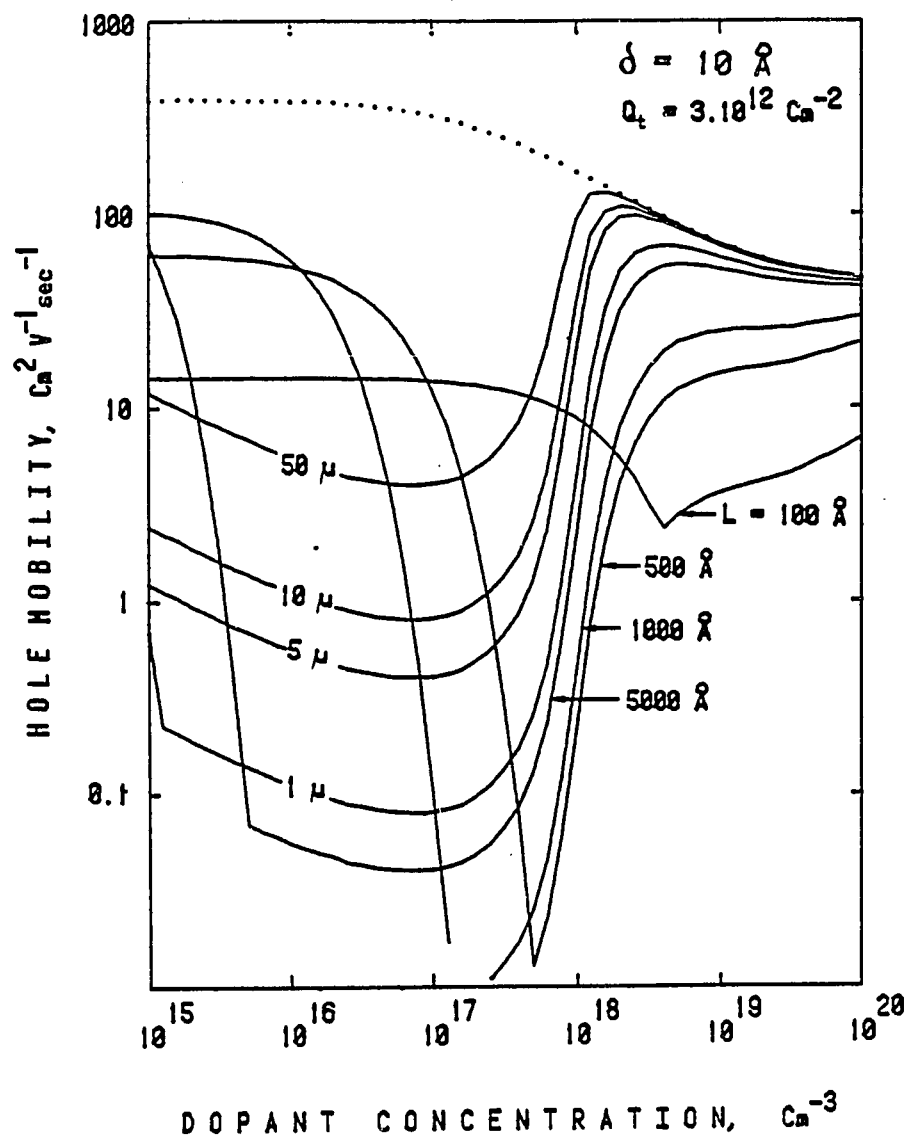


Fig. 5.12 Theoretical μ vs. N_A for different L .

small grain size, say $L = 100 \text{ \AA}$, mobility, at a level smaller than the μ_c values, varies only by a factor of about 10 over the entire range of N_A considered. The conduction in this case is entirely dominated by the inherent grain boundary properties, as mentioned earlier. As L is increased to about 3000 \AA , the mobility dip significantly enhances and μ varies by as much as 4 orders of magnitudes over the same N_A range. This is explained in terms of the barrier potential; qV_B , in this case is generated over a broad depletion depth into a large value near N^* ($\sim 0.3 \text{ eV}$) and severely reduces the number of holes available for the extended state conduction. At this value of N^* all trap states are saturated. Increasing N_A above N^* should, therefore, result in decreasing W according to $Q_t^+ \sim 2N_A W$. Consequently, $qV_B W^2$ decreases rapidly and also the amount of mobile holes in the grain also increases, i.e. $p(-L/2) = N_A$. Hence, μ should rise rapidly and become identical to the corresponding μ_c with increasing L . With further increase in L into the μm region, the mobility dip flattens and persists over an increasingly broader N_A range. This interesting new result can again be explained in terms of qV_B and the Fermi statistics. For a large L , N^* occurs at a low doping density. At this concentration the Fermi level is not lowered sufficiently to saturate the entire trap level. Any further increase in N_A is, therefore, accompanied by two opposing processes; it provides additional holes in unoccupied trap levels and qV_B grows linearly with N_A with its depletion depth pinned at $L/2$. Simultaneously, $p(-L/2)$ increases in direct proportion to N_A . These two opposite tendencies built into the mobility expression nearly compensate each other to keep the mobility dip flat until all the trap levels are saturated. Beyond this N_A value, qV_B again rapidly reduces and the polysilicon mobility rises to a level practically

identical to μ_c . The minimum μ -value at the dip is, in turn, determined by the system weighting factors for both crystalline and boundary components in μ . For the case of mobility, the effect of increasing grain size is not as straightforward as in the case of ρ . For a low dopant concentration, for example, the increase in L could actually reduce the mobility value rather than enhancing it.

5.4.2 EFFECT OF DECREASING Q_t

Figure 5.13 presents the ρ vs. N_A curves for several different Q_t values for small grain polysilicon ($L = 500 \text{ \AA}$). With decreasing trap density the ρ -values substantially reduce, as expected. Note, however, that regardless of the Q_t value considered, ρ remains considerably larger than ρ_c even in the limit of heavy doping. This is again due to the large boundary resistivity, ρ_{gb} ; in a small grain the maximum achievable weighting factor for the crystalline grain component is not sufficient to mask the effect of ρ_{gb} . In Fig. 5.14 the corresponding mobility curves are presented. With decreasing Q_t the mobility dip is suppressed, as anticipated. Nevertheless, μ remains considerably smaller than μ_c for the same reasons as mentioned above, even in the limit of zero trap density, hence no barrier potential.

5.4.3 COMBINED EFFECT OF CHANGING L AND Q_t

In Figs. 5.15 and 5.16 are shown the room temperature ρ and μ curves vs. N_A for the identical set of Q_t -values as in Figs. 5.13, 5.14. The only change in the parameter values used was to increase L from 500 \AA to 5 \mu m . As can be clearly observed, the effect of decreasing trap density in a large grain polysilicon is much more pronounced and attractive. For

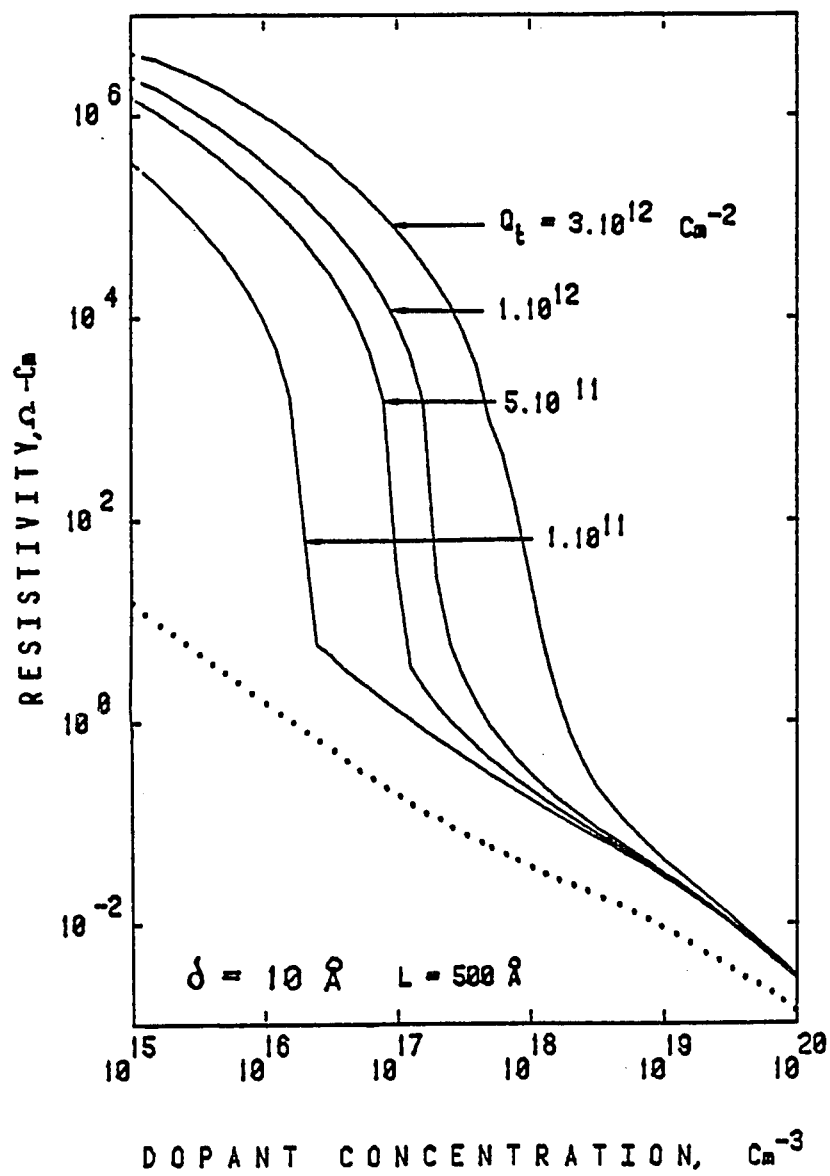


Fig. 5.13 Theoretical ρ vs. N_A for different Q_t .

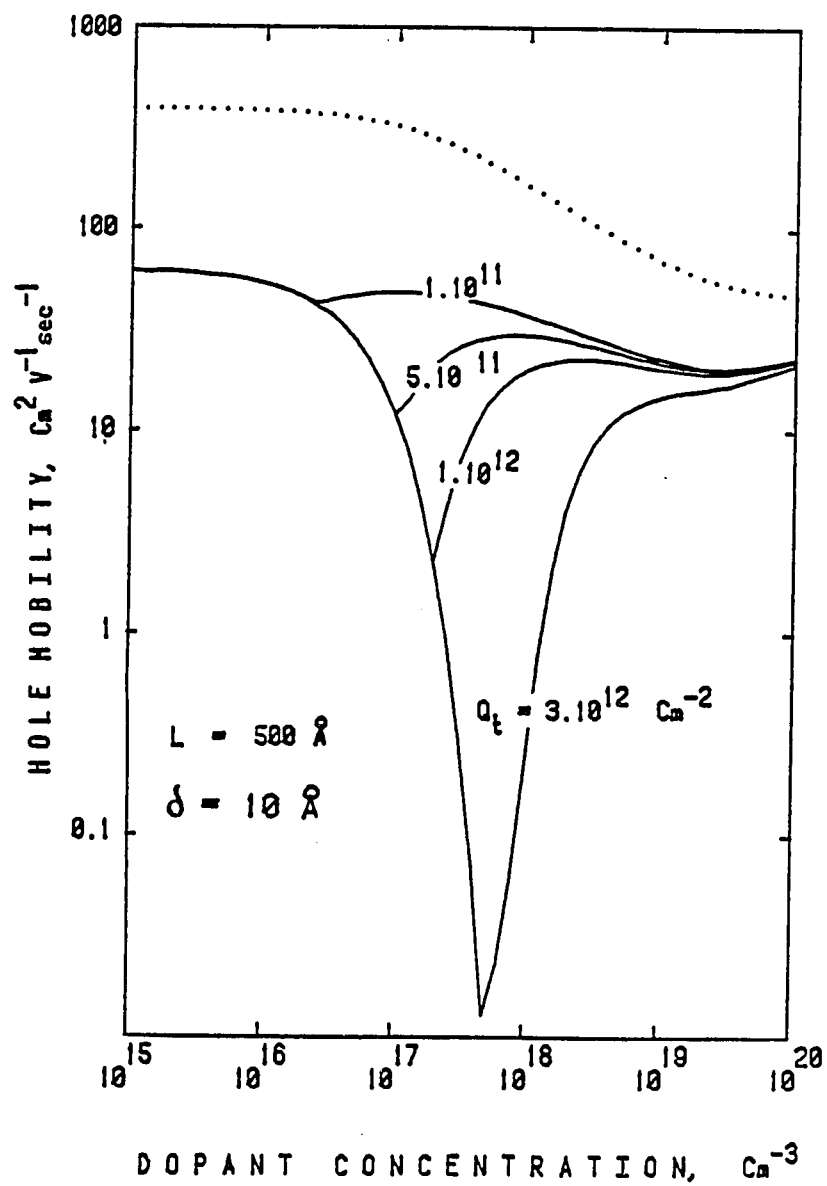


Fig. 5.14 Theoretical μ vs. N_A for different Q_t .

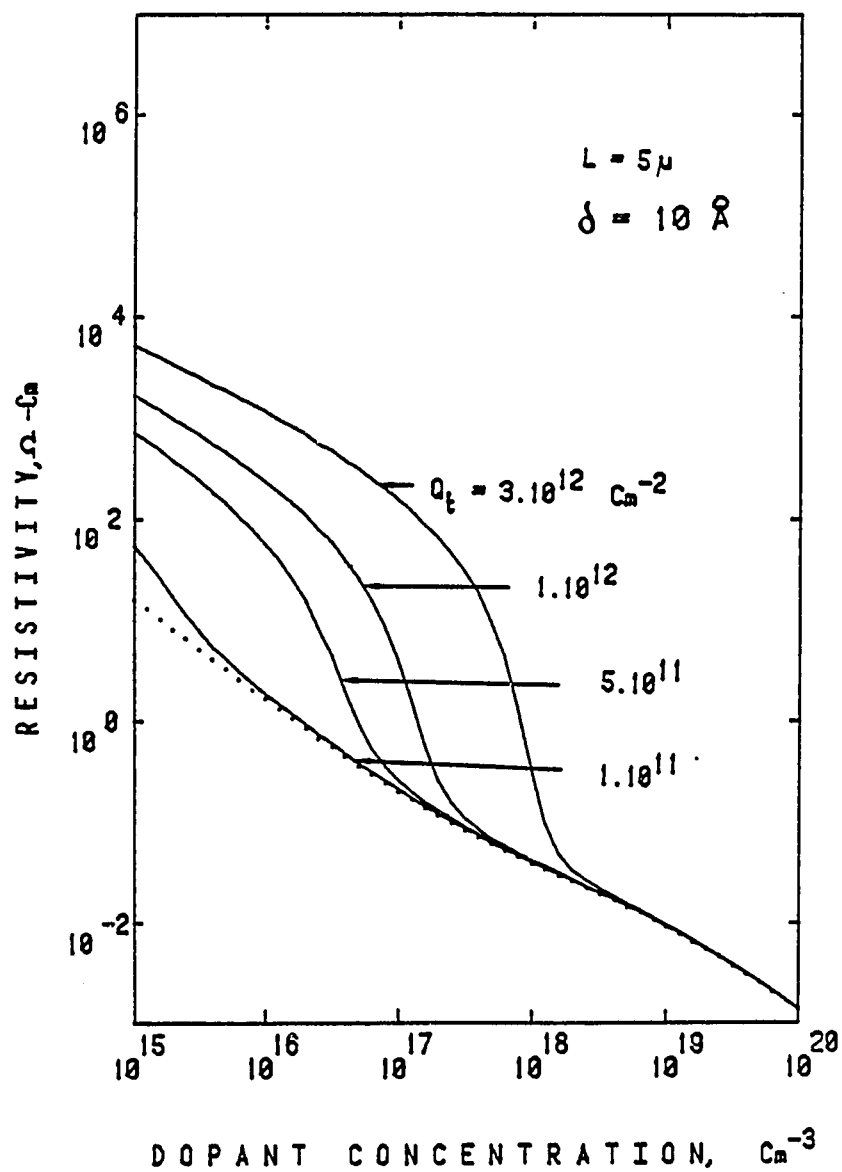


Fig. 5.15 Theoretical ρ vs. N_A for different Q_t .

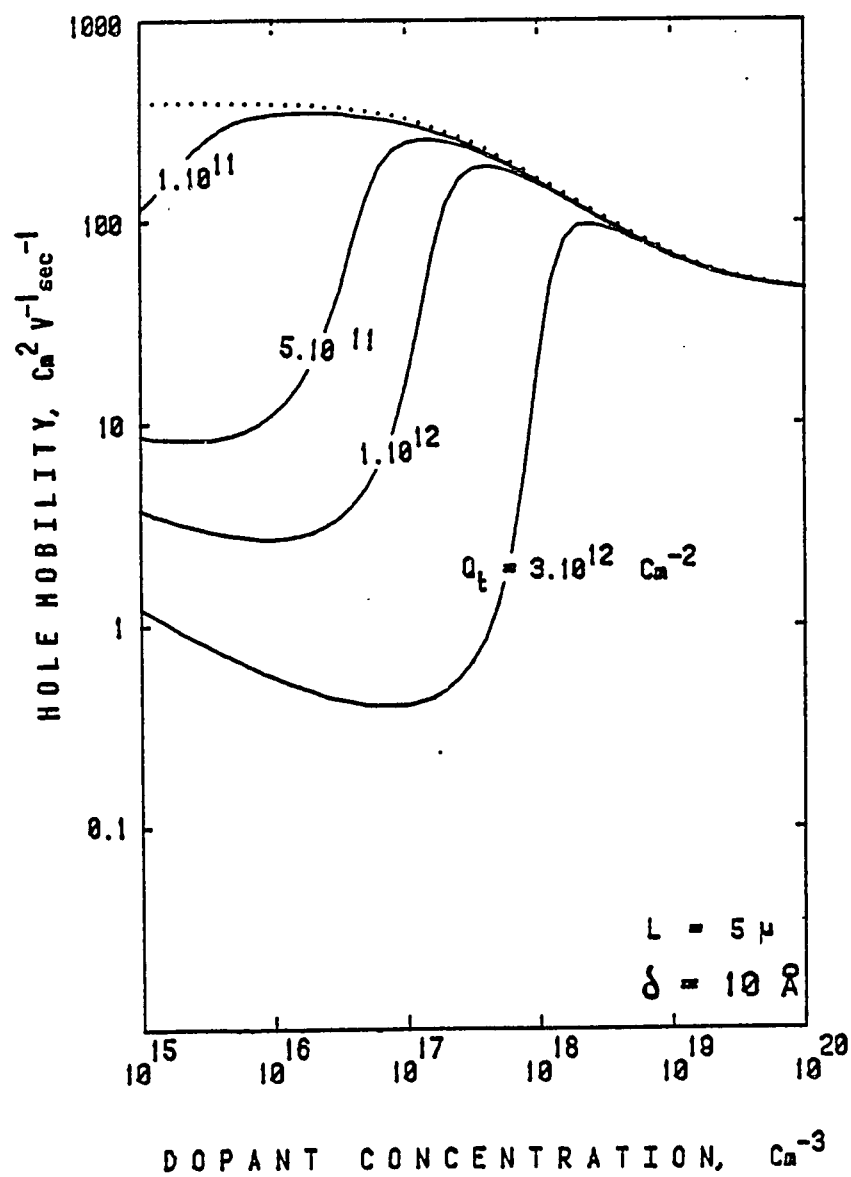


Fig. 5.16 Theoretical μ vs. N_A for different Q_t .

instance, if the trap density can be altered and reduced from a level, say 10^{12} cm^{-2} , a value typical of LPCVD polysilicon to about 10^{11} cm^{-2} , the resulting conductivity could become essentially identical to the crystalline value over the entire range of dopant concentration used for device fabrication. This brings out an interesting conclusion, namely that an efficient boundary alteration technique, if used concurrently with laser recrystallization techniques could generate a device quality film from LPCVD polysilicon.

5.5 COMPARISON WITH EXPERIMENT: GENERAL J-V CHARACTERISTICS

We have derived in eqn.(4.19) a general expression for current density, incorporating the voltage-driven redistribution of mobile holes in the grain and phenomenologically accounting for electrical switching processes in the boundary for high applied voltage. Note that at low voltages ($qV_a < kT$) this expression naturally reduces to the corresponding small signal result derived in chapter (eqn.(3.20)). We have also introduced a critical voltage, V_a^m , so that J in our formulation never exceeds the corresponding crystalline value. This theoretical consistency and appropriate incorporation of essential physical mechanisms is in contrast with the general I-V theory of Lu, et al [39,55].

We now present theoretical results. These results are obtained as follows. Given average grain size, L and dopant concentration, N_A the charge neutrality condition (eqn.(3.26) and Table I in chapter 3 is used to determine such quantities as $p(-L/2)$, qV_B , W , etc. These values are inserted into appropriate equations, together with the values for μ_c and μ_{gb} . The description of J in terms of the input voltage, V_a , is then complete with an explicit specification of $\sigma_{gb}(V_{gb})$. The switching

effect is generally attributed to electrothermal processes in amorphous thin films [72-73]. According to this model, high-field injection of carriers leads to the formation of filamentary conducting channel. The subsequent spatial and temporal growth of this filament induces an avalanche-like breakdown condition. There have been proposed various empirical expressions, which model this field enhanced conductivity. From the I-V standpoint, these expressions should describe approximately linear growth of I for small V with a slope characteristic of high resistivity medium, followed by a sharp increase in I near the threshold voltage for switching. We model this field-dependent conductivity, $\sigma_{gb}(V_{gb})$, in a manner analogous to the junction breakdown [83]:

$$\sigma_{gb}(V_{gb}) = \sigma_{gb}(0)[1 - (V_{gb}/V_{gbc})^n]^{-1} \quad (5.5)$$

Here, $\sigma_{gb}(0)$ is given by eqn.(4.16) and describes the actual boundary resistivity for $V_{gb}/V_{gbc} \ll 1$; V_{gbc} represents the critical voltage for threshold and/or memory switching and n is a parameter which determines how sharply the transition in I-V characteristic occurs near V_{gbc} . We have taken $V_{gbc} = 0.16$ volts for 16 \AA boundary width, corresponding to a value of critical field 10^6 V/cm and the parameter, n was taken to be 3. In all of the following discussions we have chosen a resistor bar of length $40 \text{ }\mu\text{m}$ and average grain size of $0.275 \text{ }\mu\text{m}$, and $Q_t = 10^{12} \text{ cm}^{-2}$.

5.5.1 VOLTAGE PARTITION

In Figure 5.17 the fractional voltages, V_{ud}/V_a , V_d/V_a , V_{gb}/V_a , dropped across the unit cells are plotted vs. N_A for fixed, L , Q_t and at room temperature and for small grain voltage ($V_a \approx 0.07 \text{ volt}$). For low dopant concentration ($N_A < N^*$) there is no undepleted region and V_a is

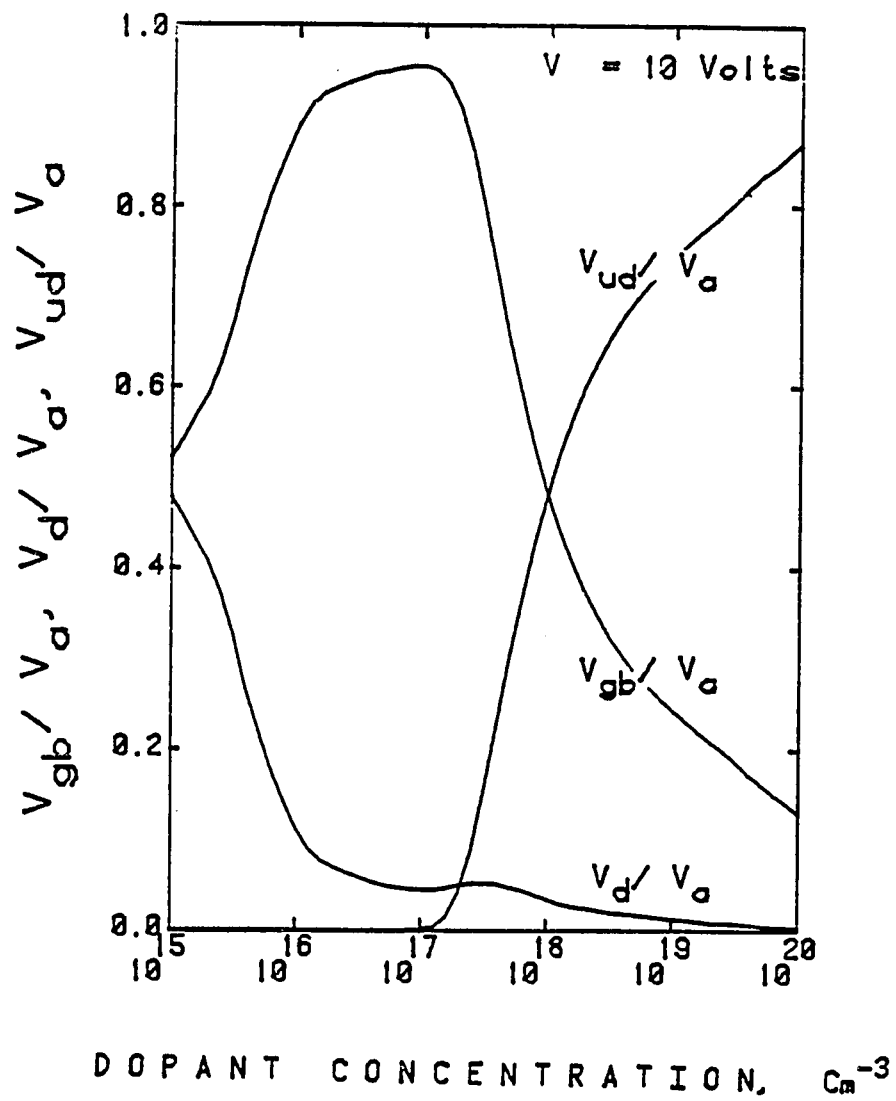


Fig. 5.17 Voltage partition in a unit cell vs. dopant concentration for $V_a = 0.07$ volt.

dropped across the total depletion depth (V_d) and the grain boundary (V_{gb}). With N_A increasing, qV_B grows linearly and the boundary resistivity, ρ_{gb} , significantly enhances because of the decrease in hole concentration beyond the mobility shoulder. Therefore, V_{gb}/V_a should increase to keep J constant within the unit cell. Once the trap states are saturated, the depletion depth, W shrinks and qV_B rapidly decreases with further increase in N_A . In this case the voltage fraction, V_{ud}/V_a assigned to the undepleted region becomes significant and V_{ud} takes up the major portion of V_a in the limit of high doping density. Note that in this voltage range V_d is always less than V_{gb} over the entire doping range considered. Equivalently, the resistivity contributed by the depleted region is less than the boundary resistivity. However this trend is drastically changed as the applied voltage is increased. In Figure 5.18 we present these fractional voltages vs. N_A for larger applied voltage ($V_a \approx 0.35$ volts). Note that, for low dopant concentration ($N_A < N^*$), V_d constitutes a larger fraction of V_a than V_{gb} . Also the growth of V_{gb}/V_a with increasing N_A is significantly suppressed. This can be understood in terms of two competing physical mechanisms operative in this voltage range; (i) lowering of mobility shoulder with increasing qV_B and accompanying increase in ρ_{gb} and (ii) considerable reduction of effective boundary resistivity arising from field enhanced conductivity, as V_{gb} approaches V_{gbc} . For $N_A > N^*$, the undepleted region in the grain again shares an increasingly appreciable fraction of V_a for the same reasons as discussed above. In Figure 5.19 we present the voltage partitioning for a very large applied voltage ($V_a \approx 0.7$ volt). Below N^* , V_d constitutes now a major portion of V_a , while V_{gb}/V_a has been reduced drastically to a small value. This reversed situation of voltage

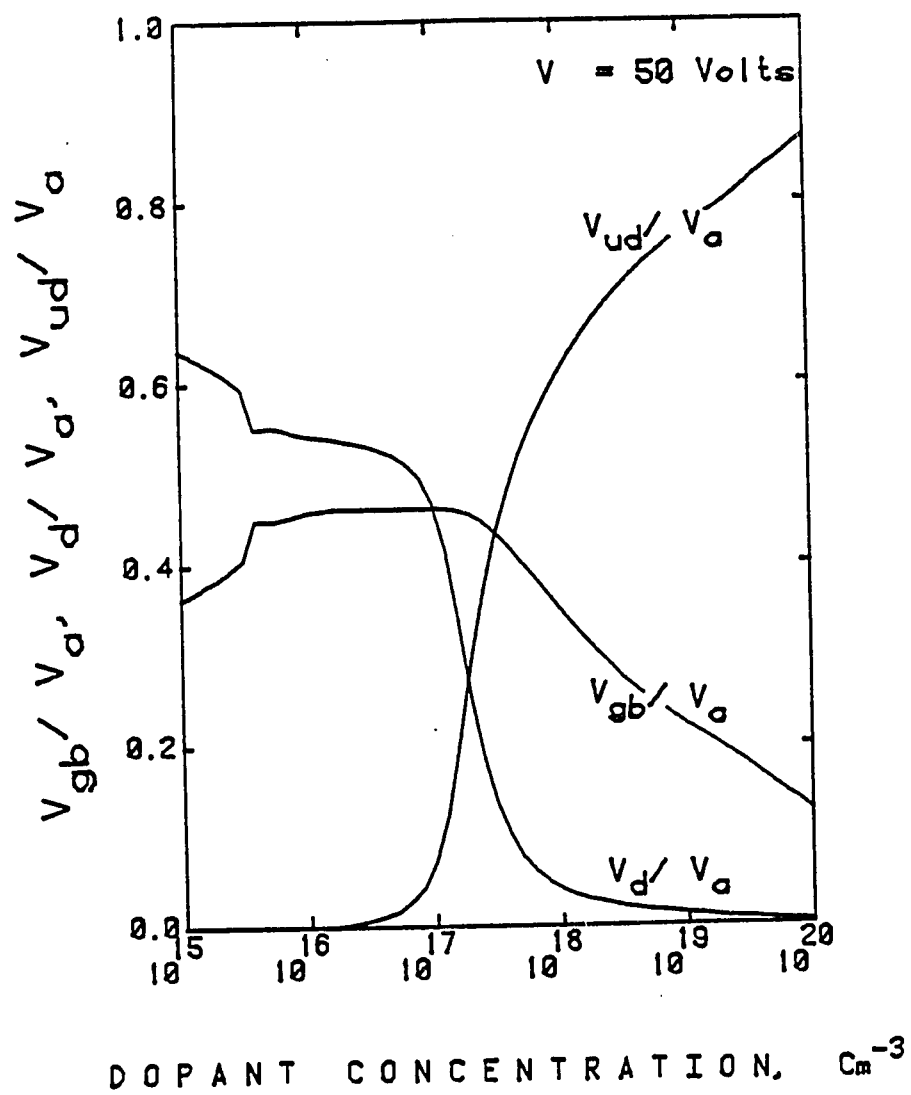


Fig. 5.18 Voltage partition in a unit cell vs. dopant concentration for $V_a = 0.35$ volt.

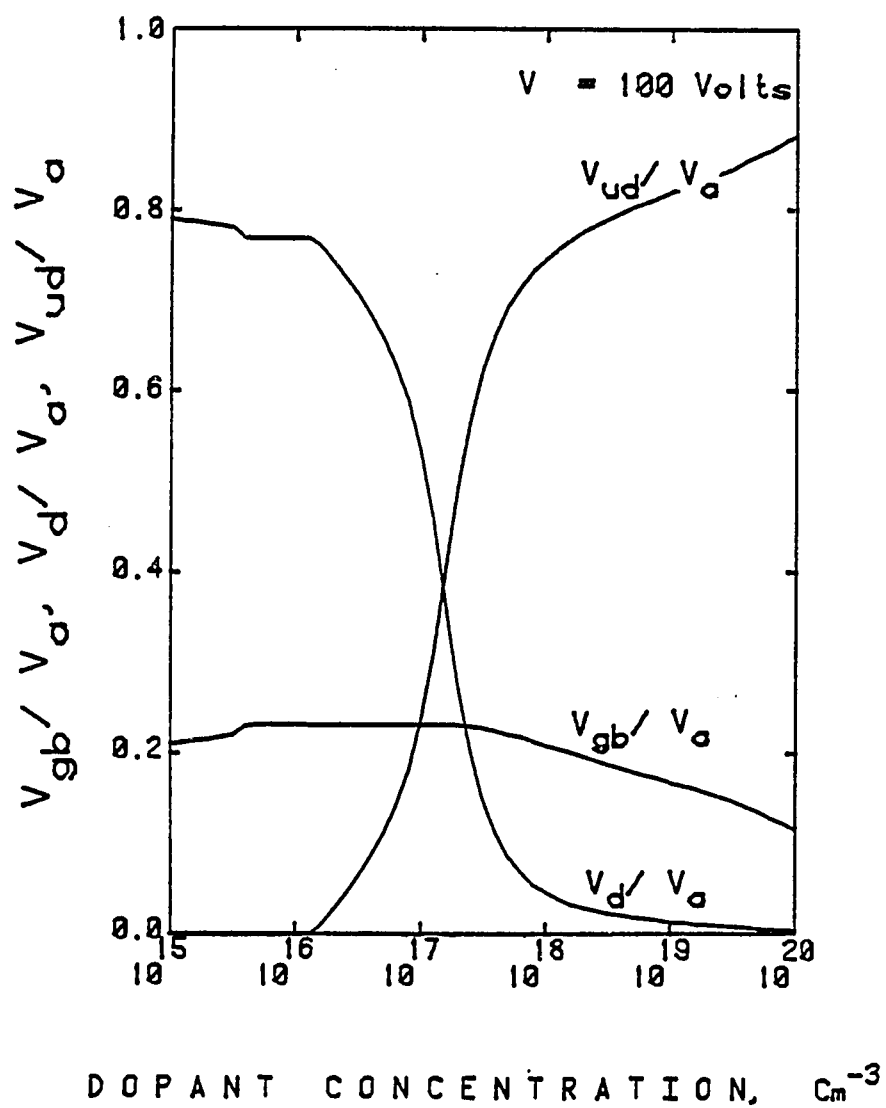


Fig. 5.19 Voltage partition in a unit cell vs. dopant concentration for $V_a = 0.7$ volt.

partitioning between depleted and boundary regions for large V_a , can be understood as follows: As the grain voltage, V_a , is increased the corresponding V_{gb} rapidly approaches the critical switching voltage. Since the grain boundary can not sustain external voltages greater than V_{gbc} , any further increase in V_a has to be dropped across the depletion depth. The small kink in these curves are due to the approximation used in this analysis (see (iv)).

Figures 5.20, 5.21, 5.22 present the voltage partition as a function of applied voltage for several different doping concentrations ($10^{15} - 10^{20} \text{ cm}^{-3}$). In Figure 5.20 is plotted V_{gb}/V_a vs. V_a . Note that for entire doping concentration considered, V_{gb}/V_a either remains flat or decreases with increasing V_a . This can be expected because $\sigma_{gb}(V_{gb})$ is approximately flat at low voltages and is enhanced very sharply near V_{gbc} . The dependence of V_{gb}/V_a on N_A , for small voltages, is correlated to that of qV_B as discussed earlier. For low and/or intermediate doping concentration, where ρ_{gb} is relatively large, a substantial portion of V_a should be dropped across the boundary. This means that with increasing V_a the onset of electrical switching is approached relatively quickly. Hence, any further increase in V_a has to be accommodated within the grain, and V_{gb}/V_a should decrease approximately as V_a^{-1} . For high dopant concentration, where the depletion depth is very small, i.e. $V_d \approx 0$, V_a divides between $V_{nd} \propto \rho_c \cdot (L - \delta)$ and $V_{gb} \propto \rho_{gb} \cdot \delta$. Since ρ_{gb} and ρ_c are of the same order of magnitude in this case and the boundary width, δ , is small, V_{gb} approaches V_{gbc} rather slowly. In Figure 5.21, V_d/V_a as a function of V_a is presented. For $N_A < N^*$, the general trend of this voltage fraction can be understood via the relation, $V_d/V_a = 1 - V_{gb}/V_a$, while for $N_A > N^*$, V_d/V_a rapidly decreases because of shrinking depletion

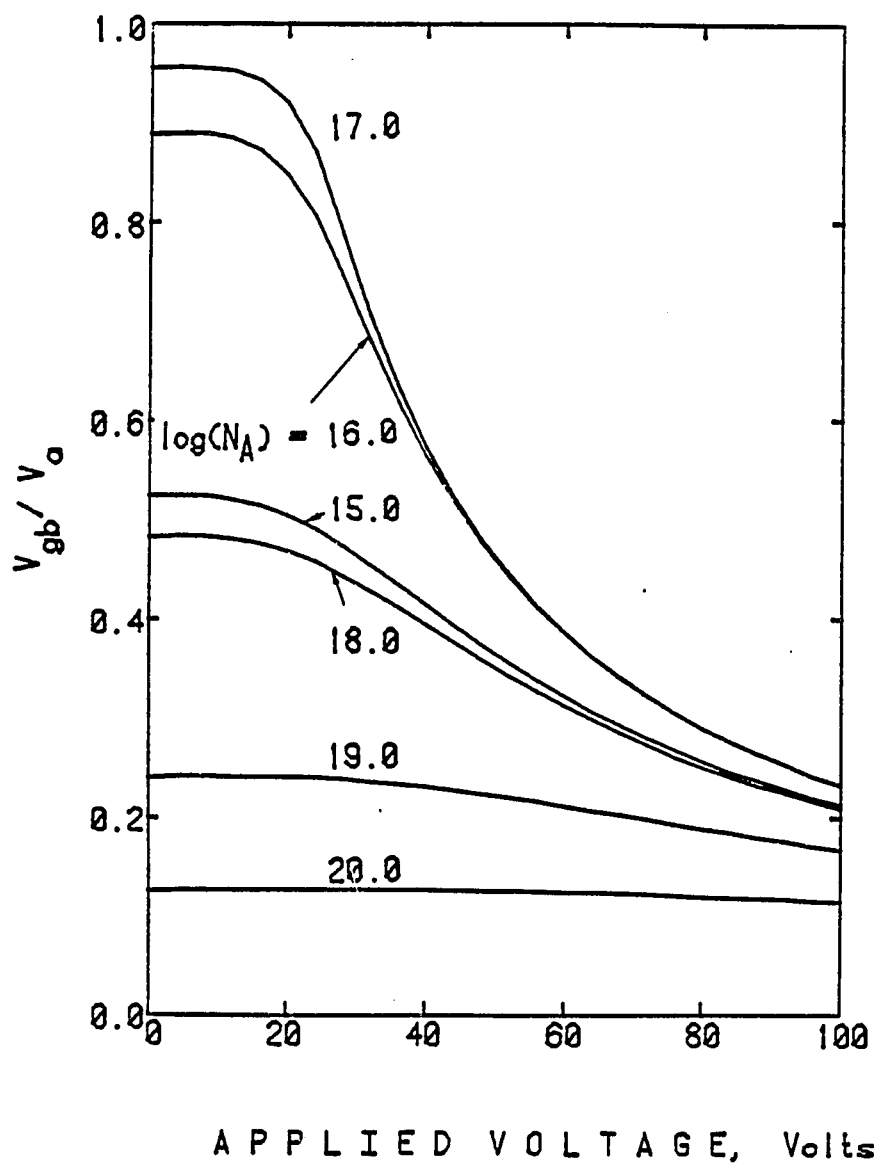


Fig. 5.20 V_{gb}/V_a vs. applied voltage for different dopant concentrations.

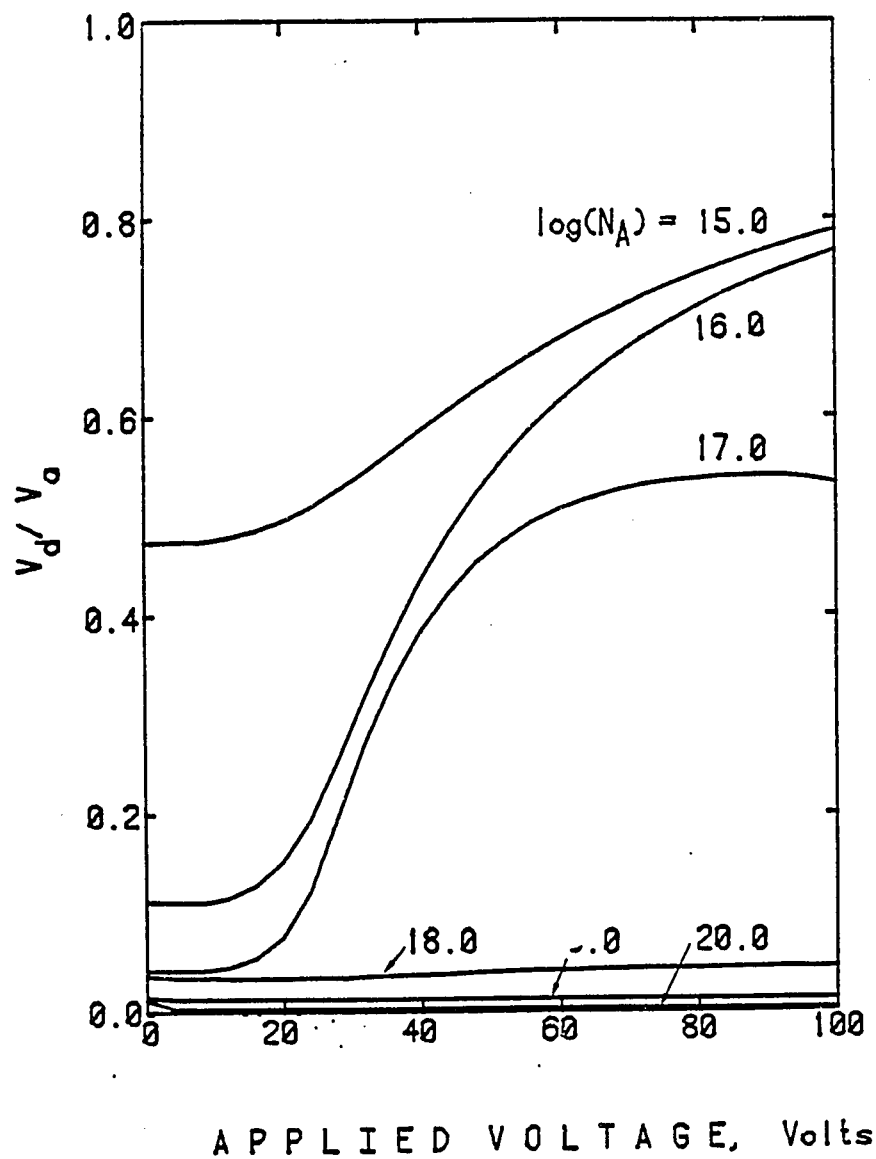


Fig. 5.21 V_d/V_a vs. applied voltage for different dopant concentrations.

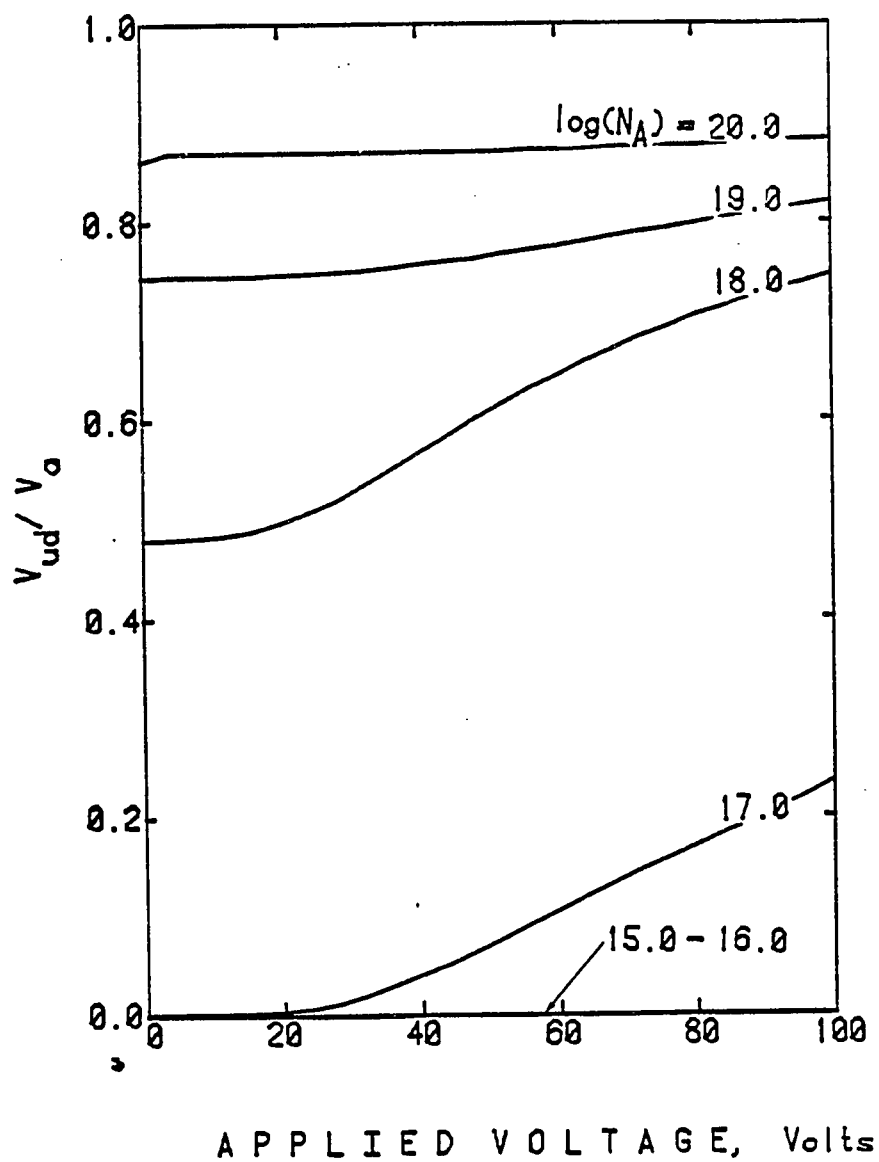


Fig. 5.22 V_{ud}/V_a vs. applied voltage for different dopant concentrations.

depth. In Fig. 5.22, the applied voltage dropped across the undepleted grain region, V_{ud}/V_a , is plotted against N_A . As can be clearly observed, V_{ud} shares an increasingly appreciable fraction of V_a with increasing N_A and eventually constitutes a major portion of V_a . This suggests that V_{ud} could be an important factor, influencing the overall I-V characteristics especially for the case of high doping concentration and high applied voltage. Neglect of this term could thus lead to erroneous I-V results. It is important to point out that in previous emission models this V_{ud} component was neglected in the voltage partition scheme. In this regard, the present approach fundamentally differs from the previous theories.

5.5.2 COMPARISON WITH EXPERIMENT

A key feature of this present I-V theory is that V_a is distributed via the relation, $V \propto J\rho$ where J is constant and ρ in each of three different regions in the unit cell is determined explicitly for given N_A , T and V_a . The theory by Mandurah, et al [54] considered the effect of mobile carrier redistribution under the influence of external voltage. Ref. [54] distributed V_a into V_d and V_{gb} , presumably for the special case where there is no undepleted region. Since the grain boundary is taken as an insulator in their model, V_{gb} is determined by electrostatic considerations associated with changing depletion depths (see Eq. (28) in Ref. [54]). An interesting consequence of this analysis is that for small N_A , say 10^{15} cm^{-3} the voltage fraction, V_{gb}/V_a is practically zero while $V_d/V_a \approx 1$, and for large N_A , $V_{gb}/V_a \approx 1$. These results are in marked contrast with the present results discussed above. These two different theoretical results can be experimentally compared in terms of the conductance data reported in Ref. [64]. Using boron-doped ($N_A = 10^{15} \text{ cm}^{-3}$)

bicrystal bar of $12 \times 3 \times 0.4 \text{ mm}^3$ with grain boundary bisecting the long edge, Werner et al [64] measured crystalline ($6 \times 3 \times 0.4 \text{ mm}^3$) conductance, G_c and grain boundary conductance, G_{gb} . Near the room temperature the ratio, G_c/G_{gb} was about 2-3. This ratio, when transcribed into fractional voltages, V_{ud}/V_a , V_d/V_a , and V_{gb}/V_a (Appendix I) leads explicitly to the conclusion that $V_{gb}/V_a > 0.5$. This result unambiguously supports the present voltage partitioning scheme.

5.5.3 I-V CURVES We now come to the final results of this theory, namely the I-V characteristics. The general current response to input voltage, V_a , can be conveniently and compactly discussed by recasting eqn.(4.19) into a new format as follows. Upon multiplying both sides of eqn.(4.19) by area, A , of the resistor and small signal resistance, $R_s(\rho_s N_g L/A)$ with N_g denoting the average number of grains in the resistor, there results

$$IR_s = \Gamma(V_a, N_g, T, L) V \quad (5.6)$$

where ρ_s is given by eqn.(3.23) and V is the total voltage applied across the resistor. Note that the output, IR_s , has now the unit of volt and is related to the input voltage, V_a , through the dimensionless response function, Γ , given by

$$\Gamma = \frac{F(0)}{F} \cdot \left[e^{\frac{qV_{aL}}{kT}} - e^{\frac{qV_{aR}}{kT}} \right] / (qV_a/kT) \quad (5.7)$$

In the limit of small applied voltage, the response function reduces to unity, as expected. Hence, the output for small V_a is always described by straight line having unity slope. Thus, the nonlinearity in I-V relationship, if any, should come via this V_a -dependent response function and is exhibited as a deviation from this straight line.

In Fig. 5.23 we present IR_s vs. V_a for several different doping concentrations ($10^{15} - 10^{20} \text{ cm}^{-3}$) at room temperature. For low dopant levels ($< 2.5 \times 10^{15} \text{ cm}^{-3}$), where $qV_B \leq 2kT$, the crystalline grain behaves as a passive resistor and the nonlinearity arises solely from the field enhanced conductivity of the grain boundary. As N_A is increased ($4 \times 10^{15} - 2.5 \times 10^{17} \text{ cm}^{-3}$), qV_B becomes much larger than kT . In this case, the redistribution of mobile holes in the grain further enhances nonlinearity as can be clearly observed in the figure. As N_A is further increased, qV_B now rapidly reduces and V_{ud} takes up substantial fraction of V_a . Consequently, the I-V relationship should closely resemble the corresponding single crystalline case. It should be noted that some of these IR_s curves have not been stretched beyond V_a^m due to limitations in ordinate scale. However, it is important to point out that all of these curves should eventually become strictly linear beyond their respective V_a^m .

As can clearly be observed in Fig. 5.23, the nonlinear behavior of IR_s vs. V_a can be drastically different, depending on the doping level used, for example. Equivalently, the response function, Γ , describing this nonlinearity should depend rather sensitively on N_A , T , Q_t , L etc. This comprehensive characterization of Γ in terms of material and structural parameters of polysilicon is in contrast with the previous I-V theories. Lu et al [39,55] described IR_s vs. V_a behavior by

$$IR_s = \left[\frac{\sinh\left(\frac{qV}{2kTN_g}\right)}{\left(\frac{qV}{2kTN_g}\right)} \right] V \quad (5.8)$$

Note that the nonlinear response function introduced by Lu et al depends only on the applied voltage dropped across the unit cell, V/N_g . This

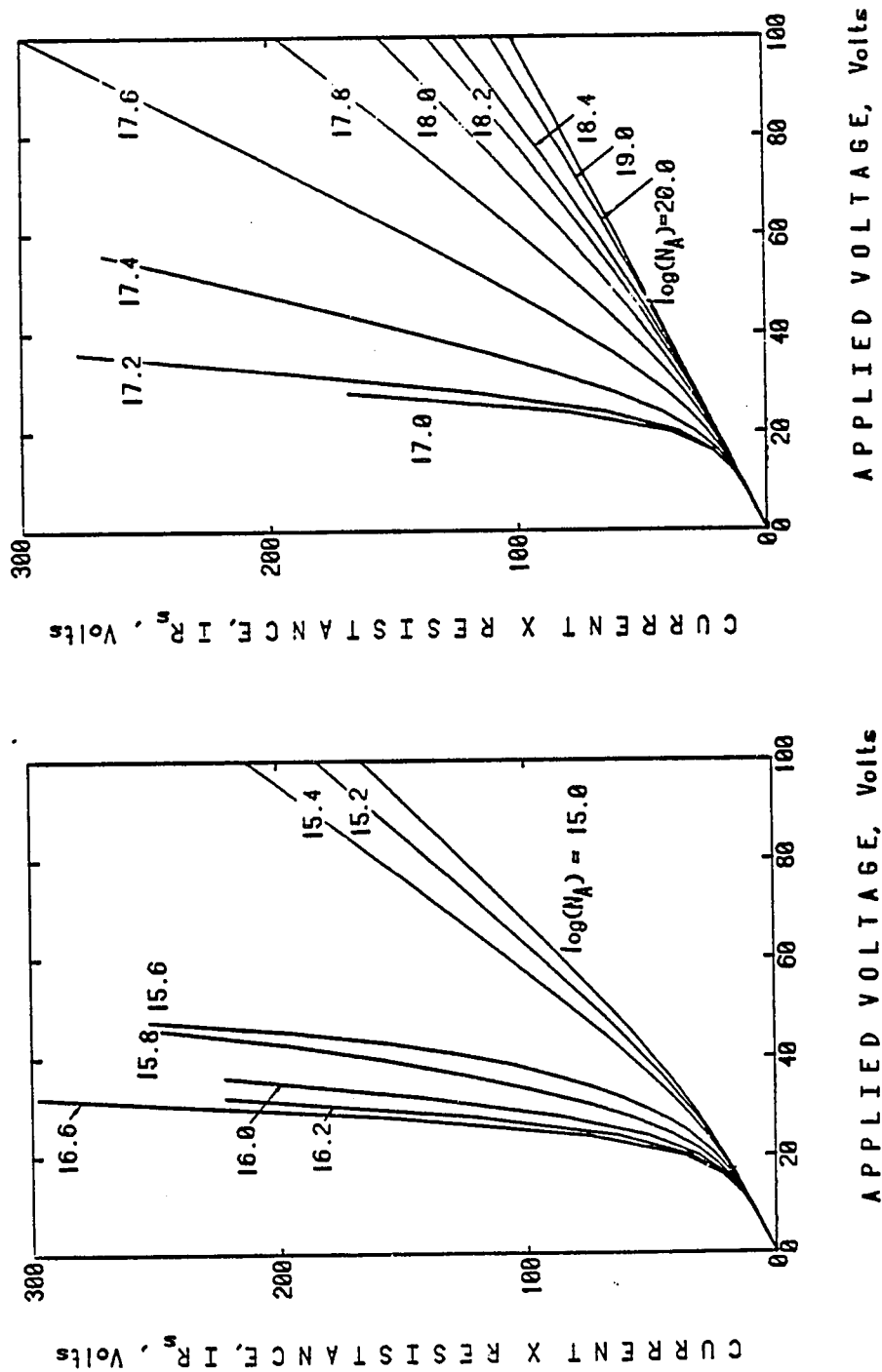


Fig. 5.23 Normalized current vs. applied voltage for different dopant concentrations.

implies that the nonlinearity in IR_s vs. V curves is strictly dictated by the strength of applied voltage for unit cell, regardless of the doping concentration N_A . It is, therefore, apparent in this approach that any departure of IR_s vs. V curves from this simple prediction can only be accommodated by adjusting the applied voltage per cell, viz. by introducing N_{eff} in place of N_g as a function of N_A and T . The present theory basically differs from the previous approach in that the nonlinearity is not only caused by V_a but also by other pertinent system parameters.

CHAPTER SIX

CONCLUSION

6.1 PRELIMINARIES

We have presented a new theory of conduction in polysilicon. The present theory differs from previous theories in the formulation of the grain boundary and the description of conduction within it. We assume that the boundary is an amorphous conductor in equilibrium contact with crystalline semiconductor. Current, therefore, is described via drift-diffusion theory. Previous theories have taken grain boundary as an insulator or a barrier-in-vacuum. Current, therefore, was accounted for via thermionic and/or field emission of carriers. These contrasting viewpoints have been examined in light of experimental data and theoretical consistency. It should also be emphasised that this alternative viewpoint has been explicitly guided by a few key experimental observations:

(i) ρ vs. T^{-1} data, taken in the limit of small applied voltage and closely resembling the corresponding data in amorphous solids, provided a direct clue for the amorphous nature of grain boundaries strongly influencing the overall conduction properties of polysilicon. We also feel that the strict linearity existing in ρ vs. $T^{-1/4}$ data, observed in undoped polysilicon [84], constitutes a further experimental support for the present point of view. Note that this temperature characteristic of ρ is, in the present approach, a natural consequence of tunneling mobility, whereas in emission models, this data may again require a new tem-

perature variation of q_x and δ in Ref. [43].

(ii) The threshold switching effect observed in polysilicon [80] for high applied voltage further attests, we feel, to the validity of the present approach. This sudden transition would be difficult to be understood within the framework of emission models. Note that in undoped polysilicon there is practically no barrier potential and also the external voltage dropped across the boundary is negligible [54]. This leaves virtually no physical mechanisms by which to explain this nonlinear I-V behavior in these models. The present viewpoint regarding the grain boundary, on the other hand, has an inherent advantage to incorporate this nonlinear switching effect as a natural consequence of high field I-V phenomena in amorphous semiconductor films. We conclude our discussion by summarizing essential physics pertaining to these conduction processes.

6.2 VOLTAGE PARTITION

Emission models based on postulating q_x suffer from the fundamental inconsistency in their voltage partition scheme. Consider, for example, undoped polysilicon or polysilicon with low dopant concentration. A voltage, V applied to a resistor bar was taken to distribute uniformly in each grain (V_g). Since the barrier potential is practically nonexistent in this case, the voltage assigned electrostatically to the 'boundary insulator' is negligible (see equation (28) in Ref. [54]), and V_g drops mainly in the grain. The energy diagram of the resistor is illustrated in Fig. 6.1.

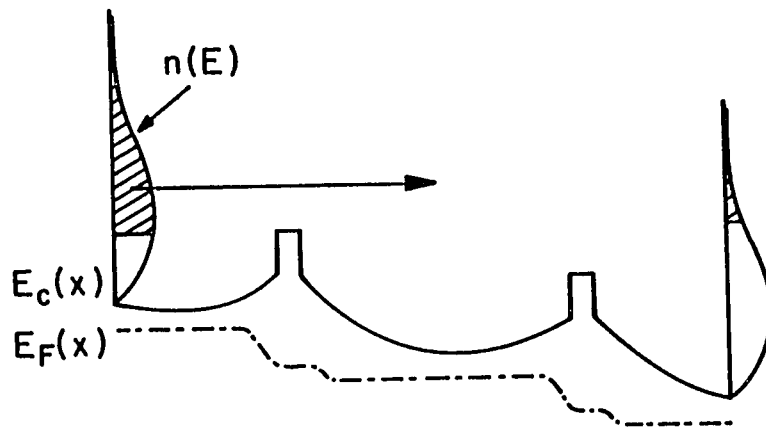


Fig. 6.1 Schematic illustration of emission mode of 2-grain polysilicon system.

Consider thermionic current. In emission models, carriers are regarded as free particles. Therefore, those carriers which overcome the first barrier, $q\chi_1$ on the left are automatically capable of passing through the rest of the barriers, i.e. remaining barriers do not provide any additional resistivity. Obviously this is in direct contradiction to the assumption that V divides equally among the grains. That is, invoking grain voltage (V_g) to describe current is not physically justified. Even a thermalization processes (ρ_c) of charge carriers in each grain, i.e. phonon and/or impurity scattering does not eliminate this inconsistency. For the case under consideration, i.e. for a completely depleted case it is not possible for these emission models to bring in these essential scattering processes. This is a fundamental drawback.

Additionally, with V increasing, all of the electrons available in the conduction band to the left of $q\chi_1$ can be thermally emitted across $q\chi_1$. This means that current should be saturated beyond a certain voltage range. This picture is again in contradiction with the hyperbolic-sine function I-V characteristics asserted by these theories.

In contrast, the present theory is firmly rooted in carrier scattering processes, both in crystalline grain (μ_c) and disordered boundary (μ_{gb}), and is, therefore, entirely consistent with the uniform partition of V into each unit cell.

6.2.1 CRITICAL VOLTAGES

In this theory, we have partitioned the voltage applied across the unit cell into three different regions therein, namely, the undepleted crystalline grain region (V_{nd}), depletion depth (V_d), and the grain boun-

dary region (V_{gb}). The basic guideline for this voltage distribution has been the continuity of current density throughout the unit cell. We have shown for the first time that the V_{nd} -component can constitute a major fraction of V_a for high doping concentrations above N^* . Hence the general I-V characteristics in polysilicon should, in this case, approach the corresponding I-V curves in single crystalline silicon. We have also shown for the first time that the V_{gb} -component can take up substantial fraction of V_a over a wide range of N . This, coupled with the fact that the boundary width is small could lead to electrical switching within the amorphous boundary region. However, the quantitative model for this field enhanced conductivity is not available at present. We, therefore, have incorporated this effect phenomenologically in the I-V analysis. We believe that this boundary switching may constitute a major mechanism responsible for rather complex and nonlinear I-V characteristics observed in polysilicon. We also feel that a comprehensive experimental and theoretical characterization of I-V behavior requires further study on switching processes in polysilicon together with extensive and explicit I-V data as a function of N , T , and V . Additionally, we have introduced the concept of a critical voltage, V_a^m associated with changing depletion depth under bias. Beyond V_a^m , the crystalline grain transforms into a passive and/or ohmic resistor and the current density in polysilicon never exceeds the corresponding single crystal value, in contrast with previous theories.

6.3 $\ln(\rho)$ VS. T^{-1}

The experimental data for $\ln(\rho)$ vs T^{-1} curves constitutes a key area in which to test the opposite viewpoints regarding grain boundary. The

slope of $\ln \rho$ at a given T is a measure of the activation energy at that temperature, namely the energy spacing, ΔE between E_F and the prevalent conduction channel. Lu, et al. [43] adjusted, in essence, this ΔE via T -dependent q_x to fit the data. This mathematical procedure was theoretically shown to be unphysical and was experimentally proven to be invalid. In the present approach ΔE is naturally dependent on T because of different conduction channels existing at different energy levels in the disordered boundary.

Inasmuch as the present approach is based on using conduction mechanisms operative in amorphous semiconductors, a clear contention of the theory is that carriers trapped near the midgap should also be amenable to tunneling conduction. As discussed earlier (sec. 6.1) the ρ - T data reported by Kobka, et al. [84] is extremely significant in this context. Using undoped polysilicon, they measured ρ in the temperature range, -14°C to 120°C , and showed that $\ln \rho$ vs. $T^{-1/4}$ plot is strictly linear. Note that E_F is pinned at midgap for undoped polysilicon and the probability of charge carriers residing in hopping and diffusive bands is practically zero. Therefore, the conduction through grain boundary should be via tunneling. The temperature dependence of μ_{tun} given in eqn.(2.5) predicts precisely this experimental curve. This constitutes one of the most direct experimental evidences that grain boundary is an amorphous semiconductor, in which all the carriers participate in conduction under bias.

6.4 ARTIFICIAL FACTOR, f

Lu, et al [39] originally introduced the f -factor in the form,

$$\rho_B \sim \frac{1}{f} \frac{kT}{q^2 2W_p(-L/2)} \frac{1}{v_T} \exp \frac{qV_B}{kT}.$$

with v_T denoting the thermal velocity of carriers in the medium. For $L \leq 0.3 \mu\text{m}$, ρ in the present theory is essentially given by the boundary component. Hence, confining to μ_{ext} or equivalently D_{ext} one can write

$$\rho \sim \frac{kT}{q^2 L_p(-\frac{1}{2}L)} \frac{1}{v_{\text{ext}}} \exp \frac{qV_B}{kT}.$$

where the quantity, $v_{\text{ext}} = D_{\text{ext}} \gamma \exp(\Delta/kT)/\delta$ has the dimension of a velocity. These two expressions have the same mathematical form, and the quantities v_T , v_{ext} can be formally regarded as an effective recombination velocity, (v_R) in Schottky diode. In the present theory v_R has been specified by structural and physical properties of the grain boundary, while in emission theories v_R has been represented by the thermal velocity. Since the grain boundary is not metallic, carriers can not be regarded as free particles. We feel that use of v_T in emission models led to an overestimation of current, necessitating the introduction of the f -factor.

(d) Limitations of the Present Theory

We have approximated polysilicon to consist of identical cubic grains and considered one-dimensional conduction processes. The effect of grain size distribution has not been taken into account. This simplifying assumption may exclude some of the pertinent physical mechanisms operative in polysilicon. For example, at the same dopant density two grains of different sizes may have different Fermi levels for $N < N^*$. In equilibrium, therefore there should ensue a band bending for the two grains to share a common E_{F0} . Consequently, a resistor consisting of

different size grains may be associated with many mini-"diodes" (Fig. 6.2) due to this band bending. Also, actual paths of charge carriers could possibly be dictated by a two-dimensional random network. The resulting current may then exhibit a rather complicated nonlinear behavior. If, on the other hand, the distribution of grain sizes can be tightly controlled, the description of I-V characteristics becomes simple, and the theoretical results presented here can be a useful basis for understanding the experimental data.

Also, for polysilicon, experimental data for band tail (Δ) and mobility shoulder (Δ') are not available at the present time. We have therefore determined these values parametrically with the aid of optimal fit to data. As mentioned earlier, the values for μ_{ext} , μ_{hop} have been chosen within the range available in the literature. Nevertheless, we feel that because grain boundary width is small, these mobility values associated with polysilicon could be larger than the corresponding mobilities in bulk amorphous semiconductors. If this could be supported by theoretical analysis in the future, it is possible to achieve better fit to the data with the choice of Δ , Δ' , such that the energy gap in the boundary could better simulate the optical bandgap data reported for amorphous silicon.

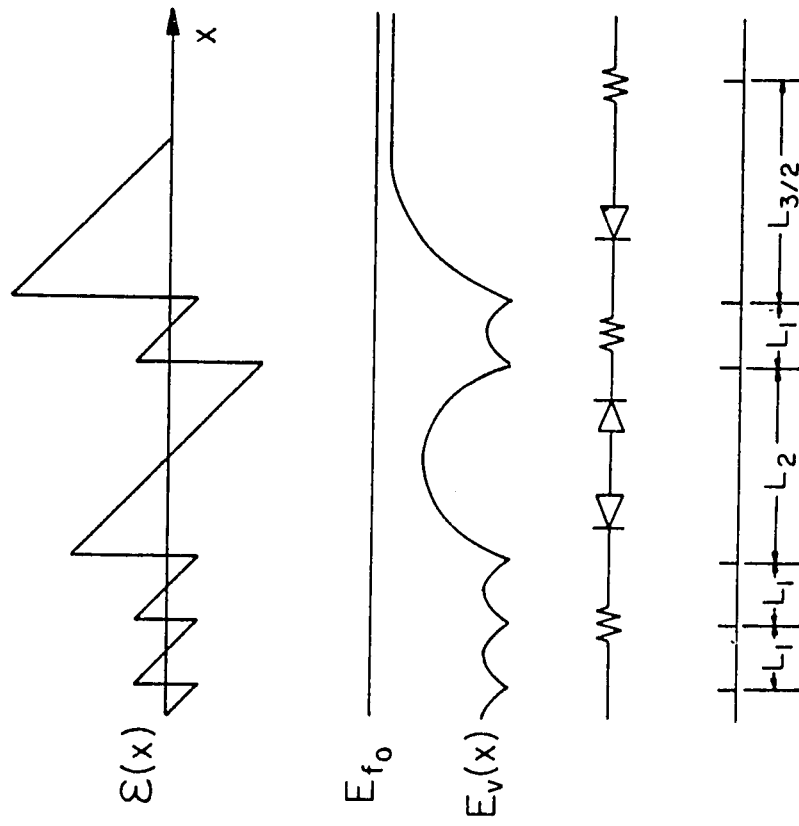


Fig. 6.2 Schematic illustration of formation of the "mini-diode" in polysilicon having different grain sizes.

REFERENCES

1. R.A. Mickelson, "Industrial application of polycrystalline thin-film devices," Polycrystalline and amorphous thin film devices, L.L. Kajmerski Ed. New York : Academic press 1980.
2. Polycrystalline and amorphous thin film devices, L.L. Kajmerski Ed. New York : Academic press 1980.
3. J.E. Mahan, D.S. Newman, M.R. Gulett, "Gigaohm-range polycrystalline silicon resistor for microelectronic applications," IEEE Trans. Electron. Devices, ED-30, pp. 45-51, 1983
4. L. Gerzberg, "Monolithic power-spectrum centroid detector," Ph.D. dissertation, Stanford Electronics Laboratories, Stanford University, May 1979.
5. D.J. Bartelink, "Potential application of poly-silicon as an electronic devices material," Material Research Soc. Meeting, Boston, 1981.
6. F. Mohammadi, K.C. Saraswat, and J.D. Meindl, " A high voltage MOS-FET in polycrystalline silicon," IEEE Trans. Electron. Devices, ED-27, pp. 293-295, 1980
7. S.W. Depp, A. Juliano, and B.G. Huth, "Polysilicon FET devices for large area input-output applications," IEDM Tech. Dig., pp. 703-706, 1980.
8. T.I. Kamins, "Field effects in polycrystalline silicon films," Solid-State Electron., vol. 156, pp. 789-799, 1972.

9. S. Onga, Y. Mizutani, K. Taniguchi, M. Kashiwagi, K. Shibata, and S. Kohyama, "Characterization of polycrystalline silicon MOS transistors and its film properties," Jpn. J. Appl. Phys., vol. 21, pp. 1472-1478, 1982.
10. R.R. Shah, D.R. Hollingsworth, and D.L. Crosthwait, "Laser recrystallized polysilicon for high performance resistors," IEEE Electron. Device Lett., vol. EDL-2, pp. 254-256, 1981.
11. R.R. Shah, D.R. Hollingsworth, G.A. DeJong, and D.L. Crosthwait, "P-N junction and Schottky barrier diode fabrication in laser recrystallized polysilicon on SiO_2 ," IEEE Electron. Device Lett., vol. EDL-2, pp. 159-161, 1981.
12. N.M. Johnson, D.K. Biegelsen, and M.D. Moyer, "Grain boundaries in p-n junction diodes fabricated in laser recrystallized silicon thin films," Appl. Phys. Lett., vol. 38, pp. 900-902, 1981.
13. G.E.J. Eggermont and J.G. Degroot, "Diode characteristics in laser recrystallized and conventional polycrystalline silicon," IEEE Electron. Device Lett., vol. EDL-3, pp. 156-158, 1982.
14. M. Schaber, M. Schelpmeir, W.M. Werner, and D. Cutter, "Schottky diodes in laser recrystallized polysilicon," in Laser and Electron-Beam Interactions with Solids, B.R. Appleton and G.K. Celler, eds., Academic Press, New York, 1982, pp. 639-641.
15. T.I. Kamins, K.F. Lee, J.F. Gibbons, and K.C. Saraswat, "A monolithic integrated circuit fabricated in laser-annealed polysilicon," IEEE Trans. Electron. Devices, ED-27, pp. 290-293, 1980

16. K.K. Ng, G.K. Celler, E.I. Povilonis, R.C. Frye, H.J. Leamy, and S.M. Sze, "Effects of grain boundary on laser crystallized poly-si MOSFET's," IEEE Electron. Devices Lett., EDL-2, pp. 316-318, 1981.
17. H.W. Lam, Z.P. Sobczak, R.F. Pinizzotto, and A.L. Tasch, "Devices fabricated in {100} silicon-on-oxide produced by a scanning CW-laser-induced lateral seeding technique," IEEE Trans. Electron. Devices, ED-29, pp. 389-394, 1981.
18. T.I. Kamins, B.P. Von Herzen, "MOSFET's in electron-beam recrystallized polysilicon," IEEE Electron. Devices Lett., EDL-2, pp. 313-315, 1981.
19. N.M. Johnson, D.K. Biegelsen, H.C. Tuan, M.D. Moyer and L.E. Fennell, "Single-crystal silicon transistors in laser crystallized thin films on bulk glass," IEEE Electron. Devices Lett., EDL-3, pp. 369-372, 1982.
20. H.P. Lee, and H.W. Lam, "Electrical characteristics of the interface between laser-recrystallized polycrystalline silicon and underlying insulator," IEEE Electron. Devices Lett., EDL-3, pp. 161-163, 1982.
21. R.D. Jolly, T.I. Kamins, and R.H. McCharles, "A dynamic RAM cell in recrystallized polysilicon," IEEE Electron. Devices Lett., EDL-4, pp. 8-11, 1983.
22. T.I. Kamins, C.I. Drowley, "Effect of laser recrystallization of polysilicon on the underlying substrate," IEEE Electron. Devices Lett., EDL-3, pp. 363-365, 1982.

23. H.S. Lee, "Channel electron conduction in laser annealed polysilicon metal-oxide-semiconductor field effect transistor," pp. 770-772, 1981.
24. A. Chiang, W.P. Meuli, N.M. Johnson, and M.H. Zarzycki, "High performance thin film transistor in CO₂ laser crystallized silicon on quartz, SPIE Symposium on Laser Processing of Semiconductor Devices, SPIE proc., vol. 385, paper no. 28, Los Angeles, 1983.
25. A.F. Tasch, T.C. Holloway, K.F. Lee, and J.F. Gibbons, "Silicon-on-insulator M.O.S.F.E.T.S. fabricated on laser annealed polysilicon on SiO₂," Electronics Lett., vol. 15, pp. 435-437, 1979.
26. K.F. Lee, J.F. Gibbons, K.C. Saraswat, and T.I. Kamins, "Thin film MOSFET's fabricated in laser annealed polycrystalline silicon," Appl. Phys. Lett., vol. 35, pp. 173-175, 1979.
27. T.I. Kamins and P.J. Marcoux, "Hydorgenation of transistors fabricated in polycrystalline-silicon films," IEEE Electron. Device Lett., vol. EDL-1, pp. 159-161, 1980.
28. R.R. Shah and S.L. Hughey, "Controlling TCR of polysilicon resistors by laser recrystallization and plasma passivation," Texas Instruments Internal Report, July 1982.
29. C.H. Seager and D.S. Ginley, "Passivation of grain boundaries in polycrystalline silicon," Appl. Phys. Lett., vol. 34, pp. 337-340, 1979.
30. D.R. Campbell, "Enhanced conductivity in plasma hydrogenated polysilicon films," Appl. Phys. Lett., vol. 36, pp. 604-606, 1980.

31. D.R. Campbell, J.C.M Hwang, I. Ohdomari, M Frisch, and W. Fitzpatrick, "Effects of hydrogenation on lightly doped polycrystalline silicon," J. Appl. Phys., vol. 53, pp. 7454-7457, 1982.
32. R.T. Young, M.C. Lu, R.D. Westbrook, and G.E. Jellison, "Effect of lithium on electrical properties of grain boundaries in silicon," Appl. Phys. Lett., vol. 38, pp. 628-630, 1981.
33. Laser and Electron Beam Processing of Materials, C.W. White and P.S. Peercy, eds., Academic, New York, 1980.
34. Laser and Electron-Beam Interactions with Solids, B.R. Appleton and G.K. Celler, eds., North-Holland, New York, 1982.
35. Grain Boundaries in Semiconductors, H.J. Leamy, G.E. Pike, and C.H. Seager, eds., North-Holland, New York, 1982.
36. Thin Films and Interfaces, P.S. Ho and K.N. Tu, eds., North-Holland, New York, 1982.
37. K.C. Saraswat, "Physical and electrical properties of polycrystalline silicon thin films," Material Research Society, Grain boundary symposium, Boston, 1981.
38. J.T. Schott, and J.J. Comer, Laser and Electron-Beam Solid Interactions and Material Processing, J.F. Gibbons, L. Hess, T. Sigmon, eds., North Holland, New York, 1981 p. 479.
39. N.C.C. Lu, L. Gerzberg, C.Y. Lu, and J.D. Meindl, "Modeling and optimization of polycrystalline silicon resistors," IEEE Trans. Electron Devices, vol. ED-28, pp. 818-830, 1981.
40. T.I. Kamins, "Hall mobility in chemically deposited polycrystalline silicon," J. Appl. Phys., vol. 42, pp. 4357-4365, 1971.

41. J.Y.W. Seto, "The electrical properties of polycrystalline silicon films," J. Appl. Phys., vol. 46, pp. 5247-5254, 1975.
42. N.C.C. Lu, L.Gerzberg, J.D. Meindl, "A quantitative model of the effect of grain size on the resistivity of polycrystalline silicon resistors," IEEE Electron Device Lett., vol. EDL-1, pp. 38-41, 1980.
43. N.C.C. Lu, L. Gerzberg, C.Y. Lu, and J.D. Meindl, "A new conduction model for polycrystalline silicon films," IEEE Trans. Electron. Device Lett., vol. EDL-2, pp. 95-98, April 1981.
44. M.M. Mandurah, K.C. Saraswat, C.R. Helms, and T.I. Kamins, "Dopant segregation in polycrystalline silicon," J. Appl. Phys., vol. 51, pp. 5755-5763, 1980.
45. G. Baccarani, B. Ricco, and G. Spadini, "Transport properties of polycrystalline silicon films," J. Appl. Phys., vol. 49, pp. 5565-5570, 1978.
46. C.H. Seager, and T.G. Castner, "Zero-bias resistance of grain boundary in neutron transmutation-doped polycrystalline silicon," J. Appl. Phys., vol. 49, pp. 3879-3889, 1978.
47. T.I. Kamins, "Resistivity of LPCVD polycrystalline-silicon films", J. Electrochem. Soc., vol. 126, pp. 833-837, 1979.
48. H.P. Maruska, A.K. Ghosh, A. Rose, T. Feng, "Hall mobility of polycrystalline silicon," Appl. Phys. Lett., vol. 36, pp. 381-383, 1980.
49. K.R. Kumer and M. Satyam, "Carrier mobility in polycrystalline semiconductor," Appl. Phys. Lett., vol. 39, pp. 898-900, 1981.

50. J.P. Colinge, E. Demonelin, F. Delannay, M. Lobet, and J.M. Temerson, "Grain size and resistivity of LPCVD polycrystalline silicon films," J. Electrochem. Soc., vol. 128, pp. 2009-2014, 1981.
51. G.J. Korsh and R.S. Muller, "Conduction properties of lightly doped polycrystalline silicon," Solid-State Electron., vol. 21, pp. 1045-1051, 1978.
52. G.E. Pike and C.H. Seager, "The dc voltage dependence of semiconductor grain-boundary resistance," J. Appl. Phys., vol. 50, pp. 3414-3422, 1979.
53. J. Martinez and J. Piqueras, "On the mobility of polycrystalline semiconductors," Solid-State Electron., vol. 23, pp. 297-303, 1980.
54. M.M. Mandurah, K.C. Saraswat, and T.I. Kamins, "A model for conduction in polycrystalline silicon -- Part I: theory," IEEE Trans. Electron Devices, ED-28, pp. 1163-1170, 1981.
55. N.C.C. Lu, C.Y. Lu, M.K. Lee, and G. Chang, "High-field conduction mechanisms in polycrystalline-silicon resistors," IEDM 82, pp. 781-786, 1982.
56. M.E. Cowher and T.O. Sedgwick, "Chemical vapor-deposited polycrystalline silicon," J. Electrochem. Soc., vol. 119, p. 1565, 1978.
57. C.M. Wu, and E.S. Yang, "Physical basis of scattering potential at grain boundary of polycrystalline semiconductors," Appl. Phys. Lett., vol. 40, no. 1, pp. 49-51, 1982.
58. M.E. Cowher, and T.O. Sedgewick, J. Electrochem. Soc., vol. 119, p.1565, 1972.

59. A.L. Fripp, and L.H. Slack, J. Electrochem. Soc., vol. 120, p. 145, 1973.
60. D. Redfield, Appl. Phys. Lett., vol. 40, P. 163, 1982.
61. T.L. Chu, J.C. Liu, H.C. Mollenkopf, S.C. Chu, and K.W. Heizer, Solar Energy, vol. 17, p. 229, 1975
62. S.M. Sze, Physics of Semiconductor Devices, John Wiley, New York, 1981.
63. R.T. Young, J. Narayan and Y.K. Chang, "Electrical and structural properties of grain boundary in polycrystalline Si," in Grain Boundaries in Semiconductors, H.J. Leamy, G.E. Pike and C.H. Seager, eds., North-Holland, New York, 1982, p. 111.
64. J. Werner, W. Jantsch, K.H. Froehner, and H.J. Queisser, "Transport across silicon grain boundaries," in Grain Boundaries in Semiconductors, H.J. Leamy, G.E. Pike, and C.H. Seager, eds., North-Holland, New York, 1982, p. 99.
65. D.M. Kim, A.N. Khondker, R.R. Shah, and D.L. Crosthwait, "Conduction in polycrystalline silicon: diffusion theory and extended state mobility model," IEEE Electron Device Lett., vol. EDL-3, pp. 141-143, 1981.
66. A.N. Khondker, D.M. Kim, and R.R. Shah, "Conduction in polycrystalline silicon: generalized thermionic emission-diffusion theory and extended state emission model," in Laser-Solid Interactions and Transient Thermal Processing of Materials, J. Narayan, W.L. Brown, and R.A. Lemons, eds., North-Holland, 1983.

67. A.N. Khondker, R.R. Shah, and D.M. Kim, "Conduction processes in polysilicon: effects of laser restructuring," SPIE/LA '83 Symposium, Jan. 17-21, 1983, Los Angeles.
68. Amorphous Semiconductors, M.H. Brodsky, ed. New York, Springer-Verlag, 1979.
69. N.F. Mott, and E.A. Davis, Electronic Processes in Non-crystalline Materials, Oxford, Clarendon Press, 1971.
70. P. Nagels, "Electronic transport in amorphous semiconductors", in [68], pp. 113-158.
71. Section 7.4 in [69], pp. 197-207.
72. C. Feldman, and K. Moorjani, "Switching in elemental amorphous semiconductors," J. Noncryst. Solids, vol. 2, pp. 82-90, 1970.
73. S.K. Dey, "Electrothermal model of switching in amorphous silicon films," J. Vac. Sci. Technol., vol. 17 (1), pp. 445-448, 1980.
74. M.H. Brodsky, R.S. Title, Phys. Rev. Lett., Vol. 23, p. 581, 1969.
75. I. Solomon, "Spin effects in amorphous semiconductors," in [68], pp. 189-213.
76. D.E. Carlson, and C.R. Wornski, "Amorphous silicon solar cells," in [68], pp. 287-329.
77. P.G. LeComber W.E. Spear, "Doped amorphous semiconductors," in [68], pp. 251-285.
78. M.H. Brodsky, "Introduction," in [68].
79. Handbook of Mathematical Functions, M. Abramowitz and I.A. Stegun, eds., Dover, New York, 1965.

80. J.E. Mahan, "Threshold and memory switching in polycrystalline silicon," Appl. Phys. Lett., vol. 41 (5), pp. 479-481, 1982.
81. NBS special publication 400-10, Semiconductor measurement technology, Spreading Resistance Symposium, U.S. Department of Commerce, 1974.
82. W.E. Taylor, N.H. Odell and H.Y. Fan, "Grain boundary barriers in germanium," Phys. Rev., vol. 88, pp. 867-875, 1952.
83. A.S. Grove, Physics and Technology of Semiconductor Devices, John Wiley, New York, 1967.
84. V.G. Kobka, R.P. Komirenko, Y.V. Karnyushin, Y.P. Medvedev, and O.V. Tretyak, "Electrical conductivity of polycrystalline semiconductors," Sov. Phys. Semicond., vol. 16 (12), pp. 1404-1405, December 1982.

APPENDIX I: ANALYSIS OF CONDUCTANCE DATA OF REF. [64]

Werner et al measured crystalline ($6 \times 3 \times 0.4 \text{ mm}^3$) conductance, G_c and the boundary conductance, G_{gb} , in a bicrystal doped with boron ($N_A = 10^{15} \text{ cm}^{-3}$). The ratio, G_c/G_{gb} , was about 2-3 at room temperature. Using the photocapacitance data, they also measured the boundary trap density, Q_t , to be about $1.4 \times 10^{11} \text{ cm}^{-2}$. Using the values of N_A and Q_t in the charge neutrality condition, one can estimate the depletion depth, W . One finds $W \sim 0.55 \text{ } \mu\text{m}$ for the trap level, E_t , at midgap and $W \sim 0.38 \text{ } \mu\text{m}$ for $E_t = 0.15 \text{ eV}$ below midgap. The corresponding barrier potential, qV_B , are 0.25 eV and 0.12 eV, respectively. Now, using eqns.(3.10) and (3.23) in Part I one can write the ratio of resistances R_{ud} , R_d in the undepleted and depleted crystalline regions, respectively, as

$$\frac{R_d}{R_{ud}} = \frac{2W}{L-2W} \exp\left(\frac{qV_B}{kT}\right) \left[D\left(\sqrt{\frac{|qV_B|}{kT}}\right) / \sqrt{\frac{|qV_B|}{kT}} \right]$$

Upon inserting the values of L (1.2 cm) and W estimated above, this ratio is found to vary from 0.12 for $qV_B = 0.25 \text{ eV}$ to 0.0012 for $qV_B = 0.12 \text{ eV}$. This clearly indicates that the voltage dropped across the depletion depth, V_d , is much smaller than V_{ud} . Also, the lower bound for V_{gb} can be estimated from the reported conductance ratio in the form, $G_c/G_{gb} = (V_{gb} + V_d)/V_{ud}$. Since $G_c/G_{gb} = 2-3$, and $V_d/V_{ud} < 0.12$ one can conclude that $V_{gb} > V_{ud}$ and $V_{gb}/V_a > 0.5$.